

①

Theory of Electron Correlation in 3d Transition Metal Oxides

1	Introduction	1
2	Cluster Model with a Transition Metal Ion	8
2.1	Introduction	8
2.2	Model Hamiltonian	9
2.3	Ground State	9
2.4	Excited States	15
2.4.1	Wave function	15
2.4.2	Resonance phenomena spectra	18
2.4.3	Fragment of N_2 and F_2	19
2.5	EXAFS in 3d TM compounds	22
2.5.1	3d RPE	23
2.5.2	7p RPE	24
2.5.3	3s RPE	26
2.6	Conclusions	26
3	Cluster Model with Multiple Transition Metal Ions	27
3.1	Introduction	27
3.2	Model Hamiltonian	28
3.3	Ground state	30
3.4	Excited states	30
3.4.1	$3d_{xy}$ plane	30
3.4.2	Effect of the electric field induced at the crystal surface	34
3.4.3	$3d_{xy}$ plane	35
3.5	Conclusions	35
4	Spin-orbital Basis Set Expansion	37
4.1	Introduction	37
4.2	Density matrix method	39
4.3	Optimal functions on the CuO_4 cluster	40
	References	48

Arata TANAKA

February 1997

*Department of Materials Science, Faculty of Science
Hiroshima University, Higashi-Hiroshima 739*

Contents

1	Introduction	1
2	Cluster Model with a Transition Metal Ion	6
2.1	Introduction	6
2.2	Model Hamiltonian	8
2.3	Quasi- <i>d</i> state	9
2.4	Resonant photoemission	15
2.4.1	Wave function	15
2.4.2	Resonant photoemission spectra	16
2.4.3	Parameters of \mathcal{H}_2 and V	18
2.5	SX-RPE in 3 <i>d</i> TM compounds	19
2.5.1	3 <i>d</i> RPE	19
2.5.2	3 <i>p</i> RPE	33
2.5.3	3 <i>s</i> RPE	34
2.6	Conclusions	34
3	Cluster Model with Multiple Transition Metal Ions	37
3.1	Introduction	37
3.2	Model Hamiltonian	38
3.3	Non-local interference effect on the spectral functions in undoped CuO ₂ plane	41
3.4	Effect of the electron and hole doping on the spectral functions in CuO ₂ plane	47
3.5	Conclusion	51
4	Systematic Basis Set Reduction	55
4.1	Introduction	55
4.2	Density matrix method	56
4.3	Spectral functions on the Cu ₅ O ₁₆ cluster	58
4.4	Conclusion	66
	Acknowledgments	67
	References	68

Abstract

Electronic structures and spectral functions of $3d$ transition metal (TM) oxides are theoretically investigated using a finite size cluster model. We first study the resonant $3d$, $3p$ and $3s$ photoemission spectroscopies (PES) at TM $2p$ threshold in late $3d$ TM monoxides and TiO_2 using a cluster model with a TM ion and its ligand oxygen ions which includes the configuration interaction and the $3d$ - $3d$ and $3d$ -core hole multipole interaction. Analyzing the experimental valence band spectra, we determine the charge transfer energy and the $3d$ - $3d$ Coulomb interaction energy and show that the spectra give reliable information about the characteristic parameters of TM oxides. We also discuss the difference in the selection rule between the direct process and the resonance process.

We next discuss the $3d$ PES, $3d$ inverse photoemission spectroscopy (IPES) and Cu $2p$ X-ray photoemission spectroscopy (XPS) spectra for the CuO_2 plane in the undoped and doped high- T_c superconductors using a Cu_nO_m cluster model containing up to four Cu ions. The model takes into account full degeneracy of the Cu $3d$ and O $2p$ orbits and on-site Cu $3d$ - $3d$ and O $2p$ - $2p$ electrostatic multipole interaction. For the $3d$ PES spectra of the undoped cluster, the main peak structure consists of two kinds of states. One has an excess hole introduced by the photoexcitation on nearest neighbor oxygen sites of the photoexcited Cu site. The other has the hole on neighboring CuO_4 units, having the Zhang-Rice singlet state on the neighboring units. Because of the non-local character of the state corresponding to the main peak structure, the structure is sensitive to the number of the nearest neighbor Cu site. The interference of the initial and final state wave functions caused by the inter- CuO_4 -unit charge transfer lead to a spectral weight transfer to the low binding energy side. For the Cu $2p$ XPS spectra for undoped systems, a hole escaping from the core hole Cu site exhibits similar way and its main peak structure consists of the two kinds of screened states. In the light of calculations for larger clusters, the results obtained from the above small clusters are reinterpreted. For the $3d$ PES spectra of the electron doped cluster, two kinds of states are created inside the insulating gap and the chemical potential moves into the conduction band. The spectral weight is transferred to the peaks corresponding to the states created inside insulating gap, drastically.

We furthermore present a formalism for a systematic basis set reduction of clusters. Using this formalism, we calculate the spectra of the clusters containing up to five Cu ions, where the number of basis set without the reduction beyond the tractable limit. We show that our formalism is a promising method to discuss spectral functions in large clusters including $3d$ TM ions other than Cu ion.

Chapter 1

Introduction

The electron correlation effect in $3d$ transition metal (TM) compounds is a long-standing problem. In 1937, de Boer and Verwey [1] pointed out that the insulating behavior of some of the $3d$ transition metal oxides can not be explained by the band theory. After this, Mott and Peierls [2] argued that the electron correlation effect is essential to understand the insulating behavior on these materials. The insulating behavior of such materials for instance NiO has once been believed to be explained by the theory proposed by Mott [3] and Hubbard [4–6]. In the theory, charge fluctuations of the type $d^n d^n \rightarrow d^{n-1} d^{n+1}$, where one of the $3d$ electrons on a site is transferred to another site, are suppressed by the on-site Coulomb interaction of the $3d$ electron and if the Coulomb interaction energy (U) becomes larger than the d -band width (W), a simple band picture breaks down and the metal-to-insulator transition takes place.

Recently, photoemission (PES) and inverse photoemission spectroscopies (IPES), which correspond to an electron removal and an electron addition, respectively, have taken an important role in the study of electronic structures of the TM systems. Using the NiO_6 octahedral cluster model with the configuration interaction for NiO, where the $d^8 \rightarrow d^7$ valence PES is supposed to occur, Fujimori *et al.* [7, 8] showed that the character of the valence band top of PES is not d^7 but $d^8 \underline{L}$ (\underline{L} stands for a hole on the O $2p$ orbit). Zaanen, Sawatzky and Allen (ZSA) [9] proposed, using the so called ZSA diagram, that the TM compounds with the d^n configuration can be classified into two categories depending on the Coulomb interaction energy U , the charge transfer energy Δ and the oxygen bandwidth. The schematic electron removal and electron addition spectra are shown on the left hand side in Fig. 1. The insulator with $U > \Delta$, where the band gap is determined not by U but by Δ , belongs to the charge transfer insulator. The valence band top has mainly $d^n \underline{L}$ character in this case (see Fig. 1(a)). The Mott-Hubbard insulator, on the other hand, corresponds to the case with $U < \Delta$ where the valence band top has mainly the

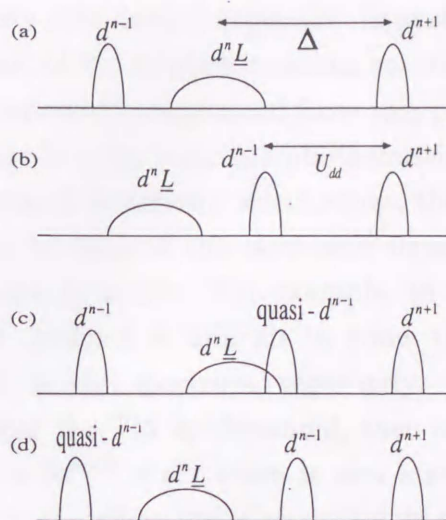


Figure 1.1: Schematic picture of the electron removal and electron addition spectra. Spectra for the two different categories proposed by Zaanen, Sawatzky and Allen: the charge-transfer insulator (a) and the Mott-Hubbard insulator (b). Spectra with the strong hybridization: the charge-transfer insulator (c) and the Mott-Hubbard insulator (d).

d^{n-1} character (see Fig. 1(b)). According to the ZSA diagram, the charge transfer insulator is realized mainly in late TM compounds, while the Mott-Hubbard one is realized mainly in light TM compounds.

The states of valence band top of both the charge transfer and Mott-Hubbard insulators are, however, highly covalent in reality and the classification of ZSA would be oversimplified one. For example, light $3d$ transition metal oxides, e.g., V_2O_3 which is believed to be a typical Mott-Hubbard insulator, however, is revealed to be highly covalent system by Uozumi *et al.* [10, 11] Moreover, for the charge transfer type insulator such as late $3d$ transition metal monoxides, the valence band top is found to be a bound state resulting from mixture of O $2p$ and $3d$ orbit pushed out of the oxygen $2p$ band. For example, the so called Zhang-Rice singlet state [12] in the CuO_2 plane is the one of such “pushed out” states. The state, in some sense, has d^{n-1} like character [13–16], though the dominant configuration of the state is $d^n \underline{L}$. We call this state the quasi- d state. The quasi- d state is very similar to the multiple charge states of transition-metal impurities in semiconductors [17]. In Chap. 2, we will discuss the quasi- d state systematically, showing why the state is appears in the top of the valence band. The schematic electron removal and electron addition spectra in this point of view are shown in Figs. 1(c) and 1(d). The valence band top of both the Mott-Hubbard and the charge transfer insulators now has a d^{n-1} like state. Thus, the distinction between the charge transfer and Mott-Hubbard

insulators is not necessarily well defined especially in systems with high covalency. We also show that the trend of the $3d$ photoemission spectroscopy ($3d$ PES) through the TM oxide can systematically be explained from this point of view.

Another topic in Chap. 2 is the resonant photoemission spectroscopy (RPES). Because of its site and orbital symmetry selectivities, the RPES is nowadays one of the most powerful tool to analyze the electronic structure of the transition or rare earth compounds experimentally. For example, in the conventional valence band PES of the $3d$ TM oxide, it is difficult to know the contribution of the O $2p$ orbit and Cu $3d$ orbit to the spectrum, separately. However, if we tune the incident photon energy near the TM $3p$ threshold, then in addition to the conventional photoprocess $3d^n \rightarrow 3d^{n-1} + e^-$, there is also a second order photoprocess $3d^n \rightarrow 3p^5 d^{n+1} \rightarrow 3d^{n-1} + e^-$, where the electric dipole transition $3p \rightarrow 3d$ is followed by the super Coster-Kronig decay. In the latter process, because the Auger decay including the $3d$ electron is dominant, the intensity corresponding to the states which have the contribution from the $3d$ orbit are selectively enhanced. Moreover, tuning the incident photon energies corresponding to various intermediate states, we can obtain more detailed information for the final state, because of different selection rule through the intermediate states. Recently, RPES experiments using soft X-ray has been carried out at the TM $2p$ threshold in $3d$ TM metals and their compounds. The RPES at the $2p$ threshold has some advantages compared to $3p$ threshold. The resonant enhancement of the spectrum is by an order larger than that of $3p$ threshold and the presence of rich structures in soft X-ray core absorption spectra (XAS) [19] enables one to discuss processes through more specific intermediate states. Furthermore, in addition to valence photoemission, we can discuss resonances in shallower core level photoemission, which can provide much information about electronic structures. In the rest of Chap. 2, we will present the calculated RPES spectra in the late $3d$ TM monoxides and TiO_2 at $2p$ threshold using a cluster model including the configuration interaction and intraatomic multipole interaction between $3d$ electrons. We will show that the RPES gives reliable information about electronic structures of $3d$ TM oxides.

In 1986, Bednorz and Müller [20] reported the discovery of the cuprate superconductor with a high critical temperature $T_c = 38\text{K}$. Since then, a lot of “high- T_c ” cuprate superconductors have been found and now a cuprate superconductor with mercury has critical temperature about $T_c = 133\text{K}$. They all have two dimensional network CuO_2 plane. In the most of the high- T_c superconductor, the CuO_2 planes are doped with holes. On the other hands, in $\text{Nd}_{2-x}\text{Ce}_x\text{CuO}_{4-\delta}$, the CuO_2 planes are shown to be doped with electrons [21].

The naive explanation for the doping effect is based on the rigid-band picture.

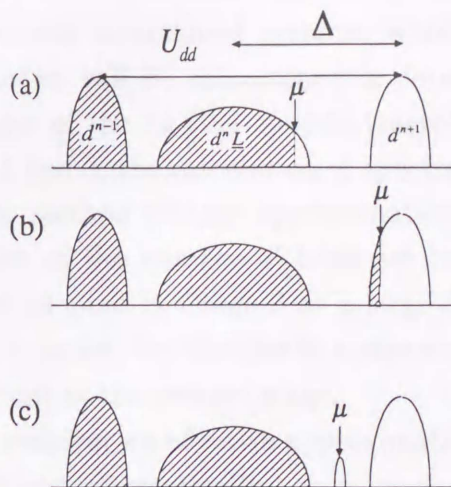


Figure 1.2: Schematic illustration of the effect of doping on the spectra. The hole doped (a) and the electron doped (b) spectra for the rigid band model. Upon hole (electron) doping, the chemical potential moves into the valence band top (the conduction band bottom). Another explanation of the effect of doping (c); New state created inside the insulating gap and the chemical potential stay inside the gap.

Figure 1.2 shows the schematic picture of the electron and hole doping effect on the PES and the IPES spectra. Upon hole doping, the chemical potential shifts into the valence band top and the IPES spectrum has new peaks in the vicinity of the valence band top (see Fig. 1.2(a)). On the other hand, upon electron doping, the chemical potential shifts into the conduction band bottom and the PES spectrum has additional peaks in the vicinity of the conduction band (see Fig. 1.2(b)). This chemical potential shift upon doping is in accordance with the result of the finite cluster calculations for the two dimensional Hubbard model [22] and d - p model [23–25]. Moreover, the many body effect lead to the spectral weight transfer to the peaks created inside the insulating gap in these models. The electron energy loss spectroscopy (EELS) [26] and XAS [27–29] data agree with the shift of the chemical potential and spectral weight transfer to the new peaks, by the doping. From the PES and IPES experimental side, on the other hand, the chemical potential is argued to lie in the state created inside the gap by the electron and hole doping (see Fig. 1.2(c)) [30–36].

In Chap. 3, we will discuss the effect of electron or hole doping on the $3d$ PES, $3d$ IPES and Cu $2p$ XPS spectra by extending the CuO₄ cluster to those containing four Cu atoms including the intraatomic multipole interaction between electrons. With the extended cluster model, the spectral weight transfer and the necessity

of including the $3d$ orbitals with other than the $x^2 - y^2$ symmetry are discussed in detail. The $3d$ PES spectrum in undoped systems, which is discussed in Chap. 2 with the small CuO_4 cluster, will be reexamined in detail. A problem about the character of the final states of the $3d$ PES spectra treated in the small cluster will be discussed. In Chaps. 2 and 3, the calculation of spectra is performed with use of the Lanczos and recursion method without approximation for a given Hamiltonian i.e. an artificial reduction of the number of basis set is not performed. For the system size beyond those adopted in Chap. 3 or a large cluster in the case $3d$ TM compounds other than Cu oxides, the number of states necessary in the calculation is beyond the tractable limit in the present stage.

In Chap. 4, we try to seek out an effective approximation to calculate spectra by reducing the number of basis systematically.

2.1 Introduction

Highly correlated $3d$ transition metal (TM) compounds have attracted much attention as materials responsible for the mechanism of high T_c superconductivity. The actual studies are based either on the local density functional approximation (LD) and its extension (LDA+ U) or many-body calculations (MCTDH, etc.) [1, 2]. The latter have several advantages. High energy resolution such as photoemission and photoabsorption is well known to resolve the ground state clearly. Electronic structure of $3d$ TM compounds, which is a topic that has been analyzed from a viewpoint of CI in the form of a finite cluster including local electron correlation. As a result, the effects of $3d$ correlation through U_d , the d-orbital energy relative to the atomic reference level d are more important than the energy components and the interactions producing the energy gap of superconductors. They however still have disadvantages of numerical U_d and d values depend on the choice of a reference level [1, 2].

Recently a recent photoemission spectroscopy (PES) experiment using soft X-ray (SX) has been carried out in $3d$ TM oxides, their compounds and $3d$ rare earths [3-5]. In parallel with experimental observations to clarify the mechanism of SC, PES have been investigated from the many-body CI viewpoint on the basis of a cluster model including full multiple occupancy [6-10]. In SC, PESs are for $3d$ TM oxides, the TM $3d$ orbitals are less populated than the $3d$ orbitals of the free TM. The Kondo (T_K) energy, the electron transfer to the conduction band and another electron is assumed to be finite. The following spectra of soft X-ray spectra compared with the vacuum ultraviolet (VUV) light spectra [11] seem to be a good approximation [1]. The occurrence of photoemission is much stronger compared with the case of VUV light excitation, which can give spectra independent of the incident

Chapter 2

Cluster Model with a Transition Metal Ion

2.1 Introduction

Electronic structures of $3d$ transition metal (TM) compounds have attracted much attention in relation to researches of the mechanism of high- T_c superconductivity. Theoretical studies on the basis of either the local density functional approximation [18] and its extension [37, 38] or many-body configuration interaction (CI) [8, 9, 39–41] have been carried out. High energy spectroscopy such as photoemission and photoabsorption is well known to contribute greatly to clarify electronic structures of $3d$ TM compounds. Various spectra have been analyzed from a viewpoint of CI on the basis of a cluster model including local electron correlation. As a result, the effective $3d$ - $3d$ interaction strength U_{dd} , the charge transfer energy between the anion and cation sites Δ etc. have been estimated for many compounds and the mechanism producing the energy gap of insulators has been discussed. There however exist some discrepancies of estimated U_{dd} and Δ values among previous analyses for a given compound [15, 42–48].

Recently a resonant photoemission spectroscopy (RPE) experiment using soft X-ray (SX) has been carried out in $3d$ TM metals, their compounds and $4f$ rare earth systems [49–53]. In parallel with experiments, theoretical studies to clarify the capability of SX-RPE have been attempted from the many-body CI viewpoint on the basis of a cluster model including full multiplet splitting [54–57]. In SX-RPE for $3d$ TM compounds, the TM $2p$ core electron is first photoexcited into valence states and then, by the Coster-Kronig (CK) decay, one electron returns to the core level and another electron is emitted outside solids. The following merits of soft X-ray region compared with the vacuum-ultraviolet (VUV) light region [58] seem to become apparent: 1) The resonance of photoemission is much stronger compared with the case of VUV light region, which can give spectra independent from off-resonance

spectra and is therefore expected contribute to a removal of discrepancies of estimated parameter values among analyses. 2) The presence of rich structures in soft X-ray core absorption spectra (XAS) [19] enables one to discuss resonant processes through more specific intermediate states. 3) In addition to valence photoemission, we can discuss resonances in shallower core level photoemission, which can provide much information about electronic structures.

Aside from these merits, there exist however debates about the relative importance between the resonant photoemission and Auger decay processes. For example in resonant $3d$ photoemission experiment at Cu $2p$ threshold for CuO, Tjeng *et al.* [49] argued the satellite resonance enhancement factor of $\sim 10^2$, while Lopetz *et al.* claimed that the resonance is mostly due to the Auger decay and the actual resonance enhancement is ~ 10 , not $\sim 10^2$ [50]. Considering the above-mentioned merits of SX-RPE, we may expect that the comparison between the calculation of SX-RPE and experiments for various photon energies at on-resonances can be very useful in an identification of observed second order optical processes.

Recently Park *et al.* reported giant resonances in $3d$ RPE at TM $2p$ core threshold for CuO, NiO, CoO, FeO, MnO, V_2O_3 and Ti_2O_3 [59] and Shin *et al.* reported the resonances on Ti oxides [60]. In this work, we present expected $3d$, $3p$ and $3s$ RPE spectra at the $2p$ core threshold of $3d$ TM ions in TM monoxides and TiO_2 calculated on the basis of the cluster model including full multiplet splitting with preassuming resonant photoemission. One of our purposes is to provide information to identify the second order photoexcitation process. Another purpose is to demonstrate the capability of SX-RPE to give more plausible parameter values such as U_{dd} and Δ .

In most of previous theoretical calculations of resonant photoemission spectra, the lifetime of the intermediate state (or the imaginary part of the self-energy) has been assumed to be an adjustable constant parameter. In this work, we take into account the off-diagonal matrix element as well as the term dependence of the imaginary part of the self-energy expected from possible various CK decay processes. The authors have adopted this approach in the calculation of the $3d$ RPE at the Ni $3p$ core threshold for ferromagnetic Ni and the resonance enhancement of $3 \sim 4$ is obtained for the 6 eV satellite [61], which is in good agreement with experiment. The application of this approach to the present problem therefore seems to be meaningful, since it has been the subject of debate.

As was discussed in Chap. 1, in systems with high covalency or with the strong TM $3d$ -O $2p$ hybridization, the distinction between the Mott-Hubbard and charge transfer insulators is meaningless especially in a discussion of PES or IPES spectra near the Fermi level, In this chapter, we try to discuss the character of $3d$ PES

spectrum at off-resonance by introducing the concept “quasi- d state”.

We present our method of calculation in Sect.2.2, discuss the quasi- d state and the off-resonant PES in Sect.2.3 and show the method of calculation and calculated result of the RPE spectra in Sect.2.4 and Sect.2.5, respectively. Section 2.6 is devoted to conclusions.

2.2 Model Hamiltonian

As a model for the TM compounds, we assume a TMO_6 cluster with the octahedral symmetry (O_h) or a TMO_4 cluster with the D_{4h} symmetry clusters where the central TM ion are surrounded by the ligand oxygen ions. The Hamiltonian of the cluster is assumed to be

$$\mathcal{H} = \mathcal{H}_1 + \mathcal{H}_2 . \quad (2.1)$$

\mathcal{H}_1 is the “non-multiplet” term describing the valence and core states and the the effective interaction between electrons given by

$$\begin{aligned} \mathcal{H}_1 = & \sum_i \varepsilon_d(\Gamma_i) \sum_{\gamma_i} d_{\gamma_i}^\dagger d_{\gamma_i} + \sum_i \varepsilon_p(\Gamma_i) \sum_{\gamma_i} p_{\gamma_i}^\dagger p_{\gamma_i} + \varepsilon_c \sum_{\xi} c_{\xi}^\dagger c_{\xi} \\ & + U_{dd} \sum_{i,j} \sum_{\gamma_i \neq \gamma_j} n_{d\gamma_i} n_{d\gamma_j} + U_{dc} \sum_{i,\gamma_i,\zeta} n_{d\gamma_i} n_{c\zeta} + \sum_i V(\Gamma_i) \sum_{\gamma_i} (d_{\gamma_i}^\dagger p_{\gamma_i} + h.c.) \end{aligned} \quad (2.2)$$

Here, the first, second, third, fourth, fifth and sixth terms, respectively, denotes the energy of the $3d$ orbit of the TM ion, of the ligand molecular orbit and of the core orbit, the effective $3d$ - $3d$ interaction, the attractive core-hole potential acting on the $3d$ electron and the hybridization between the ligand and $3d$ orbit. $\{\Gamma_i\}$ denotes, the t_{2g} and e_g representation of the O_h group or the corresponding representation of the D_{4h} and γ_i denotes the basis of each representation including spin state. The energy difference between between the t_{2g} and e_g is given by $10Dq$ for the $3d$ orbit and by $2T_{pp}$ for the ligand with the use of the O-O transfer integral T_{pp} . We assume $V(e_g) = -2V(t_{2g})$ for the O_h cluster. For CuO, we adopt the approach given in ref. [62]. We define charge transfer energy as $\Delta = E(3d^{n+1}\underline{L}) - E(3d^n)$, where $E(3d^{n+1}\underline{L})$ and $E(3d^n)$ are the average energies of $3d^{n+1}\underline{L}$ and $3d^n$ configuration, respectively. ξ stands for the orbital and spin state of the core orbit. The suffix of the core state c means the $2p$ core of TM ion in the intermediate state of the resonant photoemission and in the final state the $3p$ and $3s$ cores for $3p$ RPE and $3s$ RPE, respectively.

H_2 describes the full-multiplet $3d$ - $3d$ (\mathcal{H}_{dd}) and $3d$ -core interaction (\mathcal{H}_{dc}) described by the Slater integrals other than F^0 ($c = 2p, 3s, 3p$) and the spin-orbit interaction in the $3d$ state $\mathcal{H}_d(\zeta_d)$ with the coupling constant ζ_d and in the core

state $\mathcal{H}_c(\zeta_c)$ ($c = 2p, 3p$); [63]

$$\mathcal{H}_2 = \mathcal{H}_{dd} + \mathcal{H}_{dc} + \mathcal{H}_d(\zeta_d) + \mathcal{H}_c(\zeta_c). \quad (2.3)$$

We set the average energy of \mathcal{H}_2 in each configuration equal to zero; the present definition of U_{dd} is the same as that of U in ref. [44]. The Hamiltonian \mathcal{H} (see eq. (2.1)) is often used to discuss various core level spectroscopies.

2.3 Quasi- d state

We start discussions with the hybridization term with the spherical (SO_3) symmetry and without the multiplet and spin-orbit interaction terms. The strength of the hybridization between the $3d$ and ligand orbitals are all the same in the SO_3 symmetry and we set $V \equiv V(SO_3)$. Each $d^{n+m}\underline{L}^m$ configuration has $\binom{10}{n} \times \binom{10}{m}$ Slater determinants constructed from the $3d$ and ligand orbitals. Among many states for a given $d^{n+m}\underline{L}^m$, we define a quasi- d state in this configuration corresponding to one of Slater determinants $|d^n \alpha\rangle$ in d^n configuration as

$$|d_m^n \alpha\rangle = \frac{1}{\sqrt{\binom{10-n}{m}}} (D^\dagger)^m |d^n \alpha\rangle \quad (2.4)$$

where D^\dagger denote

$$D^\dagger = \sum_{\mu} d_{\mu}^{\dagger} p_{\mu} \quad (2.5)$$

and index α identify $\binom{10}{n}$ different Slater determinants in the d^n configuration. The most essential point to understand properties of the quasi- d^n states is that, among the couples of the states chosen arbitrary from the $d^{n-m}\underline{L}^m$ and $d^{n-m+1}\underline{L}^{m+1}$ configurations, the couple of the quasi- d^n states $|d_m^n i\rangle$ and $|d_{m+1}^n i\rangle$ maximizes the effective hybridization strength between $d^{n-m}\underline{L}^m$ and $d^{n-m+1}\underline{L}^{m+1}$ and it is $\sqrt{10-n-m}V$. Because of the strong effective hybridization of the quasi- d^n states, the ground state of the d^n system in the SO_3 symmetry without other interaction should always consist of the $\binom{10}{n}$ hold quasi- d^n states in the presence of a finite hybridization strength. Note that, even without d^n states, the ground state still consists of the quasi- d^n state in the presence of the finite hybridization strength.

Next, we switch on the multiplet and spin-orbit interaction terms. It can be easily shown that the effective Hamiltonian for the quasi- d^n state in $d^{n+m}\underline{L}^m$ configuration is the same as that of the d^n states except the parameter values for the one-body interaction terms should be reduced by a factor of

$$\frac{10-n-m}{10-n}. \quad (2.6)$$

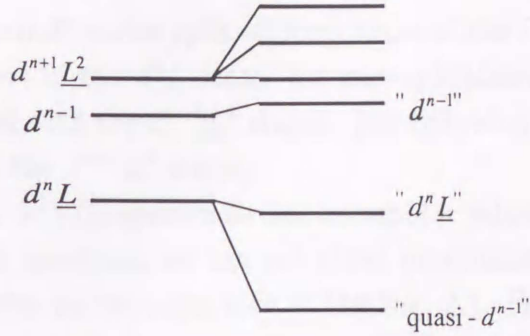


Figure 2.1: Schematic energy diagram for the final state of the 3d PES in the absence of the hybridization (left) and in the presence of the hybridization (right) are shown.

The multipole interaction terms, on the other hand, should be then reduced by a factor of

$$\frac{(10 - n - m)(9 - n - m)}{(10 - n)(9 - n)}. \quad (2.7)$$

The multipole interaction also mix the quasi- d^n states in a configuration and the rest of states in the same configuration. The quasi- d states and thus are no more rigorously defined. Even then, the ground state of the d^n system behaves as if it is an ion with the d^n configuration with the weakened multipole and spin-orbit interactions.

To understand 3d PES spectra for the TM compounds systematically, we performed calculations for various d^n systems with three different situations. 1) The hybridization with SO_3 symmetry is included and the multipole interaction is omitted. 2) Both the hybridization with SO_3 symmetry and the multipole term are included. 3) Both the hybridization with O_h symmetry and the multipole term are included. We fixed the values of parameters U_{dd} , $V(\Gamma_i)$ and Δ corresponding to the charge-transfer insulator regime. Note that, the choice of the parameter values in the Mott-Hubbard insulators does not affect overall structures of the spectra under the condition of strong hybridization. We assume that state is a superposition of d^n , $d^{n+1}\underline{L}$ and $d^{n+2}\underline{L}$. Then the final state of 3d PES is that of d^{n-1} , $d^n\underline{L}$ and $d^{n+1}\underline{L}$. First, we discuss the 3d PES of the system with the hybridization term with the SO_3 symmetry and without the multiplet terms. Figure 2.1 shows a schematic energy-level diagram of the final state of the 3d PES spectrum. On the left side of the figure, we show the energy-level diagram of in the absence of the hybridization. Three horizontal lines represent the energy-level of the configurations d^{n-1} , $d^n\underline{L}$ and $d^{n+1}\underline{L}^2$. On the right side of the figure, we show the energy-level diagram of in the presence of the hybridization. The quasi- d^{n-1} states in each configuration

are now hybridized with one another and, in $d^n \underline{L}$ and $d^{n+1} \underline{L}^2$ configurations, the energy levels of the quasi- d^n states split off from those of the remainder states in the configurations. The rest of the $d^n \underline{L}$ states are not hybridized with the d^{n-1} states and are only hybridized with the $d^{n+1} \underline{L}^2$ states. The hybridization leads to a further energy level splitting of the $d^{n+1} \underline{L}^2$ states.

In Fig. 2.2, we show $3d$ PES spectra for the parameter values $\Delta = 3\text{eV}$, $U_{dd} = 6\text{eV}$ and $V = 2\text{eV}$. In each spectrum we can see three prominent peaks corresponding to the lowest three states on the right side of the Fig. 2.1. For these peaks, we call them, in order of lowest to higher ones, “quasi- d^{n-1} ”, “ $d^n \underline{L}$ ” and “ d^{n-1} ” satellite peaks. The relative intensity of “ d^{n-1} ” satellite peak to that of “quasi- d^{n-1} ” peak is increased and the energy separation of the two is decreased with increasing n . This is the result of decrease of the effective hybridization with increasing n between quasi- d^{n-1} (quasi- d^n) states of d^{n-1} (d^n) and $d^n \underline{L}$ ($d^{n+1} \underline{L}$) in the final (initial) states: the value is $\sqrt{10 - nV}$ ($\sqrt{11 - nV}$) for the final (initial) state.

Next, in addition to the hybridization term with SO_3 symmetry, we include the the multipole term. We set values for the Slater integrals $F_{dd}^2 = 9.44\text{eV}$ and $F_{dd}^4 = 5.92\text{eV}$. The result is shown in the Fig. 2.3. Each of the “quasi- d^{n-1} ”, “ $d^n \underline{L}$ ” and “ d^{n-1} ” satellite peaks discussed above now has the multiplet structure. The relative intensity of the “ $d^n \underline{L}$ ” structure to that of the “quasi- d^{n-1} ” structure is increased compared to the corresponding spectra in the case without the multiplet (see Fig. 2.2), since the quasi- d^{n-1} states and the rest of the $d^n \underline{L}$ states (corresponding to the “ $d^n \underline{L}$ ” structure) are mixed with one another by the multiplet interaction terms. Because the energy level splitting due to the multipole interaction of the d^5 configuration is largest, the spectral weight transfer to the “ $d^n \underline{L}$ ” structure is most prominent for the system with $n = 5$, where the intensity of “ $d^5 \underline{L}$ ” structure is larger than that of the “quasi- d^4 ” structure. This is why the $3d$ PES spectra of highly covalent Mn compounds like MnCl_2 [78] and MnTe [77] have a main peak structure not in the vicinity of the valence band top but at several eV higher binding energy region from the valence band top. For the system with more than half filled d electrons in the initial state ($n > 5$), we can see each structures splits into two peaks. The lower and higher energy peaks correspond to the state obtained by removing an electron with parallel and anti-parallel spin to the spin moment in the initial states. The energy difference between the two peaks corresponds to the exchange splitting energy. The decrease of the exchange splitting energy in the “ d^{n-1} ” satellite structure with increasing n is clearly seen in the figure (Figs. 2.5(a), 2.5(b) and 2.5(c)). This can be explained by the decrease of multiplet splitting energy with increasing n . The decreasing of the exchange splitting energy in the “quasi- d^{n-1} ” structure are much faster than that of “ d^{n-1} ” satellite structure with increasing

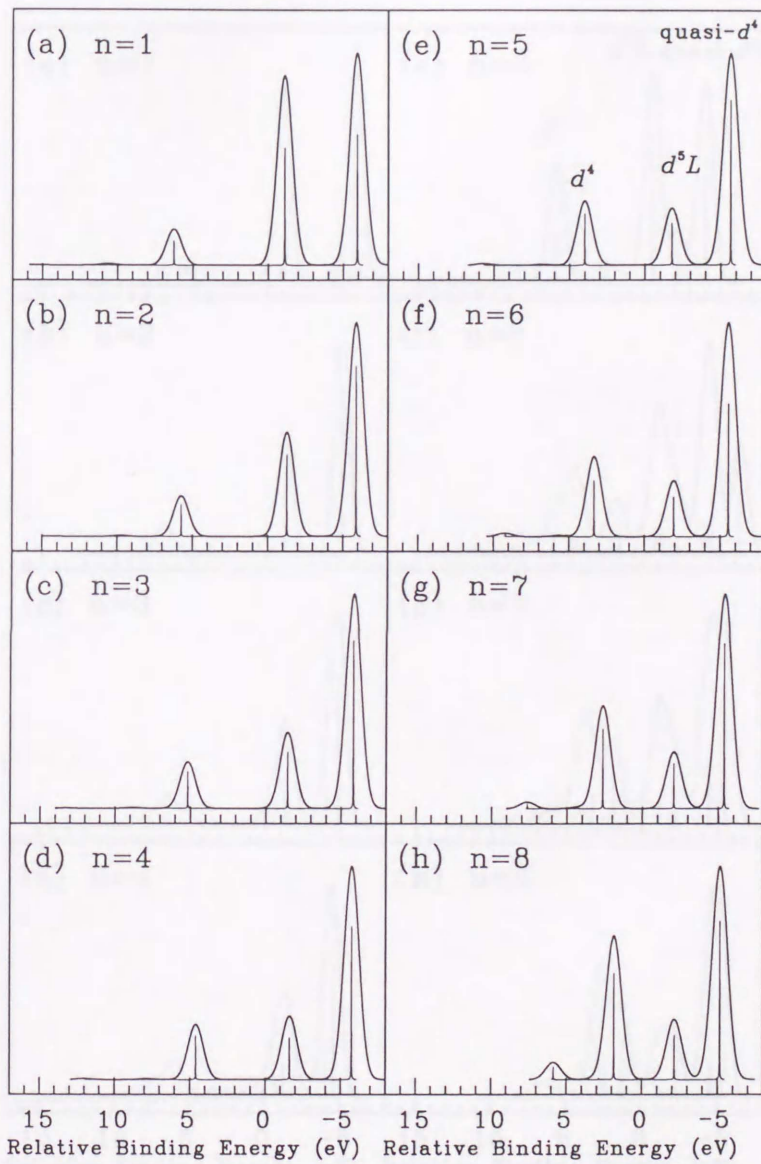


Figure 2.2: The calculated 3d PES spectra for various d^n systems with the hybridization term with the SO_3 symmetry and without the multipole term.

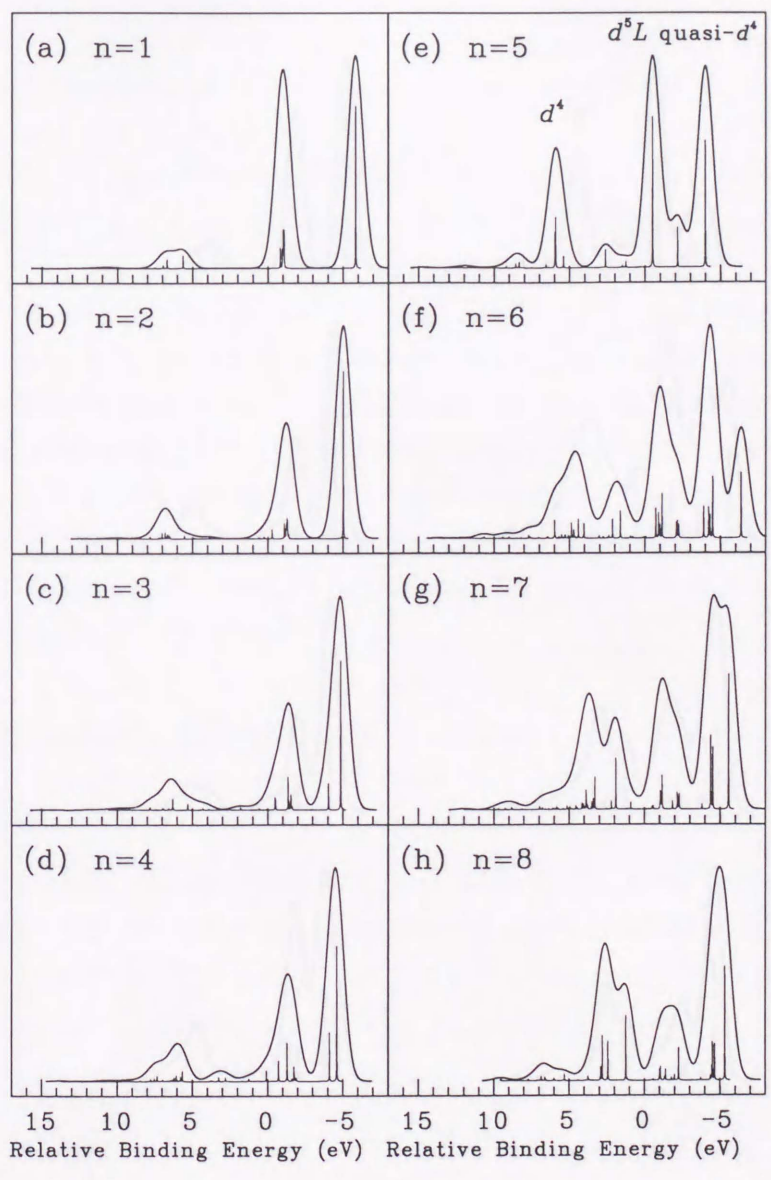


Figure 2.3: The same as Fig. 2.2 but with the multipole term.

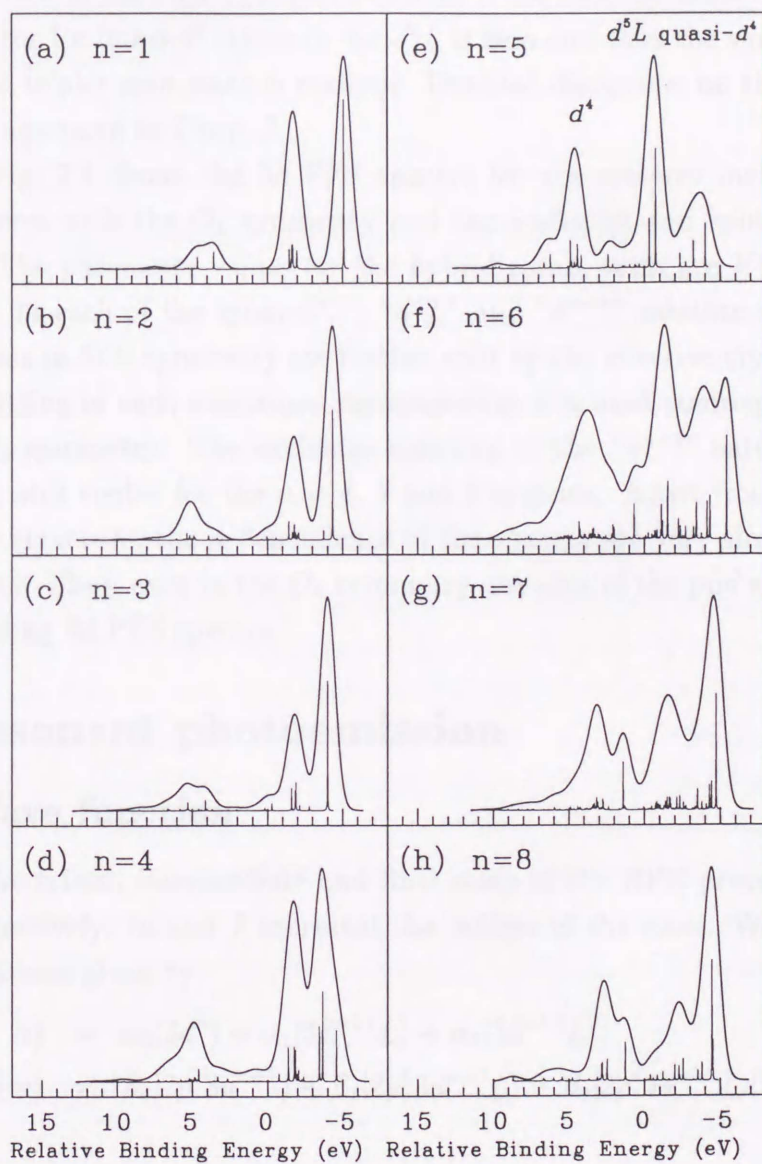


Figure 2.4: The same as Fig. 2.3 but with the hybridization term with the O_h symmetry

n , since the parameter value of the effective multipole interaction of “quasi- d^{n-1} ” states in the $d^n \underline{L}$ configuration should be reduced by the factor expressed in the eq. (2.7) from the bare value: the factors for the d^6 , d^7 and d^8 systems are 3/5, 1/2 and 1/3, respectively. This is why the d^{n-1} ion-like-state in the valence band top has the tendency to realize the low spin state compared to a d^{n-1} ion [13, 14]. The ZRS singlet state in the high- T_c superconductor is the most extreme case, where the reduction factor for quasi- d^8 states in the $d^9 \underline{L}$ is zero and thus the singlet spin state instead of the triplet spin state is realized. Detailed discussion on the ZRS singlet state will be appeared in Chap. 3.

Finally, Fig. 2.4 shows the 3d PES spectra for the systems including the hybridization term with the O_h symmetry and the multiplet and spin-orbit interaction terms. The parameter values for the hybridization term are $V(E_g)=2\text{eV}$ and $V(T_{2g})=1\text{eV}$. In each of the quasi- d^{n-1} , “ $d^n \underline{L}$ ” and “ d^{n-1} ” satellite structures, the multiplet terms in SO_3 symmetry are further split by the effective crystal field. The exchange splitting of each structures are somewhat obscured compared to the case with the SO_3 symmetry. The exchange splitting of the “ d^{n-1} ” satellite structure are, however, still visible for the $n = 6, 7$ and 8 systems. Apart from the detail of the multiplet structure, the n dependence of the spectra are very similar to that of SO_3 symmetry. Thus, even in the O_h symmetry, the idea of the ppd state is capable of understanding 3d PES spectra.

2.4 Resonant photoemission

2.4.1 Wave function

We denote the initial, intermediate and final state of the RPE process by $|i\rangle$, $|m\rangle$ and $|f\rangle$, respectively: m and f represent the indices of the state. We then assume the superpositions given by

$$|i\rangle = \alpha_0|3d^n\rangle + \alpha_1|3d^{n+1}\underline{L}\rangle + \alpha_2|3d^{n+2}\underline{L}^2\rangle \quad (2.8)$$

$$|m\rangle = \beta_0|2p^5 3d^{n+1}\rangle + \beta_1|2p^5 3d^{n+2}\underline{L}\rangle + \beta_2|2p^5 3d^{n+3}\underline{L}d^2\rangle \quad (2.9)$$

and

$$|f\rangle = \gamma_0|3d^{n-1}\rangle + \gamma_1|3d^n\rangle + \gamma_2|3d^{n+1}\underline{L}^2\rangle \quad (2.10)$$

for 3d RPE,

$$|f\rangle = \gamma_0|3p^5 3d^n\rangle + \gamma_1|3p^5 3d^{n+1}\underline{L}\rangle + \gamma_2|3p^5 3d^{n+2}\underline{L}^2\rangle \quad (2.11)$$

for 3p RPE, or

$$\begin{aligned} |f\rangle = & \gamma_0|3s^1 3d^n\rangle + \gamma_1|3s^1 3d^{n+1}\underline{L}\rangle + \gamma_2|3s^1 3d^{n+2}\underline{L}^2\rangle \\ & + \gamma_3|3p^4 3d^{n+1}\rangle + \gamma_4|3p^4 3d^{n+2}\underline{L}\rangle + \gamma_5|3p^4 3d^{n+3}\underline{L}^2\rangle \end{aligned} \quad (2.12)$$

for 3s RPE, where n is assumed to be 9, 8, 7, 6, 5 and 0 for Cu, Ni, Co, Fe, Mn and Ti compounds, respectively and \underline{L} denote a ligand hole; the photoelectron state is not contained in $|f\rangle$.

2.4.2 Resonant photoemission spectra

The RPE spectrum for the incident photon energy ω and the photoelectron energy ε $F(\varepsilon, \omega)$ is expressed as

$$F(\varepsilon, \omega) = \sum_f |\langle f\varepsilon|T(\omega)|i\rangle|^2 \delta(\omega + E_i - \varepsilon - E_f) \quad (2.13)$$

where E_i and E_f are the energy of $|i\rangle$ and $|f\rangle$, respectively. The T-matrix $T(\omega)$ is defined as

$$T(\omega) = V + V \frac{1}{\omega + E_i - \mathcal{H} - \mathcal{H}_{pe} - V} V \quad (2.14)$$

with \mathcal{H} given by eq. (2.1) and \mathcal{H}_{pe} being the Hamiltonian of a photoelectron the use of the perturbation V given by

$$V = V_D + V_R + V_{CK} + h.c. \quad (2.15)$$

Here V_D is the operator to represent the direct dipole transition from the $3d$, $3p$ or $3s$ orbit to the continuum state εl with the energy ε and the orbital angular momentum l for $3d$, $3p$ or $3s$ PE, respectively, which is described by the dipole matrix element such as $\langle 3d|r|\varepsilon l\rangle$ etc. V_R is the operator to represent the $2p \rightarrow 3d$ dipole transition expressed with the use of the matrix element $\langle 2p|r|3d\rangle$. V_{CK} describes the $2p3d3d$, $2p3d3p$, $2p3d3s$ and $2p3p3p$ CK decay processes which connect the above-mentioned intermediate state and various final states and are expressed with the use of the radial integrals such as $R^k(2p, \varepsilon l; 3d, 3d)$ etc. of the above-mentioned operator. We calculate the T-matrix by taking into account V_D and V_R to the lowest order and V_{CK} to an infinite order. Then $T(\omega)$ is expressed as [64, 67]

$$T(\omega) = V_D + V_{CK} \frac{1}{\omega + E_i - \mathcal{H}_m - \Sigma(\omega)} (V_R + V_{CK}^\dagger \frac{1}{\omega + E_i - \mathcal{H}_f - \mathcal{H}_{pe}} V_D). \quad (2.16)$$

$$\text{with } \Sigma(\omega) = V_{CK}^\dagger \frac{1}{\omega + E_i - \mathcal{H}_f - \mathcal{H}_{pe}} V_{CK} \quad (2.17)$$

Here \mathcal{H}_m and \mathcal{H}_f denote the Hamiltonian of the intermediate and the final state, respectively; $|m\rangle$ (see eq. (2.8)) and $|f\rangle$ (see eq. (2.10)-(2.12)) are the eigen state of \mathcal{H}_m and \mathcal{H}_f , respectively. The first, second and third term of eq. (2.16), respectively, represents the direct photoemission, the second-order resonant process and the interference term between the first and the second processes.

In eq. (2.16), the term

$$V_{\text{CK}}^\dagger \frac{1}{\omega + E_i - \mathcal{H}_f - \mathcal{H}_{\text{pe}}} V_{\text{D}} \quad (2.18)$$

is, with the use of the complete set $\{|f\varepsilon\rangle\}$ which is the direct product of $|f\rangle$ and the photoelectron state $|\varepsilon\rangle$ ($\mathcal{H}_{\text{pe}}|\varepsilon\rangle = \varepsilon|\varepsilon\rangle$) with the density of states $\rho(\varepsilon)$ and with neglecting the real part, rewritten as

$$\begin{aligned} & -i\pi V_{\text{CK}}^\dagger \int d\varepsilon \sum_f |f\varepsilon\rangle \langle f\varepsilon| \delta(\omega + E_i - E_f - \varepsilon) \rho(\varepsilon) V_{\text{D}} \\ & = -i\pi V_{\text{CK}}^\dagger \sum_f |f\rangle \langle f| \rho(\omega + E_i - E_f) V_{\text{D}}. \end{aligned} \quad (2.19)$$

Here we abbreviate the final state with $\varepsilon = \omega + E_i - E_f$ as $|f\rangle$ which forms a complete set in the subspace excluding the photoelectron. We furthermore replace $\rho(\varepsilon)$ by a constant ρ . Then eq. (2.19) (i.e. eq. (2.18)) reduces to

$$-i\pi\rho V_{\text{CK}}^\dagger V_{\text{D}} \quad (2.20)$$

; we assume ω contains a positive infinitesimal as its imaginary part. By the same approximation, the resolvent in eq. (2.16)

$$\frac{1}{\omega + E_i - \mathcal{H}_m - \Sigma(\omega)}$$

is expressed as

$$\frac{1}{\omega + E_i - \mathcal{H}_m + i\Gamma} \quad (2.21)$$

with $\Gamma = \pi\rho V_{\text{CK}}^\dagger V_{\text{CK}}$ whose columns and lows are specified within the subspace of intermediate states.

Our T-matrix is then expressed as

$$T(\omega) = V_{\text{D}} + V_{\text{CK}} \frac{1}{\omega + E_i - \mathcal{H}_m + i\Gamma} (V_{\text{R}} - i\pi\rho V_{\text{CK}}^\dagger V_{\text{D}}). \quad (2.22)$$

Putting eq. (2.22) into eq. (2.13), we obtain the expression of the RPE spectra as a function of ω and the binding energy $E_{\text{B}} = \omega - \varepsilon$:

$$F(E_{\text{B}}, \omega) = -\frac{1}{\pi} \langle i|T(\omega)^\dagger \left\{ \text{Im} \frac{1}{E_{\text{B}} + E_i - \mathcal{H}_f} \right\} T(\omega)|i\rangle. \quad (2.23)$$

We calculate the spectrum by using the recursion method [66] within the subspace given in Sect.2.4.1, which is, within an arbitrary error, equivalent to the result obtained from the exact diagonalization of the Hamiltonian. Our calculation takes into account the off-diagonal matrix element of the imaginary part of the self-energy

of the intermediate state as well as its term dependence, which arise from the $2p3d3d$, $2p3d3p$, $2p3s3d$ and $2p3p3p$ decay processes.

By the present treatment of RPE, we can explicitly show that the quantity $G(\omega)$ defined by

$$G(\omega) = \int \rho \, dE_B \, F(E_B, \omega) \quad (2.24)$$

is, if the origin of core lifetime is the CK decay only, the same as a generalized X-ray absorption spectrum which includes the $3s$, $3p$ and $3d \rightarrow \epsilon l$ transitions as well as the $2p \rightarrow 3d$ one. This relation is in every aspect plausible one, but is not necessarily satisfied if the self-energy is replaced by an approximate expression. Here we show that $G(\omega)$ with $F(E_B, \omega)$ arising only from the above-mentioned second order process is the same as the $L_{2,3}$ absorption ($2p \rightarrow 3d$) spectrum $F_L(\omega)$ defined by

$$F_L(\omega) = -\frac{1}{\pi} \text{Im} \langle i | V_R^\dagger \frac{1}{\omega + E_i - \mathcal{H}_m + i\Gamma} V_R | i \rangle. \quad (2.25)$$

By noting eq. (2.23), $G(\omega)$ is expressed as

$$\begin{aligned} G(\omega) &= -\frac{1}{\pi} \int dE_B \, \text{Im} \langle i | T(\omega)^\dagger \sum_f |f\rangle \langle f| \frac{1}{E_B + E_i - E_f} T(\omega) | i \rangle \\ &= \rho \langle i | T(\omega)^\dagger \sum_f |f\rangle \langle f| T(\omega) | i \rangle \\ &= \rho \langle i | V_R^\dagger \frac{1}{\omega + E_i - \mathcal{H}_m - i\Gamma} V_{\text{CK}}^\dagger V_{\text{CK}} \frac{1}{\omega + E_i - \mathcal{H}_m + i\Gamma} V_R | i \rangle. \end{aligned} \quad (2.26)$$

Noting that $V_{\text{CK}}^\dagger V_{\text{CK}} = \Gamma/(\pi\rho)$ and $(1/2i)((x - i\Gamma)^{-1} - (x + i\Gamma)^{-1})$ is equal to $(x - i\Gamma)^{-1} \Gamma (x + i\Gamma)^{-1}$, we see that $G(\omega)$ reduces to $F_L(\omega)$ given by eq. (2.25). We note that $G(\omega)$ can be also shown to give $F_L(\omega)$ in a more general case with including the interference process.

2.4.3 Parameters of \mathcal{H}_2 and V

Putting off the presentation of the parameters in \mathcal{H}_1 (see eq. (2.2)) which specifies each compound, we show the adopted values of the Slater integrals and spin-orbit interactions (see eq. (2.3)) for Cu, Ni, Co, Fe, Mn and Ti in Tables 2.1(a), 2.1(b), 2.1(c), 2.1(d), 2.1(e) and 2.1(f), respectively, which are obtained by the Hartree-Fock (HF) or local density-functional approximation (LDA) for a given configuration of an atom.

In the calculation of the parameters of V_D , V_{CK} and R^k , we adopt the wavefunction of the continuum state used by Igarashi [67], with which resonant photoemission in TM compounds at TM $3p$ threshold is discussed, with an appropriate choice of ϵ . The results for Cu, Ni, Co, Fe, Mn and Ti atoms are given in Tables 2.2(a), 2.2(b), 2.2(c), 2.2(d), 2.2(e) and 2.2(f), respectively. In the calculation of spectra, we adopt

the values reduced by 20 % from those given in Tables 2.1 and 2.2 for the Slater integrals F^k 's and G^k 's and R^k 's to take into account the intraatomic configuration interaction effect, except for those of $3s^13d^n$ and $3p^43d^{n+1}$ configurations where the mutual configuration interaction is included and reduction of the parameter values is therefore not carried out.

2.5 SX-RPE in 3d TM compounds

We present in Table 2.3 the adopted parameters of the Hamiltonian \mathcal{H}_1 (see eq. (2.2)) and the weight of $3d^n$, $3d^{n+1}\underline{L}$ and $3d^{n+2}\underline{L}^2$ configurations in the initial (ground) state calculated with the use of the parameters and those in Tables 2.1(a)-2.1(f) for the monoxides and TiO_2 . The charge transfer energy Δ is here defined as the difference of the weighted average energy of each configuration (composed of many multiplets) $E(3d^{n+1}\underline{L}) - E(3d^n)$. $E(3d^{n+2}\underline{L}^2) - E(3d^n)$ is then equal to $2\Delta + U_{dd}$ with the use of the effective $3d$ - $3d$ interaction; our definition of U_{dd} is the same as that in ref. [43]. For CuO and NiO, $U_{dd} > \Delta$, for CoO $U_{dd} \sim \Delta$ and for FeO and MnO $U_{dd} > \Delta$. In the case of TiO_2 , U_{dd} , Δ and the hybridization strength are comparable to one another [65]. The adopted values of U_{dd} and Δ are rather similar to those in refs. [15] - [45], while the present Δ values for NiO and CoO are twice those adopted in ref. [46] and [47]. (see Table 2.4) We will show that the SX- $3d$ RPE will contribute to a removal of ambiguities about the estimated U_{dd} and Δ values.

In Fig. 2.5, the calculated $3d$, $3p$ and $3s$ RPE spectra are shown as a function of the binding energy $E_B = \omega - E$ for ω indicated in the calculated $2p$ XAS spectrum for CuO, NiO, CoO, FeO, MnO and TiO_2 with the use of the above-mentioned parameters; the spectrum for off-resonance is also shown for comparison. The calculated intensity of maximum on-resonance spectra is of the order of $\sim 10^2$ compared with those at off-resonance. The result for CuO is consistent with that by Tjeng *et al.* [49] but is one order of magnitude larger than that by Lopetz *et al.* [50].

2.5.1 3d RPE

In Fig. 2.6, we show the calculated $3d$ RPE at $2p_{3/2}$ on-resonance (a) and at off-resonance (b) for our TM oxides, where the final-state lifetime broadening larger than that in Fig. 2.5 is adopted for the convenience of comparison with the experiment by Park *et al.* [59]; the scale of the off-resonance spectra is enlarged. Our result shown in Fig. 2.6 is found to correspond well to their experiment.

We first show that the relative magnitude of U_{dd} and Δ is directly reflected in the SX-RPE with strong resonances. In the final state of $3d$ photoemission, the average

Table 2.1: The values of the Slater integral and the spin-orbit interaction in units of eV for various electron configuration involved in the resonant photoemission. (see eq. (2.3)); for the $3s$ - $3d$ interaction G^1 should be read as G^2

Table 2.1(a)

Cu Config.	$3d$ - $3d$		$3d$ -core			ζ_{3d}	ζ_c
	F^2	F^4	F^2	G^1	G^3		
$3d^8$	14.410	8.996	-	-	-	0.149	-
$3d^9$	-	-	-	-	-	0.137	-
$2p^5 3d^{10}$	-	-	-	-	-	-	13.498
$3p^5 3d^9$	-	-	15.350	18.835	11.525	0.149	1.813
$3p^5 3d^{10}$	-	-	-	-	-	-	1.813
$3s^1 3d^9$	-	-	-	14.280	-	0.149	-
$3p^4 3d^{10}$	-	-	-	-	-	-	1.818
$(3p - 3p)$	17.028						
$R^1(3s3d; 3p3p)$		20.441					

Table 2.1(b)

Ni Config.	$3d$ - $3d$		$3d$ -core			ζ_{3d}	ζ_c
	F^2	F^4	F^2	G^1	G^3		
$3d^7$	13.783	8.608	-	-	-	0.123	-
$3d^8$	12.744	7.914	-	-	-	0.112	-
$3d^9$	-	-	-	-	-	0.074	-
$2p^5 3d^9$	13.548	8.422	7.721	5.787	3.291	0.102	11.507
$2p^5 3d^{10}$	-	-	-	-	-	0.102	11.507
$3p^5 3d^8$	13.860	8.660	14.716	18.075	11.059	0.124	1.547
$3p^5 3d^9$	-	-	14.048	17.322	10.523	0.114	1.508
$3p^5 3d^{10}$	-	-	-	-	-	-	1.508
$3s^1 3d^8$	13.885	8.678	-	13.726	-	0.124	-
$3s^1 3d^9$	-	-	-	13.110	-	0.114	-
$3p^4 3d^9$	-	-	14.768	18.136	11.102	0.125	1.551
$(3p - 3p)$	16.342						
$3p^4 3d^{10}$	-	-	-	-	-	-	1.514
$(3p - 3p)$	16.108						
$R^1(3s3d; 3p3p)$		19.629					

Table 2.1(c)

Co Config.	3d-3d		3d-core			ζ_{3d}	ζ_c
	F^2	F^4	F^2	G^1	G^3		
$3d^6$	13.231	8.271	-	-	-	0.102	-
$3d^7$	12.097	7.513	-	-	-	0.091	-
$3d^8$	10.932	6.742	-	-	-	0.082	-
$3d^9$	-	-	-	-	-	0.074	-
$2p^5 3d^8$	12.396	7.708	7.260	5.397	3.069	0.083	9.746
$2p^5 3d^9$	-	-	6.624	4.869	2.767	0.075	9.750
$2p^5 3d^{10}$	-	-	-	-	-	-	9.754
$3p^5 3d^7$	13.231	8.271	14.076	17.589	10.589	0.102	1.310
$3p^5 3d^8$	12.236	7.605	13.396	16.539	10.044	0.092	1.276
$3p^5 3d^9$	-	-	12.643	15.634	9.432	0.084	1.250
$3s^1 3d^7$	13.256	8.291	-	13.166	-	0.102	-
$3s^1 3d^8$	12.236	7.629	-	12.534	-	0.093	-
$3s^1 3d^9$	-	-	-	11.796	-	0.089	-
$3p^4 3d^8$	13.307	8.322	14.131	17.373	10.633	0.103	1.314
($3p - 3p$)	15.652						
$3p^4 3d^9$	-	-	13.486	16.646	10.118	0.094	1.280
($3p - 3p$)	15.414						
$3p^4 3d^{10}$	-	-	-	-	-	-	1.256
($3p - 3p$)	15.232						
$R^1(3s3d; 3p3p)$		18.811					

Table 2.1(d)

Fe Config.	3d-3d		3d-core			ζ_{3d}	ζ_c
	F^2	F^4	F^2	G^1	G^3		
$3d^5$	12.503	7.816	-	-	-	0.082	-
$3d^6$	11.437	7.104	-	-	-	0.073	-
$3d^7$	10.248	6.317	-	-	-	0.065	-
$3d^8$	8.887	5.432	-	-	-	0.056	-
$2p^5 3d^7$	11.779	7.325	6.793	5.003	2.844	0.067	8.200
$2p^5 3d^8$	10.623	6.557	6.143	4.466	2.538	0.059	8.202
$2p^5 3d^9$	-	-	5.498	3.959	2.249	0.053	8.203
$3p^5 3d^6$	12.592	7.876	13.427	16.532	10.112	0.083	1.101
$3p^5 3d^7$	11.596	7.261	12.743	15.744	9.555	0.075	1.068
$3p^5 3d^8$	10.485	6.473	11.960	14.807	8.924	0.067	1.046
$3s^1 3d^6$	12.625	7.898	-	12.597	-	0.083	-
$3s^1 3d^7$	11.629	7.201	-	11.946	-	0.075	-
$3s^1 3d^8$	10.530	6.502	-	11.180	-	0.067	-
$3p^4 3d^7$	12.675	7.932	13.487	16.602	10.161	0.083	1.105
($3p - 3p$)	14.959						
$3p^4 3d^8$	11.725	7.296	12.833	15.860	9.635	0.076	1.073
($3p - 3p$)	14.716						
$3p^4 3d^9$	-	-	12.112	14.993	9.048	0.068	1.052
($3p - 3p$)	14.529						
$R^1(3s3d; 3p3p)$		17.985					

Table 2.1(e)

Mn Config.	3d-3d		3d-core			ζ_{3d}	ζ_c
	F^2	F^4	F^2	G^1	G^3		
$3d^5$	11.844	7.407	-	-	-	0.066	-
$3d^6$	10.760	6.684	-	-	-	0.058	-
$3d^7$	9.541	5.977	-	-	-	0.051	-
$3d^8$	8.135	4.965	-	-	-	0.045	-
$2p^5 3d^6$	11.155	6.941	6.321	4.606	2.617	0.053	6.846
$2p^5 3d^7$	9.972	6.153	5.653	4.059	2.305	0.046	6.847
$2p^5 3d^8$	8.595	5.247	4.988	3.542	2.011	0.040	6.849
$3p^5 3d^5$	11.944	7.475	12.745	15.745	9.627	0.066	0.917
$3p^5 3d^6$	10.930	6.797	12.060	14.933	9.056	0.059	0.887
$3p^5 3d^7$	9.807	6.052	11.260	13.956	8.401	0.053	0.867
$3s^1 3d^5$	11.980	7.499	-	12.018	-	0.067	-
$3s^1 3d^6$	10.974	6.826	-	11.344	-	0.060	-
$3s^1 3d^7$	9.857	6.085	-	10.544	-	0.053	-
$3p^4 3d^6$	12.034	7.535	12.820	15.820	9.680	0.067	0.921
(3p - 3p)	14.261						
$3p^4 3d^7$	11.078	6.895	12.169	15.062	9.144	0.060	0.892
(3p - 3p)	14.012						
$3p^4 3d^8$	10.033	6.201	11.423	14.167	8.539	0.059	0.873
(3p - 3p)	13.821						
$R^1(3s3d; 3p3p)$		17.150					

Table 2.1(f)

Ti Config.	3d-3d		3d-core			ζ_{3d}	ζ_c
	F^2	F^4	F^2	G^1	G^3		
$3d^0$	-	-	-	-	-	-	-
$3d^1$	-	-	-	-	-	0.027	-
$3d^2$	8.565	5.315	-	-	-	0.025	-
$2p^5 3d^1$	-	-	6.302	4.628	2.633	0.032	3.776
$2p^5 3d^2$	10.343	6.499	5.580	3.991	2.267	0.027	3.776
$2p^5 3d^3$	9.214	5.744	4.850	3.378	1.917	0.023	3.776
$3p^5 3d^0$	-	-	-	-	-	-	0.555
$3p^5 3d^1$	-	-	11.393	14.027	8.644	0.035	0.523
$3p^5 3d^2$	9.901	6.205	10.707	13.276	8.099	0.031	0.496
$3s^1 3d^0$	-	-	-	-	-	-	-
$3s^1 3d^1$	-	-	-	10.817	-	0.036	-
$3s^1 3d^2$	9.955	6.241	-	10.182	-	0.031	-
$3p^4 3d^1$	-	-	12.025	14.663	9.128	0.041	0.556
(3p - 3p)	12.755						
$3p^4 3d^2$	10.934	6.898	11.446	14.084	8.686	0.036	0.526
(3p - 3p)	12.427						
$3p^4 3d^3$	10.029	6.291	10.805	13.388	8.178	0.031	0.500
(3p - 3p)	12.122						
$R^1(3s3d; 3p3p)$		15.468					

Table 2.2: The values of the Coulomb integral of CK decay in units of $(13.6)^{1/2}\text{eV}$ and the dipole matrix element in units of 13.6a.u. ($\langle 2p|r|3d \rangle$) and $(13.6)^{3/2}\text{a.u.}/\sqrt{\epsilon V}$ (others).

Cu	Auger decay				Dipole	
	direct		exchange			
					$\langle 2p r 3d \rangle = 1.7713$	
$R^k(3d3d; 2p\epsilon l)$						
		$k = 1$	$k = 3$			
$l = p$	-0.20837	-0.17134			$\langle 3d r \epsilon p \rangle = 0.01654$	
f	0.74645	0.48244			$\langle 3d r \epsilon f \rangle = 0.07420$	
h		0.2959				
$R^k(3p3d; 2p\epsilon l)$						
		$k = 0$	$k = 2$	$k = 1$	$k = 3$	
$l = s$	-0.11160			-0.27981		$\langle 3p r \epsilon s \rangle = 0.04873$
d	0.18645	0.18735		0.43865	0.20128	$\langle 3p r \epsilon d \rangle = 0.13856$
g		-0.33670		-0.42787		
$R^k(3s3d; 2p\epsilon l)$						
		$k = 1$		$k = 1$		
$l = p$	0.02830			-0.07352		$\langle 3s r \epsilon p \rangle = 0.11361$
f	0.01134			0.28375		
$R^k(3p3p; 2p\epsilon l)$						
		$k = 0$	$k = 2$			
$l = p$	0.26669	0.18725				
f		0.27346				

Ni	Auger decay				Dipole	
	direct		exchange			
					$\langle 2p r 3d \rangle = 1.83761$	
$R^k(3d3d; 2p\epsilon l)$						
		$k = 1$	$k = 3$			
$l = p$	-0.20345	-0.16729			$\langle 3d r \epsilon p \rangle = 0.01759$	
f	0.74645	0.47358			$\langle 3d r \epsilon f \rangle = 0.07809$	
h		0.29565				
$R^k(3p3d; 2p\epsilon l)$						
		$k = 0$	$k = 2$	$k = 1$	$k = 3$	
$l = s$	-0.10850			-0.27368		$\langle 3p r \epsilon s \rangle = 0.05234$
d	0.18440	0.18605		0.43414	0.19992	$\langle 3p r \epsilon d \rangle = 0.14844$
g		-0.33492		-0.42501		
$R^k(3s3d; 2p\epsilon l)$						
		$k = 1$		$k = 1$		
$l = p$	0.02782			-0.07397		$\langle 3s r \epsilon p \rangle = 0.12183$
f	0.01417			0.28384		
$R^k(3p3p; 2p\epsilon l)$						
		$k = 0$	$k = 2$			
$l = p$	0.26624	0.18727				
f		0.27256				

Table 2.2(c)

Co	Auger decay				Dipole	
	direct		exchange			
$R^k(3d3d; 2p\epsilon l)$					$\langle 2p r 3d \rangle =$	1.908
	$k = 1$	$k = 3$				
$l = p$	-0.19963	-0.16410			$\langle 3d r \epsilon p \rangle =$	0.01854
f	0.73560	0.46677			$\langle 3d r \epsilon f \rangle =$	0.08391
h		0.29374				
$R^k(3p3d; 2p\epsilon l)$						
	$k = 0$	$k = 2$	$k = 1$	$k = 3$		
$l = s$	-0.10652		-0.26975		$\langle 3p r \epsilon s \rangle =$	0.05721
d	0.18440	0.18337	0.42676	0.19595	$\langle 3p r \epsilon d \rangle =$	0.16181
g		-0.33443		-0.42253		
$R^k(3s3d; 2p\epsilon l)$						
	$k = 1$		$k = 1$			
$l = p$	0.02635		-0.07813		$\langle 3s r \epsilon p \rangle =$	0.13257
f	0.02029		0.28788			
$R^k(3p3p; 2p\epsilon l)$						
	$k = 0$	$k = 2$				
$l = p$	0.26586	0.18681				
f		0.27269				

Table 2.2(d)

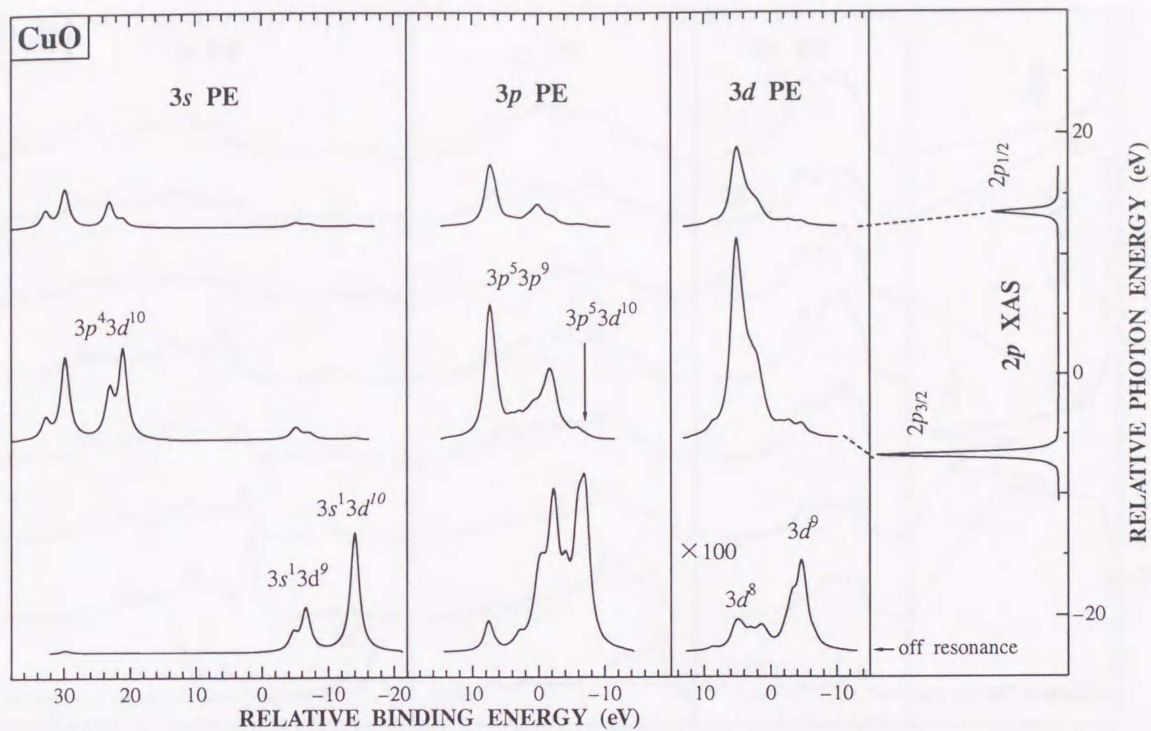
Fe	Auger decay				Dipole	
	direct		exchange			
$R^k(3d3d; 2p\epsilon l)$					$\langle 2p r 3d \rangle =$	1.984
	$k = 1$	$k = 3$				
$l = p$	-0.19545	-0.16060			$\langle 3d r \epsilon p \rangle =$	0.02032
f	0.72310	0.45892			$\langle 3d r \epsilon f \rangle =$	0.09031
h		0.29088				
$R^k(3p3d; 2p\epsilon l)$						
	$k = 0$	$k = 2$	$k = 1$	$k = 3$		
$l = s$	-0.10380		-0.26424		$\langle 3p r \epsilon s \rangle =$	0.06236
d	0.18051	0.18036	0.41837	0.19176	$\langle 3p r \epsilon d \rangle =$	0.17607
g		-0.33361		-0.41974		
$R^k(3s3d; 2p\epsilon l)$						
	$k = 1$		$k = 1$			
$l = p$	0.02649		-0.08206		$\langle 3s r \epsilon p \rangle =$	0.14446
f	0.02649		0.29078			
$R^k(3p3p; 2p\epsilon l)$						
	$k = 0$	$k = 2$				
$l = p$	0.26569	0.18628				
f		0.27380				

Table 2.2(e)

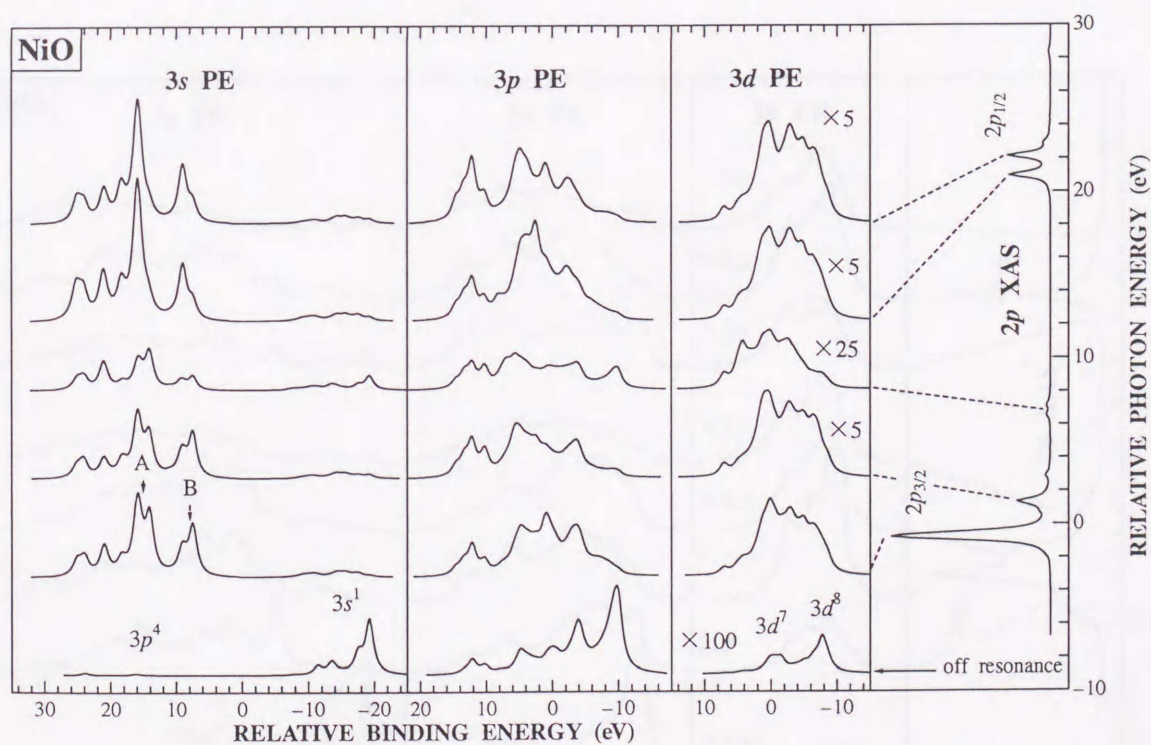
Mn	Auger decay				Dipole		
	direct		exchange				
$R^k(3d3d; 2p\epsilon l)$					$\langle 2p r 3d \rangle =$	2.064	
		$k = 1$	$k = 3$				
$l = p$	-0.19047		-0.15644		$\langle 3d r \epsilon p \rangle =$	0.02161	
f	0.7079		0.44937		$\langle 3d r \epsilon f \rangle =$	0.09695	
h			0.28778				
$R^k(3p3d; 2p\epsilon l)$							
		$k = 0$	$k = 2$	$k = 1$	$k = 3$		
$l = s$	-0.10106			-0.25871		$\langle 3p r \epsilon s \rangle =$	0.06838
d	0.17814		0.17690	0.40892	0.18686	$\langle 3p r \epsilon d \rangle =$	0.19277
g			-0.33229		-0.41596		
$R^k(3s3d; 2p\epsilon l)$							
		$k = 1$		$k = 1$			
$l = p$		0.02321		-0.08612		$\langle 3s r \epsilon p \rangle =$	0.15772
f		0.03324		0.29372			
$R^k(3p3p; 2p\epsilon l)$							
		$k = 0$	$k = 2$				
$l = p$		0.26526	0.18530				
f			0.27483				

Table 2.2(f)

Ti	Auger decay				Dipole		
	direct		exchange				
$R^k(3d3d; 2p\epsilon l)$					$\langle 2p r 3d \rangle =$	2.622	
		$k = 1$	$k = 3$				
$l = p$	-0.21127		-0.17358		$\langle 3d r \epsilon p \rangle =$	0.02426	
f	0.7916		0.50757		$\langle 3d r \epsilon f \rangle =$	0.11620	
h			0.35081				
$R^k(3p3d; 2p\epsilon l)$							
		$k = 0$	$k = 2$	$k = 1$	$k = 3$		
$l = s$	-0.10109			-0.20249		$\langle 3p r \epsilon s \rangle =$	0.08778
d	0.19517		0.20249	0.46387	0.21917	$\langle 3p r \epsilon d \rangle =$	0.24108
g			-0.36594		-0.46186		
$R^k(3s3d; 2p\epsilon l)$							
		$k = 1$		$k = 1$			
$l = p$		0.02701		-0.08612		$\langle 3s r \epsilon p \rangle =$	0.19971
f		0.03629		0.30700			
$R^k(3p3p; 2p\epsilon l)$							
		$k = 0$	$k = 2$				
$l = p$		0.28064	0.20733				
f			0.26417				

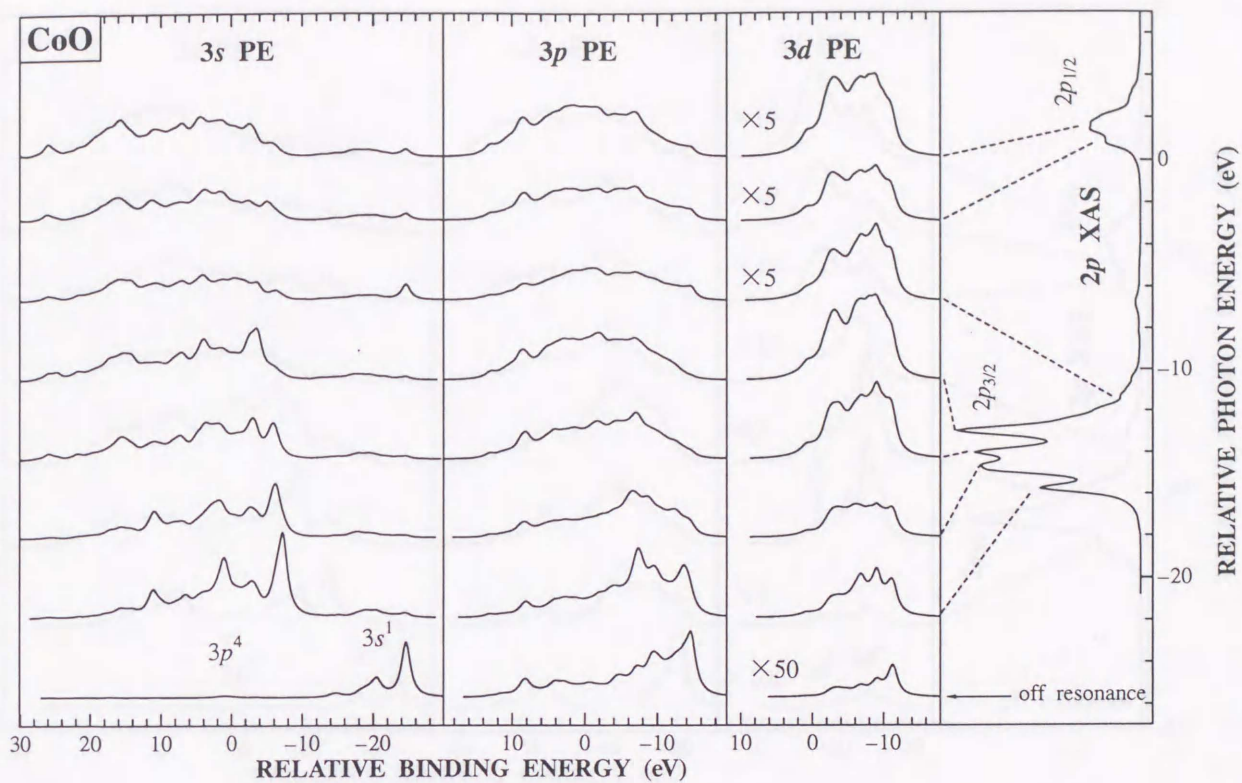


(a)

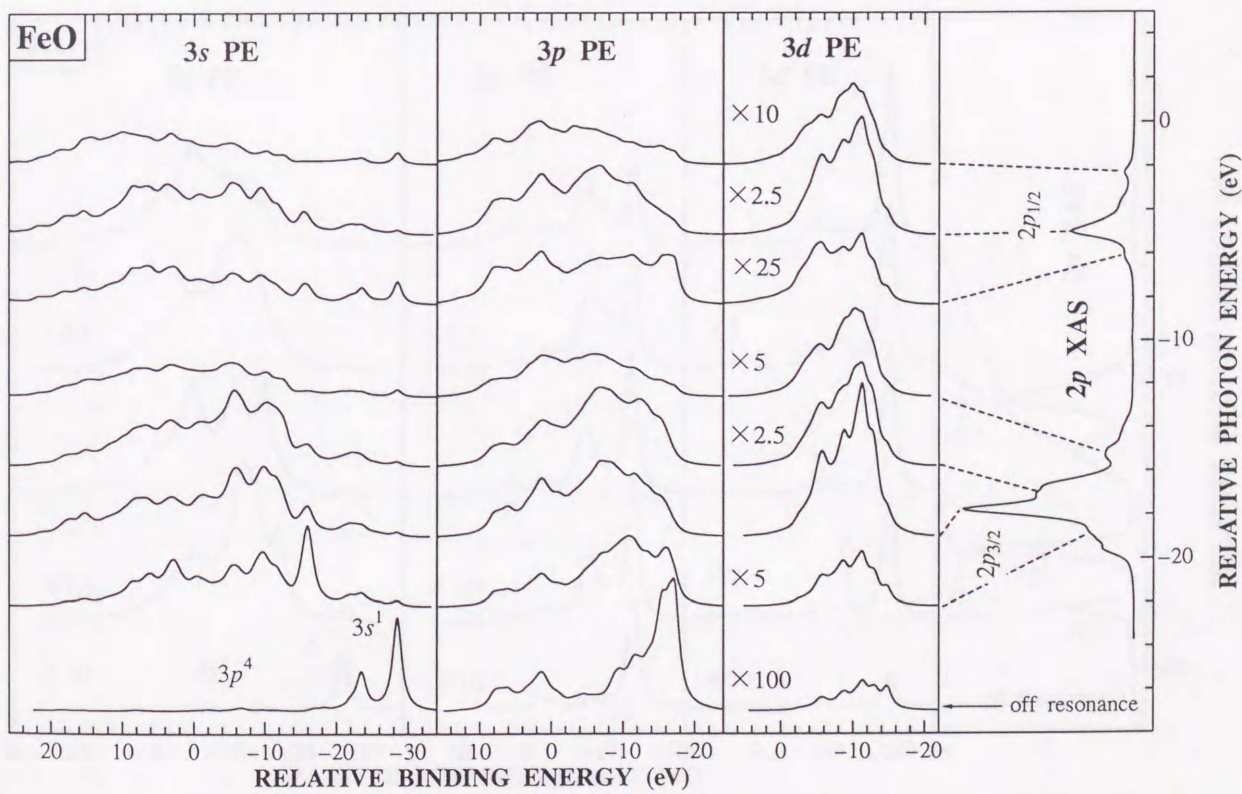


(b)

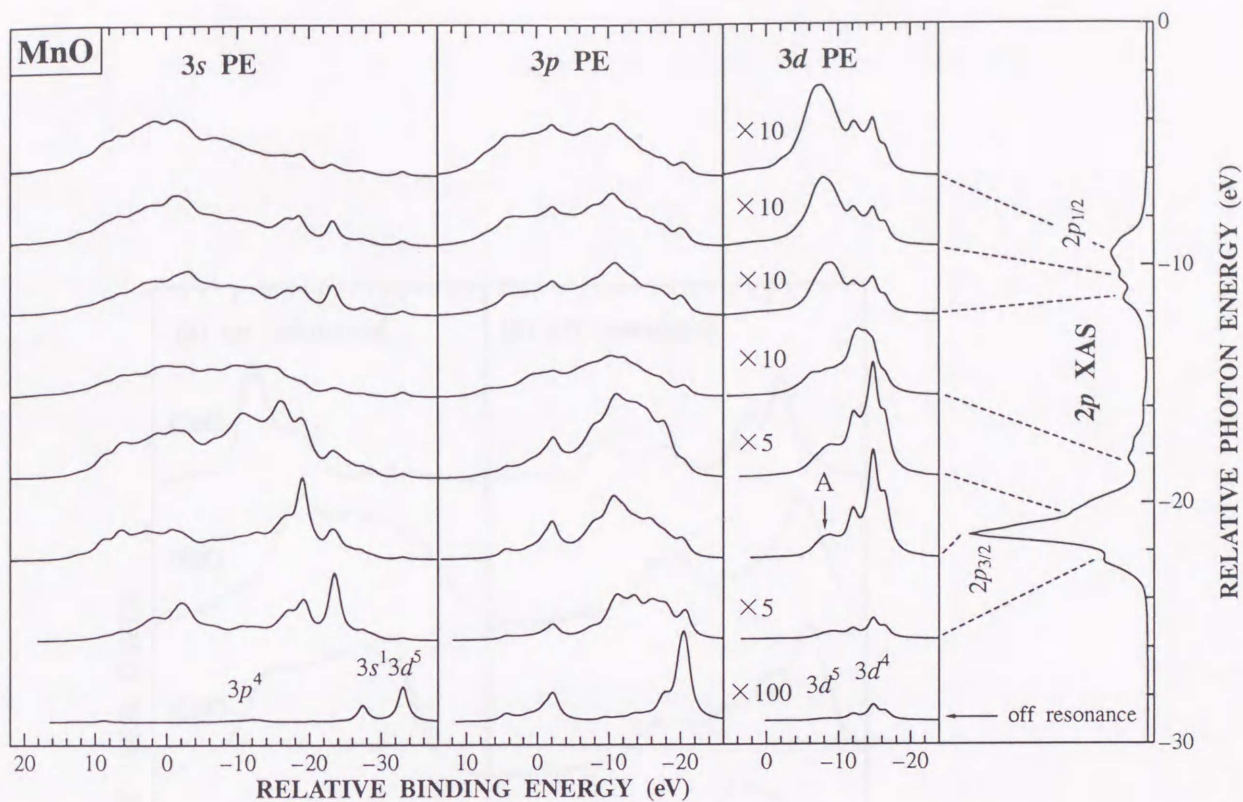
Figure 2.5: Calculated 3d, 3p and 3s RPE spectra of TM oxides for photon energies corresponding to various multiplets of 2p XAS; the off-resonance spectrum is also shown; the Lorentzian broadening in the final state of $2\Gamma_f=1.4\text{eV}$ is adopted.



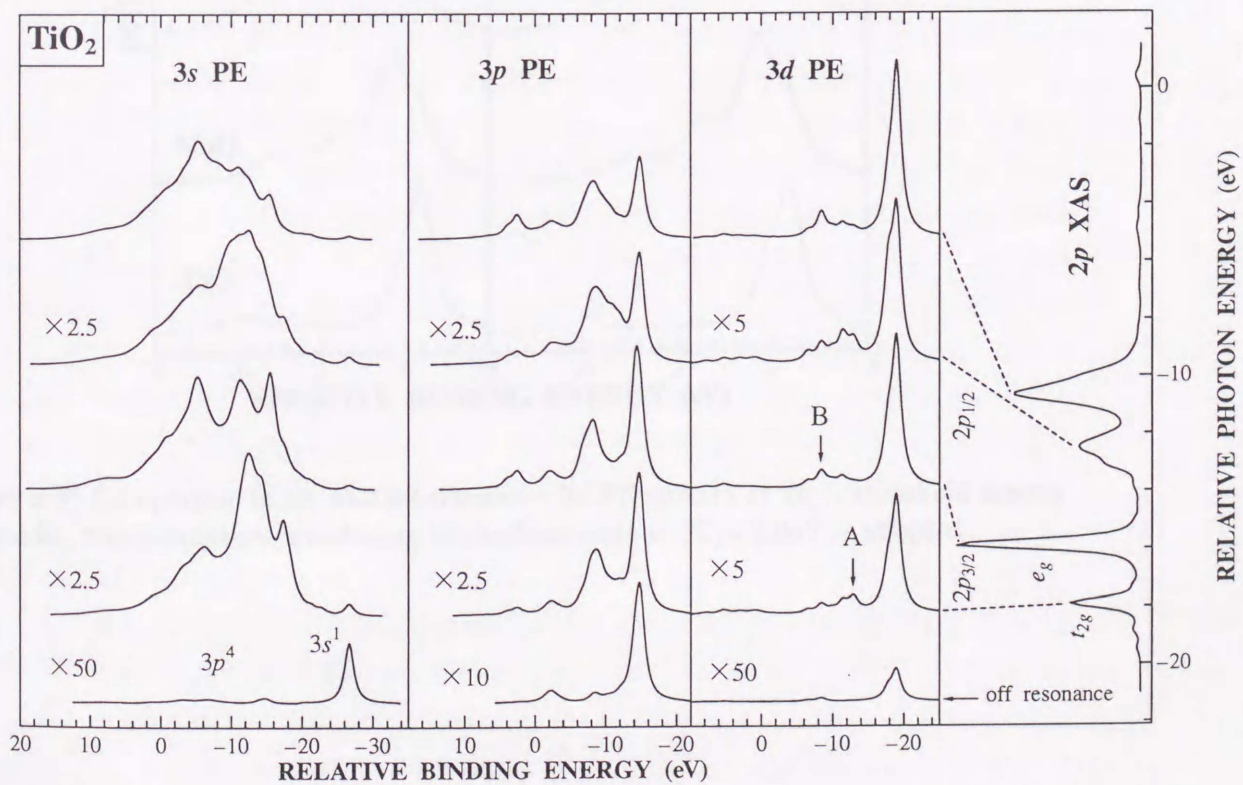
(c)



(d)



(e)



(f)

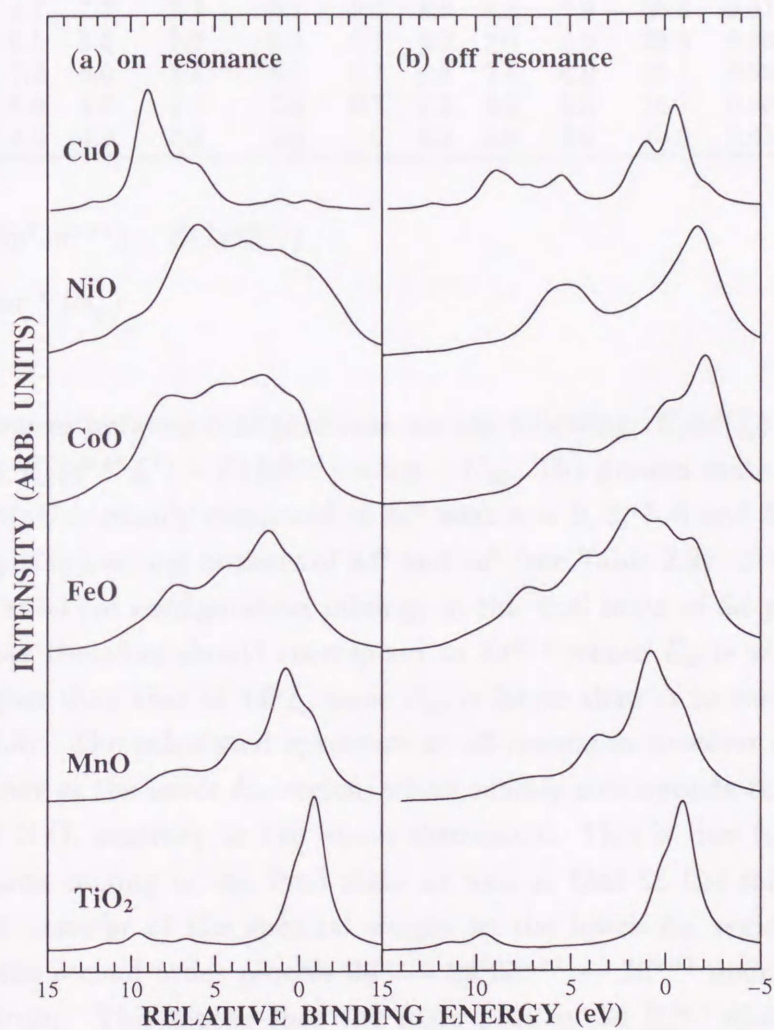


Figure 2.6: Comparison of on- and off-resonance 3d PE spectra at $2p_{3/2}$ threshold among TM oxides; the Lorentzian broadening in the final state of $2\Gamma_f=2.0\text{eV}$ is adopted

Table 2.3: The adopted parameter values in \mathcal{H}_1 (see eq. (2.2)) and the calculated weight of $3d$ configuration.

Compound	Δ	U_{dd}	$V(e_g)$	$10Dq$	T_{pp}	U_{dc}			Δ_{ps}^*	Weight		
						$2p$	$3p$	$3s$		$3d^n$	$3d^{n+1}$	$3d^{n+2}$
CuO	3.0	7.8	2.7**	0.0	1.3	9.0	8.8	7.8	30.2	0.673	0.327	-
NiO	4.7	7.3	2.2	0.7	0.7	8.5	8.3	7.3	26.8	0.811	0.184	0.005
CoO	6.5	6.5	2.2	0.5	0.7	8.2	7.5	6.5	23.5	0.869	0.128	0.003
FeO	7.0	6.0	2.1	0.5	0.7	7.5	7.0	6.0	20.1	0.882	0.115	0.003
MnO	8.0	5.5	2.1	0.5	0.7	7.2	6.5	5.5	16.7	0.900	0.097	0.003
TiO ₂	4.0	4.0	3.0	1.0	1.0	6.0	5.0	5.0	10.0	0.417	0.470	0.113

* $\Delta_{ps} = E(3p^4 3d^{n+1}) - E(3s^1 3d^n)$

** a value for $V(b_{1g})$

energy differences between configurations are the following: $E(3d^n \underline{L}) - E(3d^{n-1}) = \Delta - U_{dd}$ and $E(3d^{n+1} \underline{L}^2) - E(3d^{n-1}) = 2\Delta - U_{dd}$. The ground state of CuO, NiO, CoO, FeO, MnO is mainly composed of $3d^n$ with $n = 9, 8, 7, 6$ and 5 , respectively and for TiO₂ it is a strong mixture of $3d^0$ and $3d^1$ (see Table 2.3). In the absence of the hybridization (or configuration mixing) in the final state of $3d$ photoemission, the main peak therefore should correspond to $3d^{n-1}$ whose E_B is at least in CuO and NiO higher than that of $3d^n \underline{L}$, since U_{dd} is larger than Δ in these compounds (see Table 2.3). The calculated spectrum at off-resonance however always have a strong intensity at the lower E_B region, which mainly corresponds to $3d^n \underline{L}$ at least in CuO and NiO, contrary to the above discussion. This is due to the presence of configuration mixing in the final state as well as that in the initial state and the resultant transfer of the spectral weight to the lower E_B region. [68, 69] At resonances, the second order process $3d^n \rightarrow 2p^5 3d^{n+1} \rightarrow 3d^{n-1}$ mainly contributes to the spectrum. This means that the main peak of $3d$ RPE directly gives the position of $3d^{n-1}$ relative to that of $3d^n \underline{L}$: 1) For CuO and NiO with $U_{dd} > \Delta$, the main peak is in the higher E_B region. 2) For FeO and MnO with $U_{dd} < \Delta$, it is in the lower E_B region similarly to the spectrum at off-resonance. 3) CoO seems to corresponds to the case intermediate between the cases 1) and 2). 4) For TiO₂ (see Fig. 2.5(f)), the lower E_B main peak corresponds to the bonding state of $3d^0 \underline{L}$ and $3d^1 \underline{L}^2$ and the higher E_B satellite ($5 \sim 10$ eV above the main peak) to the antibonding state of the two.

In NiCl₂, whose RPE spectra are not shown in Figs. 2.5 and 2.6, U_{dd} is supposed to be the same as that of NiO and Δ is much smaller (see ref. [55]). The initial

Table 2.4: The previously estimated values of Δ and U_{dd} by Fujimori *et al.* [43], van Elp *et al.* [15] and Okada and Kotani (OK) [46–48]

Compound	Δ			U_{dd}		
	Fujimori	van Elp	OK	Fujimori	van Elp*	OK
CuO	2.2	2.8	-	8.8	6.7	-
NiO	5.0	6.2	2.0	7.5	6.9	7.3
CoO	-	5.5	2.5	-	5.4	7.0
FeO	5.5	7.0	6.0	6.5	5.7	7.0
MnO	7.0	8.8	10.5	6.0	4.0	7.0

* The estimated values are converted to values in the present definition

state is therefore a rather strong mixture (bonding state) of $3d^8$ and $3d^9L$ compared with NiO. In the final state, the $3d^7$ peak, which is in much higher E_B region compared with that for NiO and is not necessarily prominent at off-resonance, is much enhanced. This is consistent with the recent experiment by Okusawa *et al.* [53] and is one example to show the capability of the SX-RPE. Recently Suga *et al.* [52] observed for NiS₂ the $3d$ RPE. In this system, both U_{dd} and Δ are smaller than those of NiO and $U_{dd} - \Delta$ is approximately equal to that of NiO. As a result, the resonance behavior similar to the calculation for NiO is seen.

In Table 2.4, we list up the estimated U_{dd} and Δ for MO (M=Cu ~ Mn) by Fujimori *et al.* [43], van Elp [15] and Okada and Kotani (OK) [46–48] (a small difference in definition of Δ among authors is not essential to our discussion).

Our estimation of Δ for NiO and CoO (see Table 2.3) are much larger than those estimated from an analysis of TM $2p$ core photoemission ($2p$ PE) by OK. [46, 47] Figures 2.7 compares the $3d$ RPE and $2p$ PE for NiO and CoO, calculated with the use of the parameters adopted in Table 2.3 (a) and those adopted by OK (b) (a small difference in model other than Δ between OK and ours is not essential). For $2p$ PE, the difference between the two parameter sets is rather small, while for the $3d$ RPE the difference between the two is large. The intensity ratio and relative position of the main peak and its satellite of the $2p$ PE spectrum are strongly dependent on the value of $\Delta - U_{dc}$ with U_{dc} being the $2p$ core hole potential acting on the $3d$ electron, which means that the analysis of $2p$ PE is not necessarily a direct way to estimate $\Delta - U_{dd}$ of the TM oxides. In the analysis of $3d$ RPE, although the value of U_{dc} is needed to describe the intermediate state, the calculated spectrum is rather insensitive to U_{dc} , while sensitive to $\Delta - U_{dd}$. In addition to $2p$ PE and $3d$ PE, the analysis of SX $3d$ RPE therefore greatly contributes to the estimation of U_{dd} , Δ and U_{dc} . The values of U_{dd} and Δ in principle depend on the electron configuration

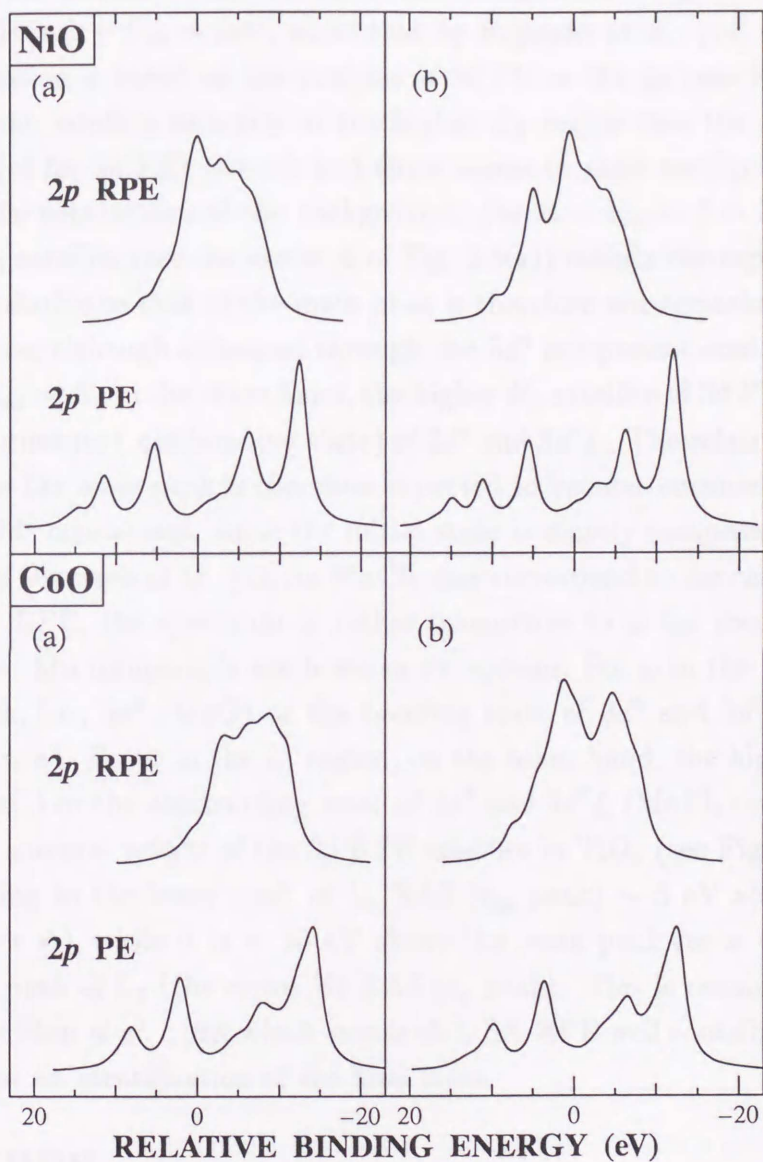


Figure 2.7: Comparison of the 3d RPE at $2p_{3/2}$ threshold and 2p PE for NiO and CoO between the present choice of parameters shown in Table III(a) and the parameters adopted by OK (b).

of TM atom. If we excessively attached to this, we have to give up the estimation of U_{dd} and Δ in the ground state from the $2p$ PE. In our opinion, to find out the parameter set giving an overall agreement with many experiments would be a sound basis for discussion of electronic structures.

For MnO, the estimation by van Elp *et al.* [45] gives $\Delta - U_{dd} \sim 4eV$ and Okada and Kotani gives $\Delta - U_{dd} \sim 2eV$, while that by Fujimori *et al.* [44] gives $\Delta \sim U_{dd}$. Their estimation is based on the analysis of $3d$ PE or Mn $2p$ core PE. In both of the spectra, the satellite intensity in the higher E_B region (see the arrow marked A of Fig. 2.5(e) for $3d$ PE) is weak and there seems to exist ambiguities about its intensity in the subtraction of the background. For $\Delta - U_{dd} = 2 \sim 3$ eV or more, the higher E_B satellite (see the arrow A of Fig. 2.5(e)) mainly corresponds to $3d^5\bar{L}$. Its intensity relative to that of the main peak is therefore not remarkably enhanced at on-resonance, although enhanced through the $3d^4$ component contained to some extent. For $U_{dd} \sim \Delta$, on the other hand, the higher E_B satellite of $3d$ PE corresponds to the strong mixture (antibonding state) of $3d^4$ and $3d^5\bar{L}$. The relative intensity of the satellite to the main peak is therefore expected to become considerably stronger through the $3d^4$ component, since the initial state is mainly composed of $3d^5$. The experiment by Okusawa *et al.* [53] for $MnCl_2$ may correspond to the case of $U_{dd} \sim \Delta$.

As for $3d$ RPE, the spectrum is rather insensitive to ω for most compounds discussed here. Mn compounds are however exceptions. For ω in the L_3 region, the lower E_B peak, i.e., $3d^4$ (MnO) or the bonding state of $3d^4$ and $3d^5\bar{L}$ ($MnCl_2$) is strongly enhanced. For ω in the L_2 region, on the other hand, the higher E_B peak, i.e., $3d^5\bar{L}$ (MnO) or the antibonding state of $3d^4$ and $3d^5\bar{L}$ ($MnCl_2$) is enhanced.

The main spectral weight of the $3d$ RPE satellite in TiO_2 (see Fig. 2.5(f)) is for ω corresponding to the lower peak of L_3 XAS (t_{2g} peak) ~ 5 eV above the main peak (the arrow A), while it is ~ 10 eV above the main peak for ω corresponding to the higher peak of L_3 (the arrow B) XAS (e_g peak). This is consistent with the experiment by Shin *et al.*, [60] which means that SX-RPE well contributes to giving information for an identification of the final state.

2.5.2 $3p$ RPE

Among the final states of $3p$ PE discussed above (see eq. (2.11), the $3p^53d^{n+1}\bar{L}$ state is in the lower E_B region and the $3p^53d^n$ state in the higher E_B region at least for Cu and Ni compounds. At off-resonance, due to the transfer of spectral weight to the lower E_B region caused by the hybridization which is similar to that discussed in $3d$ PE, the main peak is in the lower E_B region, regardless of the relative position of $3p^53d^n$ and $3p^53d^{n+1}\bar{L}$. At on-resonances, since the $3d^n$ state is the main component of the initial state, the final state containing $3p^53d^n$ with multiplet structures, which

is usually in the higher E_B region, is strongly enhanced.

In Fig. 2.8, we show the U_{dc} (see eq. (2.3)) dependence of $3p$ PE spectra for a Ni compound, where the parameters other than U_{dc} are the same as in NiO, at $2p_{3/2}$ on-resonance (a) and at off-resonance (b). The off-resonance spectrum is seen to be rather insensitive to the value of U_{dc} , while the resonance spectrum is sensitive to it. Although the $3d^{n+2}\underline{L}^2$ state is in the higher energy region in the initial state, the $3p^53d^{n+2}\underline{L}^2$ final state is pulled down due to the core hole potential U_{dc} and couples with other configurations. This means that the high resolution on-resonance spectrum is expected to give detailed information about U_{dc} in addition to U_{dd} and Δ . Furthermore the spectrum is seen to be more dependent on ω corresponding to specific intermediate state compared with the $3d$ RPE, which is very useful to identify the second order process.

2.5.3 $3s$ RPE

Among the final states of $3s$ PE, the $3s^13d^{n+1}\underline{L}$ state is in the lower E_B than the $3s^13d^n$ state at least for Cu and Ni compounds, since the magnitude of the core hole attractive potential acting on $3d$ electrons is larger than Δ . As in the cases of $3d$ and $3p$ PE, the spectral intensity is, at off-resonance, again stronger in the lower E_B region ($3s^13d^{n+1}\underline{L}$), while at on-resonances stronger in the higher E_B region ($3s^13d^n$) (see Figs. 2.5(a) and 2.5(b)). This is consistent with the experiment for NiS₂ by Suga *et al.* and for NiCl₂ by Okusawa *et al.* In $3s$ PE, the intraatomic configuration interaction (CI) between $3s^13d^n$ and $3p^43d^{n+1}$ is expected to affect the spectral shape to some extent, since the energy difference between the two is rather small (~ 20 eV). Okada and Kotani calculated for some $3d$ TM compounds the $3s$ PE spectrum at off-resonance by taking into account such interactions [48].

Our calculation of $3s$ RPE, which takes into account the decay process $2p^53d^{n+1} \rightarrow 3p^43d^{n+1}$ as well as the above-mentioned intraatomic CI, shows a strong resonance for the $3p^43d^{n+1}$ final state. This is consistent with recent various experiments. The two peaks marked A and B in the Ni compound (see Fig. 2.5(b)) are also observed in NiCl₂ and NiS₂ at L_3 on-resonances. The resonance behavior is furthermore seen to be strongly dependent on ω , the utilization of which is expected to contribute to an identification of the photoexcitation process.

2.6 Conclusions

We have presented in the preceding section calculated TM $3d$, $3p$ and $3s$ PE spectra at $2p$ core threshold of TM ions for TM monoxides from Cu to Mn and TiO₂ on the basis of a cluster model taking into account full multiplet. The imaginary part of

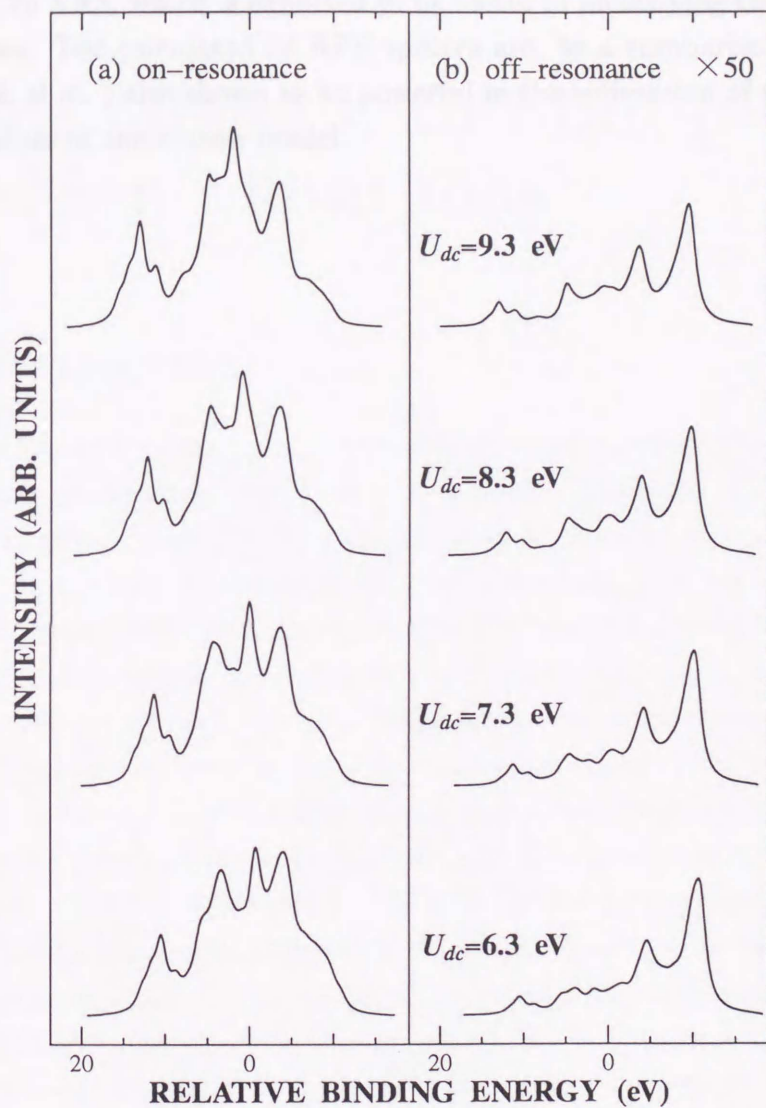


Figure 2.8: U_{dc} (the 3p core hole potential; see text) dependence of the 3p RPE at $2p_{3/2}$ threshold (a) and the off-resonance 3p PE (b) for a compound with the parameters of other than U_{dc} same as those of NiO.

the self-energy of the intermediate state is directly calculated from the CK decay without introducing adjustable parameters. The calculated resonance enhancement factor is of the order of 10^2 .

The calculated 3p and 3s PE spectra (and 3d PE for Mn compounds) are shown to be strongly dependent on the incident photon energy corresponding to various multiplets of 2p XAS, which is expected to be useful in identifying the second order optical process. The calculated 3d RPE spectra are, by a comparison with experiment by Park *et al.*, also shown to be powerful in the estimation of more plausible parameter values of the cluster model.

Transition Metal Ions

1.1 Introduction

In studies of the photochemistry of high temperature catalytic reactions in copper (Cu) clusters, photoelectron spectroscopy experiments have revealed a resonance (RPE) and resonant photoemission enhancement (RPEE) effect due to the cluster photoionization transition (T_{21}) to the region between cluster ionization potential (I_p) and $I_p + \Delta E$, which is associated by many authors with RPE experiments that the hole ($2p$ or $3d$) ionization [16, 17] leads to a resonance spectral weight in the gap of the continuum and the resonant vertical photoemission from the core states in the gap. First a theoretical approach, on the other hand, many authors and resonance enhanced photoemission spectroscopy have been performed on metal clusters, e.g., the Hubbard model, and a resonance is observed near the resonance energy (antibonding band edge for both electrons) during [21, 24, 25, 70], which also agrees the evidence from the PE and RPEE data except for X-ray absorption [26, 27]. Most of the theoretical models for excited, however, take into account only the Cu $3d_{5/2}$ and $3d_{3/2}$ shells. Although a numerical study including the effect of orbitals with $2s, 2p, 3s$ and $3p$ symmetries in addition to $3d_{5/2}$ has been carried out, the system is restricted to site to two Cu atoms and core d states [71, 72]. In a system of this size, the transfer integral of the strong $3d-3d$ overlap [12], for example, may be estimated but for the discussion of RPEE effects the size seems to be insufficient.

One of the purposes of this work is to determine the effect of electron density on PE and RPEE spectra by Cu clusters containing up to 4 Cu atoms and several d shells including the full Cu d and $4s$ orbitals and the f interatomic overlap is considered by means of the Hubbard and restricted Hartree-Fock (RHF) methods. The photoionization region of more than a few eV below I_p is adopted or adopted. The effect of the presence of the full multiplet interaction is considered to be necessary

Chapter 3

Cluster Model with Multiple Transition Metal Ions

3.1 Introduction

In studies of the mechanism of high-temperature superconductivity in doped Cu-oxides, electron spectroscopy experiments such as photoemission (PES) and inverse photoemission spectroscopy (IPES) yield direct information on electronic structures [21]. In the doping-induced insulator-to-metal transition, it is indicated by many PES and IPES experiments that the hole [30–33] or electron doping [34–36] leads to a growth of spectral weight in the gap of the insulator and the chemical potential μ lies within the new states in the gap. From a theoretical viewpoint, on the other hand, many Lanczos and recursion method numerical studies have been performed for simplified models *e.g.*, the Hubbard model, and μ was shown to lie very near the insulator valence (conduction) band edge for hole (electron) doping [21, 24, 25, 70], which contradicts the evidence from the PES and IPES experiments except for X-ray absorption [28, 29]. Most of the theoretical models so far adopted, however, take into account, at most, only the Cu $d_{x^2-y^2}$ and O p_σ orbitals. Although a numerical study taking into account d orbitals with xy, yz, zx and $3z^2 - r^2$ symmetries in addition to $x^2 - y^2$ has been carried out, the system is restricted in size to two Cu atoms and several O atoms [71, 72]. In a system of this size, the transfer integral of the Zhang-Rice (ZR) singlet [12], for example, may be estimated but for the discussion of doping effects the size seems to be insufficient.

One of the purposes of this work is to determine the effect of electron doping on PES and IPES spectra for Cu-oxides containing up to 4 Cu atoms and several O atoms including the full Cu d and O p orbitals and the full intraatomic multipole interaction by means of the Lanczos and recursion methods. In order to discuss PES in the energy region of more than a few eV below μ of doped or undoped Cu-oxides, the inclusion of the full multipole interaction is considered to be necessary

(for example the d^8 final state) [72]. In the energy region within ~ 1 eV below or above μ of doped and undoped Cu-oxides, on the other hand, it seems to be generally accepted that the inclusion of only Cu $d_{x^2-y^2}$ and O p_σ orbits is sufficient. In the present work, we show that this is not true by showing that electron doping with finite concentration leads to an upward shift of the upper valence band edge and μ relative to the $d^9 \rightarrow d^8$ peak, and the character of the upper edge state is changed from “ $d^9 \rightarrow d^9 \underline{L}$ ” to “ $d^{10} \rightarrow d^9$ ”, although the spectral shapes of undoped and doped systems are similar. This means that the “mid-gap μ and new states” of the doped metals inferred from the experimental results are interpreted as consequences of the disregard of the character change and upward shift of the upper valence band edge. This finding, which is obtained for the first time using the present approach, removes the discrepancy in the behavior of μ between the arguments from the experimental and theoretical viewpoints.

The TM $2p$ XPS of the TM compound has been believed to be well explained by using a cluster model containing a single TM atom. Van Veenendaal *et al.* recently argued that the $2p$ XPS spectra of TM compounds are strongly influenced by the presence of more-than-one TM atoms [74, 75]. For the high- T_C superconductors, they showed that by using Cu_3O_{10} cluster with a reduced basis, the main structure of the Cu $2p$ XPS spectra consists of two peaks corresponding to two different kinds of the screen states. One corresponds to the state having a hole pushed out from a core hole site to the nearest neighboring oxygen sites and the other to that having the hole on the neighboring CuO_4 unit. A similar effect should be expected in the $3d$ PES spectrum for the high- T_C superconductors. Another purpose of this work is to investigate the multiple-Cu-ion effect on the undoped $3d$ PES using a cluster model containing up to four Cu atoms. It will be shown that though the models with a Cu ion is appeared to successfully reproduce the experimental spectra of $3d$ PES in Cu-oxide, the success is only accidental and the main peak feature is very different from that expected in such models. In the state corresponding to the main peak structure, the hole introduced by the photoemission is not only on the nearest neighboring oxygen sites but also on the neighboring CuO_4 units forming the ZRS state.

3.2 Model Hamiltonian

Our model Hamiltonian \mathcal{H} for the Cu_nO_m clusters is given by

$$\mathcal{H} = \mathcal{H}_1 + \mathcal{H}_2 + \mathcal{H}_c$$

where \mathcal{H}_1 , \mathcal{H}_2 and \mathcal{H}_c are the Hamiltonians for the one-body term, the Cu $3d$ - $3d$ and O $2p$ - $2p$ Coulomb interactions and the interaction between the Cu $3d$ electron

and the Cu 2*p* core hole, respectively. \mathcal{H}_1 is given by

$$\begin{aligned}\mathcal{H}_1 &= \varepsilon_d \sum_{i\mu} d_{i\mu}^\dagger d_{i\mu} + \varepsilon_p \sum_{j\nu} p_{j\nu}^\dagger p_{j\nu} \\ &+ \sum_{\langle i,j \rangle} \sum_{\mu,\nu} V_{\text{Cu-O}}(\mu,\nu) (d_{i\mu}^\dagger p_{j\nu} + h.c.) \\ &+ \sum_{\langle j,j' \rangle} \sum_{\nu,\nu'} V_{\text{O-O}}(\nu,\nu') (p_{j\nu}^\dagger p_{j'\nu'} + h.c.)\end{aligned}\quad (3.1)$$

where the indices i and j run over the copper and oxygen sites, respectively and the indices μ and ν label the azimuthal and spin quantum number of Cu 3*d* and O 2*p* orbit, respectively. The operators $d_{i\mu}^\dagger$ and $p_{j\nu}^\dagger$ create electrons in the Cu 3*d* orbit and O 2*p* orbit specified by their indices, respectively. The ε_d and ε_p denote the one-body energy of the Cu 3*d* and O 2*p*. $V_{\text{Cu-O}}(\mu,\nu)$ and $V_{\text{O-O}}(\nu,\nu')$ denote the nearest neighbor copper-oxygen and oxygen-oxygen hopping integrals, respectively. The hopping integrals are parameterized by the Slater-Koster integrals $pd\sigma$ and $pd\pi$ for $V_{\text{Cu-O}}(\mu,\nu)$ and $pp\sigma$ and $pp\pi$ for $V_{\text{O-O}}(\nu,\nu')$. \mathcal{H}_2 is given by,

$$\begin{aligned}\mathcal{H}_2 &= \sum_{i,\mu_1,\dots,\mu_4} g_{\text{Cu}3d}(\mu_1,\mu_2;\mu_3,\mu_4) d_{i\mu_1}^\dagger d_{i\mu_2}^\dagger d_{i\mu_4} d_{i\mu_3} \\ &+ \sum_{j,\nu_1,\dots,\nu_4} g_{\text{O}2p}(\nu_1,\nu_2;\nu_3,\nu_4) p_{j\nu_1}^\dagger p_{j\nu_2}^\dagger p_{j\nu_4} p_{j\nu_3}\end{aligned}\quad (3.2)$$

where the first and second terms denote the on-site Cu 3*d*-3*d* and the O 2*p*-2*p* multipole Coulomb interaction, respectively. The coefficient $g_{\text{Cu}3d}(\mu_1,\mu_2;\mu_3,\mu_4)$ is expressed in terms of the Slater integrals F_{dd}^0 , F_{dd}^2 and F_{dd}^4 and $g_{\text{O}2p}(\nu_1,\nu_2;\nu_3,\nu_4)$ F_{pp}^0 and F_{pp}^2 .

Finally, the Hamiltonian \mathcal{H}_c , which is used in the discussion of Cu 2*p* XPS, is given by

$$\begin{aligned}\mathcal{H}_c &= \zeta_c \sum_{\xi_1,\xi_2} \langle \xi_1 | \vec{l} \cdot \vec{s} | \xi_2 \rangle c_{\xi_1}^\dagger c_{\xi_2} \\ &+ \sum_{\mu_1,\mu_2,\xi_1,\xi_2} g_{\text{Cu}3d-2p}(\mu_1,\xi_1;\mu_2,\xi_2) d_{0\mu_1}^\dagger c_{\xi_1}^\dagger c_{\xi_2} d_{0\mu_2},\end{aligned}\quad (3.3)$$

where the first and second terms denote the Cu 2*p* spin-orbit interaction and the Cu3*d*-2*p* Coulomb multipole interaction. The operator c^\dagger creates 2*p* core electron on the 0-th Cu site, where the core electron is photoexcited. ζ_c is the spin-orbit coupling constant and the coefficient $g_{\text{Cu}3d-2p}(\mu_1,\xi_1;\mu_2,\xi_2)$ is expressed in terms of the Slater integrals F_{dc}^0 , F_{dc}^2 , G_{dc}^1 and G_{dc}^3 ; ξ_1 and ξ_2 denote the azimuthal and spin quantum numbers of the Cu 2*p* core orbit.

The multiplet-averaged Cu 3*d*-3*d* (U_{dd}), Cu 2*p*-3*d* (U_{dc}) and O 2*p*-2*p* (U_{pp}) Coulomb interactions are expressed in terms of the the Slater integrals:

$$U_{dd} = F_{dd}^0 - \frac{2}{63}(F_{dd}^2 + F_{dd}^4),$$

Table 3.1: Parameter values used for the calculation in units of eV

F_{dd}^2	F_{dd}^4	F_{pp}^2	F_{dc}^2	G_{dc}^1	G_{dc}^3	ζ_c	
11.4	7.308	7.49	7.03	5.29	3.01	13.498	
Δ	U_{dd}	U_{pp}	U_{dc}	$pd\sigma$	$pd\pi$	$pp\sigma$	$pp\pi$
3.5	7.8	5.0	9.0	-1.5	0.7	1.0	-0.3

$$\begin{aligned}
 U_{dc} &= F_{dc}^0 - \frac{1}{15}G_{dc}^1 - \frac{3}{70}G_{dc}^3 \\
 \text{and } U_{pp} &= F_{pp}^0 - \frac{2}{25}F_{pp}^2.
 \end{aligned} \tag{3.4}$$

The charge transfer energy Δ is defined as an averaged energy cost moving a hole from a Cu site with nine $3d$ electron to an oxygen site with six $2p$ electrons in the absence of the hybridization.

The parameters we adopt for the Hamiltonian are presented in Table 3.1. For ζ_c , we use the value of the Hatree-Fock calculation of Cu atom and for the multipole terms of the Slater integrals we use the value reduced to 80% of the calculation. For the values of the U_{dd} , U_{dc} , Δ , $pd\sigma$ and $pd\pi$, they are adopted so as to reproduce experimental results of $2p$ XPS, valence band XPS and $3d$ RPES at the Cu $2p$ threshold in CuO, by using CuO₄ cluster model.

The intensity of angle integrated $3d$ PES spectrum $I_{3d\text{PES}}(\varepsilon)$, which is a function of the energy difference between the photoelectron and incident photon ε is given by

$$I_{3d\text{PES}}(\varepsilon) = -\frac{1}{\pi} \text{Im} \sum_{\mu} \langle g | d_{0\mu}^{\dagger} \frac{1}{E_g + i\delta - \varepsilon - \mathcal{H}} d_{0\mu} | g \rangle,$$

where E_g and $|g\rangle$ denote the eigenvalue and the eigenfunction of the ground state ; δ denotes the positive infinitesimal. The expression for the the intensity of Cu $2p$ XPS is obtained with replacing $d_{0\mu}^{\dagger}$ and $d_{0\mu}$ by c_{ξ}^{\dagger} and c_{ξ} , respectively. Similarly, the intensity of $3d$ IPES spectrum $I_{3d\text{IPES}}(\varepsilon)$, which is a function of energy difference between the incident electron and emitted photon ε is given by

$$I_{3d\text{IPES}}(\varepsilon) = -\frac{1}{\pi} \text{Im} \sum_{\mu} \langle g | d_{0\mu} \frac{1}{E_g + i\delta + \varepsilon - \mathcal{H}} d_{0\mu}^{\dagger} | g \rangle.$$

The procedure of the calculation is the following. First, the ground state eigen value and function are obtained using the Lanczos method. After applied the annihilation (for PES) or the creation (for IPES) operators to the ground state eigen function, the Green function of the final state is transformed to a continued fraction using the recursion method. The number of iterations in the continued fraction

necessary to get a well converged spectrum depends on the size of the cluster, and the typical value is about 1000.

3.3 Non-local interference effect on the spectral functions in undoped CuO_2 plane

In Chap. 2, we plotted various PES spectra as a function of the binding energy. In this chapter, in order to discuss both PES and IPES spectra, we plot them as a function of the energy ε defined in to discuss both PES and IPES spectra, we plot them as defined in Sect.3.2. For IPES, the higher energy corresponds to the final state with the higher ε . For PES, on the other hand, the lower ε corresponds to that with the higher energy final state.

Figure 3.1 shows calculated $3d$ PES and $3d$ IPES for various clusters:(a) CuO_4 , (b) Cu_2O_7 , (c) the linear chain Cu_3O_{10} , and (d) the square lattice Cu_4O_8 with 2D periodic boundary condition. The geometry of the clusters is also shown in the figure.

In the undoped CuO_4 cluster, the $3d$ PES spectrum can be roughly divided into four structures labeled A, B, C and D in Fig. 3.1(a). They are the ZRS state, which consists of the mainly $d^9\bar{L}$ configuration having both the d and ligand holes (\bar{L}) on the $x^2 - y^2$ symmetry orbits with opposite spins (A), the main peaks, which consist mainly of the $d^9\bar{L}$ configuration having one of the two holes on the orbits other than the $x^2 - y^2$ symmetry and the other on the $x^2 - y^2$ orbit (B), the states mainly consist of $d^9\bar{L}$ with the triplet spin state having both holes on the $x^2 - y^2$ symmetry orbits (C), and the “ d^8 ” satellite structure (D). In the Chap. 2, we have shown that, in the PES spectra, the state located near the valence top is d^{n-1} like states, though they consist mainly of $d^n\bar{L}$ configuration. This is also the case for the PES spectra of the CuO_2 plane. The main peak structure (labeled B in Fig. 3.1(a)) and the state, which is well known as the ZRS state, located at the valence top (labeled A in Fig. 3.1(a)) correspond to this quasi- d^8 states.

In terms of the quasi- d states discussed in the Chap. 2, the stabilization of the ZRS can easily be understood. Since the p - d hopping integral for the orbit with the $x^2 - y^2$ symmetry is especially larger than that for orbits with other symmetry, the effective one-body energy of the quasi- d orbits with $x^2 - y^2$ symmetry is about 1eV higher in energy compared to the orbit with other symmetry. Having no multipole interaction in the $d^9\bar{L}$ section of its effective Hamiltonian, the quasi- d^8 states have the smaller effective exchange energy compared to the effective ligand field splitting of quasi- d orbit between the $x^2 - y^2$ symmetry and others. Thus the lowest energy state among the one-electron removal states should have two holes on the $x^2 - y^2$

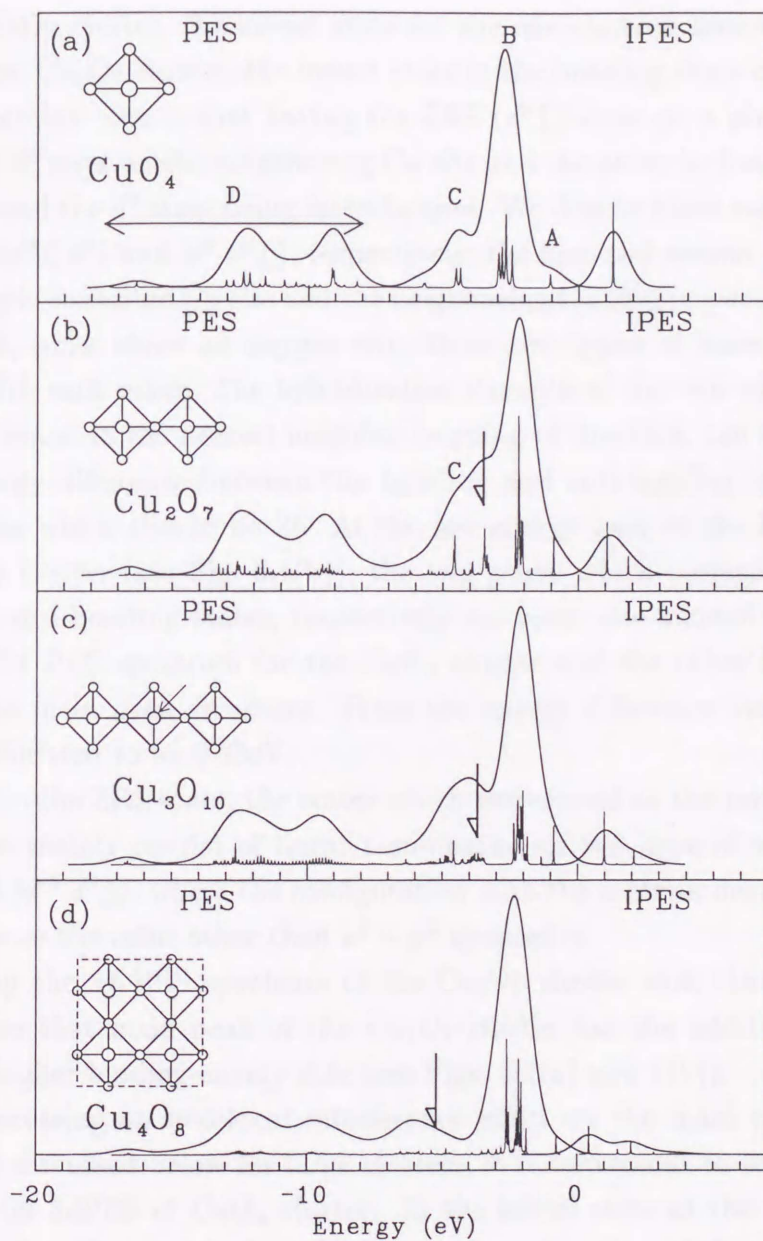


Figure 3.1: Calculated 3d PES and 3d IPES spectra for undoped CuO_4 (a), Cu_2O_7 (b), Cu_3O_{10} (c) and Cu_4O_8 (d) clusters shown in the figure; the large (small) circles denote Cu (O) atoms; the chemical potential is at the origin.

quasi- d orbit with opposite spins (in other word the low spin state) and this is called the ZRS. The main peak structure, on the other hand, corresponds to the state with a hole in $x^2 - y^2$ quasi- d orbit and another one on a quasi- d orbit other than $x^2 - y^2$ symmetry.

For the CuO_4 cluster, the lowest state for the one electron removal is the ZRS states. For the Cu_2O_7 cluster, the lowest state is the bonding state of two types of the wave functions: one is that having the ZRS ($d^9\bar{L}$) state on a photoexcited Cu site and , the d^9 state on the neighboring Cu site and the other is that with the sites of ZRS state and the d^9 state being interchanged. We denote these two type of wave functions by $|d^9\bar{L} d^9\rangle$ and $|d^9 d^9\bar{L}\rangle$, respectively; the first and second configurations stand for the photoexcited Cu site and the neighboring Cu site, respectively. Because the two CuO_4 units share an oxygen site, these two types of wave functions are hybridized with each other. The hybridization strength of the two wave function t , which is also equal to the nearest neighbor hopping of the ZRS, can be determined from the energy difference between the bonding and anti-bonding states of those wave functions which should be $2t$. At the low energy part of the PES spectrum of the Cu_2O_7 cluster (see Fig. 3.1(b)), the two peaks which corresponding to the bonding and anti-bonding states, respectively are seen: one located near the ZRS state of the $3d$ PES spectrum for the CuO_4 cluster and the other located in the vicinity of the main peak structure. From the energy difference between the two peaks, t is estimated to be 0.25eV.

Similarly to the ZRS state, the states which correspond to the main peak structure would be mainly consist of linear combination of two type of wave functions $|d^9\bar{L}^* d^9\rangle$ and $|d^{*9} d^9\bar{L}\rangle$, where the configuration with the asterisk denotes the states having a hole on the orbit other than $x^2 - y^2$ symmetry.

Comparing the $3d$ PES spectrum of the Cu_2O_7 cluster with that of the CuO_4 cluster, we see that main peak of the Cu_2O_7 cluster has the additional shoulder structure in higher binding energy side (see Figs. 3.1(a) and 1(b)).

Before discussing on non-local interference effect on the main peak structure which will be discussed below for large clusters, it is convenient to remember what is happening in $3d$ PES of CuO_4 cluster. In the initial state of the CuO_4 cluster, the wave function of the ground state is a linear combination of the wave functions $|d^9\rangle$ and $|d^{10}\bar{L}\rangle$. After removing an electron from the $3d$ orbit with the symmetry other than $x^2 - y^2$, these wave functions became $|d^{*8}\rangle$ and $|d^{*9}\bar{L}\rangle$ of the final state, respectively. The two wave functions are hybridized with each other both in the initial state and the final state through the Cu $3d$ -O $2p$ hopping, forming the bonding and anti-bonding states. In the final state, the main peak corresponds to the $d^9\bar{L}$ -configuration-dominant bonding state and the satellite structure to the d^8 -

configuration-dominant anti-bonding state. The interference of the initial and final state wave functions leads to the spectral weight transfer to the peak corresponding to the bonding state of the final state, i.e. “ $d^9 \underline{L}$ ” peak. This is why the main peak has the large spectral weight compared to the “ d^8 ” satellite, although the weight of the $d^{10} \underline{L}$ configuration is only about 20% in the initial state. Because the interference effect is caused by the charge transfer restricted in the CuO_4 unit, we call this local interference effect.

Now we discuss the $3d$ PES spectrum of the Cu_2O_7 cluster. In the initial state, the most dominant states of the ground state are the $|d^9 d^9\rangle$ and the $|d^{10} \underline{L} d^9\rangle$ states, which correspond to the $|d^9\rangle$ and $|d^{10} \underline{L}\rangle$ states on the CuO_4 cluster. In addition to these, there is also the $|d^{10} d^9 \underline{L}\rangle$ state, where the excess hole on the ligand of the neighboring Cu site forms ZRS state on this neighboring CuO_4 unit. This state is hybridized with the $|d^{10} \underline{L} d^9\rangle$ state via the oxygen site shared by the two CuO_4 units. After removing an electron from the $3d$ orbit other than $x^2 - y^2$ symmetry, the $|d^9 d^9\rangle$, $|d^{10} \underline{L} d^9\rangle$ and $|d^{10} d^9 \underline{L}\rangle$ states are transferred to the $|d^{*8} d^9\rangle$, $|d^{*9} \underline{L} d^9\rangle$ and $|d^{*9} d^9 \underline{L}\rangle$ states in the final state. Since the energy difference between the $|d^{*9} \underline{L} d^9\rangle$ and $|d^{*9} d^9 \underline{L}\rangle$ states in the final states is an order of 1eV and they also hybridized with each other. The states corresponding to the main peak structure mainly consist of the mixture of the two. The main peak and its shoulder structure of the $3d$ PES spectrum of the Cu_2O_7 cluster, corresponds to the bonding and anti-bonding states of the $|d^{*9} \underline{L} d^9\rangle$ and $|d^{*9} d^9 \underline{L}\rangle$ states, respectively. We should stress that the interference of the wave functions is caused not only by the charge transfer within the photoexcited CuO_4 but by that in the much more extended region including the neighboring CuO_4 units.

In addition to this, there are also the states having a hole on the orbit other than $x^2 - y^2$ symmetry in the neighboring Cu site of photoexcited Cu site, i.e. $d^9 \underline{L} d^{*9}$ and $d^9 d^{*9} \underline{L}$ in final state, they less affect the spectrum compared to the states discussed in the preceding paragraph. Because the holes mainly exist in the orbits with the $x^2 - y^2$ symmetry on the both Cu sites in the initial state of the PES, and the wave functions mentioned above are not directly reached by the photoexcitation and the interference effect does not take place for these states. (They affect the spectrum only by the hybridization through the intersite charge transfer to the wave functions the reached by the photoexcitation.) In the next chapter, we will show that the inclusion of the full set of the basis on Slater determinants constructed from Cu $3d$ and O $2p$ orbit is required only on the photoexcited CuO_4 unit and, for remainder of the cluster, it is sufficient to reproduce the spectra to use a reduced basis set which is extracted from the ground state wave functions of the CuO_4 units other than the photoexcited one by the density matrix method.

Because of the non-local feature of the interference effect, the main peak structure is expected to be strongly influenced by the arrangement of the surrounding CuO_4 units. It is clearly seen in the Figs. 3.1(b)-(d) that, with increasing the number of the nearest-neighbor Cu sites of the excited Cu N (N is equal to 1 (b), 2 (c) and 4 (d)), the energy separation of the anti-bonding and bonding state peaks is increased and the spectral weight is transferred to the bonding peak. This is the result of the increasing strength of the effective hybridization with the increase of N between the state with the excess hole on the ligand of the photoexcited Cu site and that with the hole on the ligand of the neighboring Cu site as the N is increased. However, the effective hybridization of the Cu_4O_8 cluster is too large for $N = 4$ and in reality, the effective hybridization of the $N = 4$ is in the middle of the Cu_3O_{10} and the Cu_4O_8 clusters.

The non-local interference also affects the Cu $2p$ XPS spectra. Figure 3.2 shows the calculated Cu $2p$ XPS spectra in various clusters: (a) CuO_4 , (b) Cu_2O_7 , (c) the linear chain Cu_3O_{10} , and (d) the square Cu_4O_8 with the 2D periodic boundary condition. The Cu $2p$ PES for the undoped CuO_4 cluster has a main peak with mainly the $|\underline{c}d^{10}\underline{L}$ character and satellite structures with mainly $|\underline{c}d^9$ character in each of $2p_{1/2}$ and $2p_{3/2}$; \underline{c} denotes the Cu $2p$ core hole. For undoped Cu_2O_7 cluster, the main peak structure of Cu $2p$ PES consists of two peaks A and B. The high (B) and low (A) binding energy peaks correspond to the bonding and antibonding states of the two types of the screened states: they are that having a hole in the ligand of the core hole site ($|\underline{c}d^{10}\underline{L}d^9$) and that having the hole in the ligand of the neighboring CuO_4 unit ($|\underline{c}d^{10}d^9\underline{L}$). Similarly to the $3d$ PES spectrum, the interference of the initial and final state wave functions of the above mentioned states leads to the spectral weight transfer to the lower binding energy peak A (the bonding state of the two) of the main structure. It is also analogous to the $3d$ PES spectrum, in the Figs. 3.1(b)-(d) that, with increasing N , the energy separation of the anti-bonding and bonding state peaks of the main structure is increased and the spectral weight is transferred to the bonding-state peak A, indicating the increasing strength of the effective hybridization between the above mentioned two types of the screened states.

3.4 Effect of the electron and hole doping on the spectral functions in CuO₂ plane

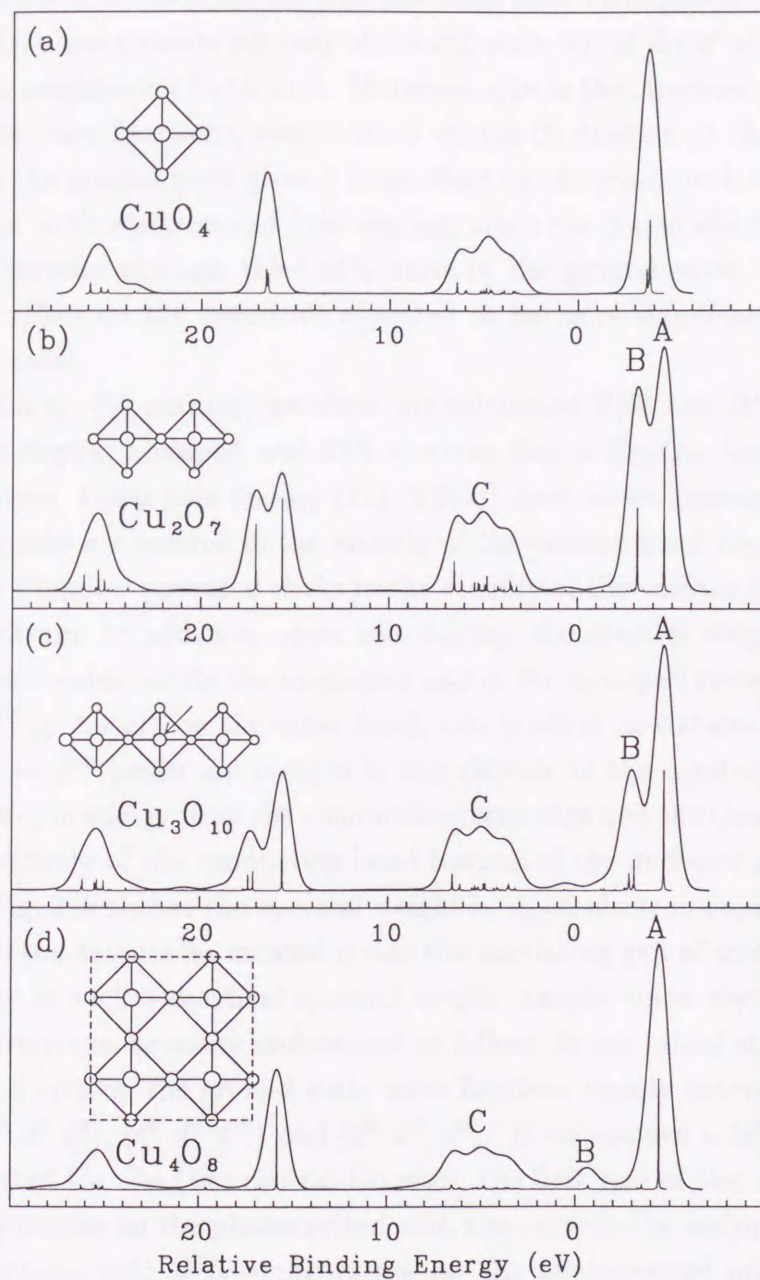


Figure 3.2: Calculated Cu 2p XPS spectra for undoped CuO₄ (a), Cu₂O₇ (b), Cu₃O₁₀ (c) and Cu₄O₈ (d) clusters shown in the figure; the large (small) circles denote Cu (O) atoms.

3.4 Effect of the electron and hole doping on the spectral functions in CuO_2 plane

In previous section, we have shown that the main peak structure of $3d$ PES for the undoped CuO_2 plane consists not only of the $d^9 \underline{L}$ state but of the d^9 states having the excess hole on neighboring CuO_4 unit. Moreover, due to the interference of the initial and final state wave functions, even a small charge fluctuation at the photoexcited CuO_4 unit in the ground state gives a large effect on the main peak structure of the spectrum. For both electron and hole doping, since the doped electrons and holes could easily transfer through the CuO_4 units in the ground state, the “non-local interference” effect on the spectrum expected to be more significant compared to the undoped cases.

In Figs. 3.3(a), (b) and (c), we show the calculated PES and IPES spectra for the 33% hole doped, undoped and 33% electron doped Cu_3O_{10} linear chain clusters, respectively. Upon hole doping (Fig. 3.3(a)), new states corresponding to the “ $d^9 \underline{L} \rightarrow d^9$ ” peaks are created in the vicinity of the valence band top in IPES spectrum and the chemical potential shifts in the vicinity of the valence band top of the undoped spectrum. In addition, upon hole doping, the spectral weight transfers to the new states created inside the insulating gap of the undoped system. Upon electron doping (Fig. 3.3(c)), on the other hand, two types of new states corresponding to the “ $d^{10} \underline{L} \rightarrow d^9$ ” peaks are created in the vicinity of the conduction band and about 1eV lower in energy from the conduction band edge and the chemical potential shifts in the vicinity of the conduction band bottom of the undoped spectrum. It is also seen in Fig. 3.3(c) that the spectral weight is, upon electron doping, drastically transferred to the new states created inside the insulating gap of undoped system.

The reason of such a drastical spectral weight transfer upon electron doping in $3d$ PES spectrum can be easily understood as follow. In the initial state of the 33% electron doped system, the ground state wave function mainly consists of the wave functions $|d^{10} d^9 d^9\rangle$, $|d^9 d^9 d^{10}\rangle$ and $|d^9 d^{10} d^9\rangle$. If we remove a $3d$ electron from the photoexcited Cu site (the central Cu site), the first two of the wave functions with d^9 configuration on the photoexcited unit, the same as the undoped case, reach the wave functions with $d^9 \underline{L}$ configuration on the photoexcited unit in the final state through the hybridization of the final state, respectively, whereas the last one, which has d^{10} configuration on the photoexcited unit, reaches the final state wave function with the d^9 configuration on the photoexcited unit $|d^9 d^9 d^9\rangle$. The energy of the wave function $|d^9 d^9 d^9\rangle$ is lower by Δ compared to those of $|d^{10} d^9 \underline{L} d^9\rangle$ and $|d^9 d^9 \underline{L} d^{10}\rangle$, in the absence of the hybridization in the final state. Thus even in the presence of hopping terms, the peaks inside gap are corresponding to the states

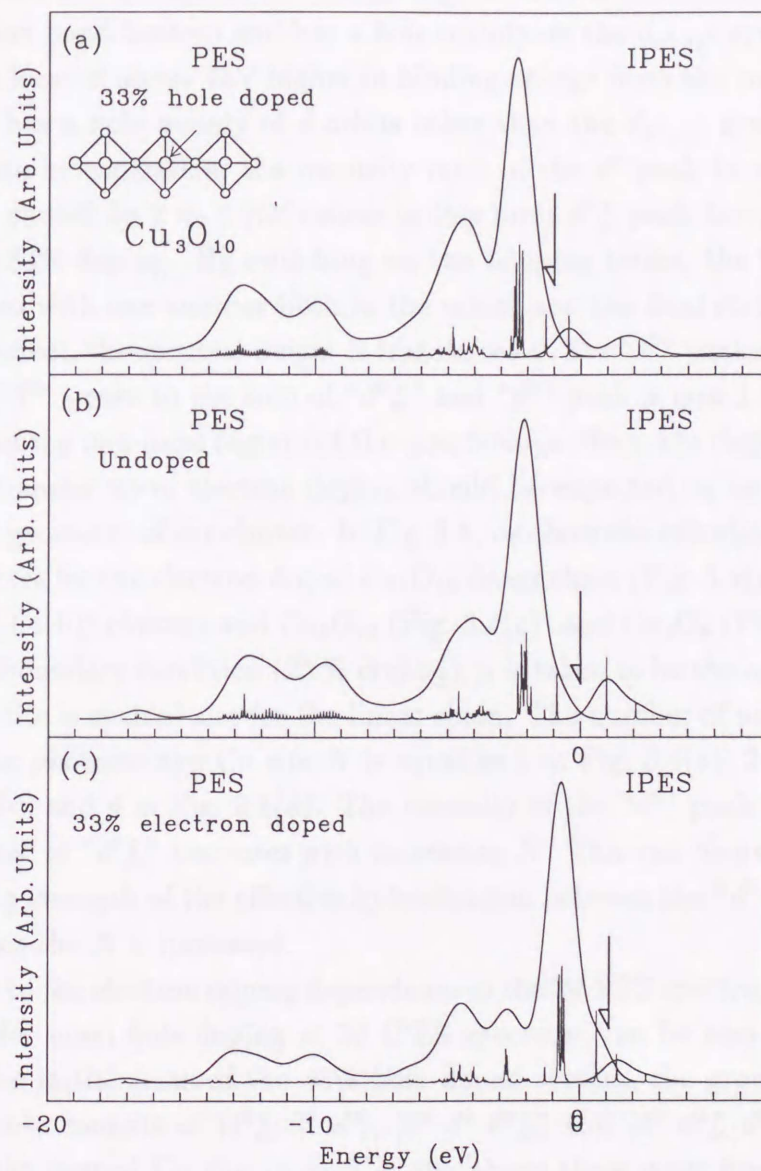


Figure 3.3: Calculated 3d PES and 3d IPES spectra for the 33% hole doped (a), undoped (b) and 33% electron doped (c) Cu_3O_{10} linear chain clusters; the chemical potentials in each clusters are indicated by arrows.

mainly d^9 configuration on the photoexcited unit and the peaks located in the energy region of 0eV to 1eV has mainly the $d^9\bar{L}$ configuration on photoexcited unit. Since the hybridization between the $d_{x^2-y^2}$ orbit and surrounding oxygen orbits is much stronger compared to the orbit with the symmetries xy , yz , zx and $3z^2 - r^2$, the d^9 state splits into two groups in the energy region. One is located in the vicinity of the conduction band bottom and has a hole mainly on the $d_{x^2-y^2}$ symmetry orbits. The other is located about 1eV higher in binding energy from the conduction band bottom and has a hole mainly of d orbits other than the $d_{x^2-y^2}$ symmetry. In the absence of the hybridization, the intensity ratio of the $d^9\bar{L}$ peak to sum of the $d^9\bar{L}$ and d^8 peak should be 2 to 1 (Of course in this limit $d^9\bar{L}$ peak has no intensity) if we note the 33% doping. By switching on the hopping terms, the wave functions are hybridized with one another both in the initial and the final states. Due to the interference effect, the spectral weight is transferred to the “ d^9 ” peaks. The intensity ratio of the “ d^9 ” peaks to the sum of “ $d^9\bar{L}$ ” and “ d^8 ” peak is now 1 to 0.47.

Because of the non-local feature of the interference effect, the degree of the spectral weight transfer upon electron doping should be expected to be strongly influenced by the geometry of the cluster. In Fig. 3.4, we show the calculated $3d$ PES and $3d$ IPES spectra for the electron-doped Cu_4O_{13} linear chain (Fig. 3.4(a)) and Cu_4O_{12} square (Fig. 3.4(b)) clusters and Cu_4O_{10} (Fig. 3.4(c)) and Cu_4O_8 (Fig. 3.4(d)) with the periodic boundary condition (25 % doping); μ is taken to be the origin of energy; the edge Cu site is excited site for the linear chain. The number of nearest-neighbor Cu site of the photoexcited Cu site N is equal to 1 in Fig. 3.4(a), 2 in Fig. 3.4(b), 3 in Fig. 3.4(c) and 4 in Fig. 3.4(d). The intensity of the “ d^9 ” peak ($-1 \sim -3$ eV) relative to that of “ $d^9\bar{L}$ ” increases with increasing N . This can be explained by the the increasing strength of the effective hybridization between the “ d^9 ” state and the “ $d^9\bar{L}$ ” state as the N is increased.

Similarly to the electron doping dependence of the $3d$ PES spectrum, the spectral weight transfer upon hole doping in $3d$ IPES spectrum can be also understood as follow. In the initial state of the 33% hole doped system, the ground state wave function mainly consists of $|d^9\bar{L} d^9 d^9\rangle$, $|d^9 d^9 d^9\bar{L}\rangle$ and $|d^9 d^9\bar{L} d^9\rangle$. Adding an electron to the central Cu site in each of the above three wave functions reached to the wave functions $|d^9\bar{L} d^{10} d^9\rangle$, $|d^9 d^{10} d^9\bar{L}\rangle$ and $|d^9 d^9 d^9\rangle$ through the final state hybridization. In the absence of hopping terms, the last wave function are energetically lower by Δ compared to the other two. Thus, the first and second wave functions are the main component of the states located in the vicinity of the conduction band bottom of the undoped IPES spectrum and the last one is that of the state inside the gap located in the vicinity of the valence band top. The interference of the initial and final state wave functions leads to the spectral weight

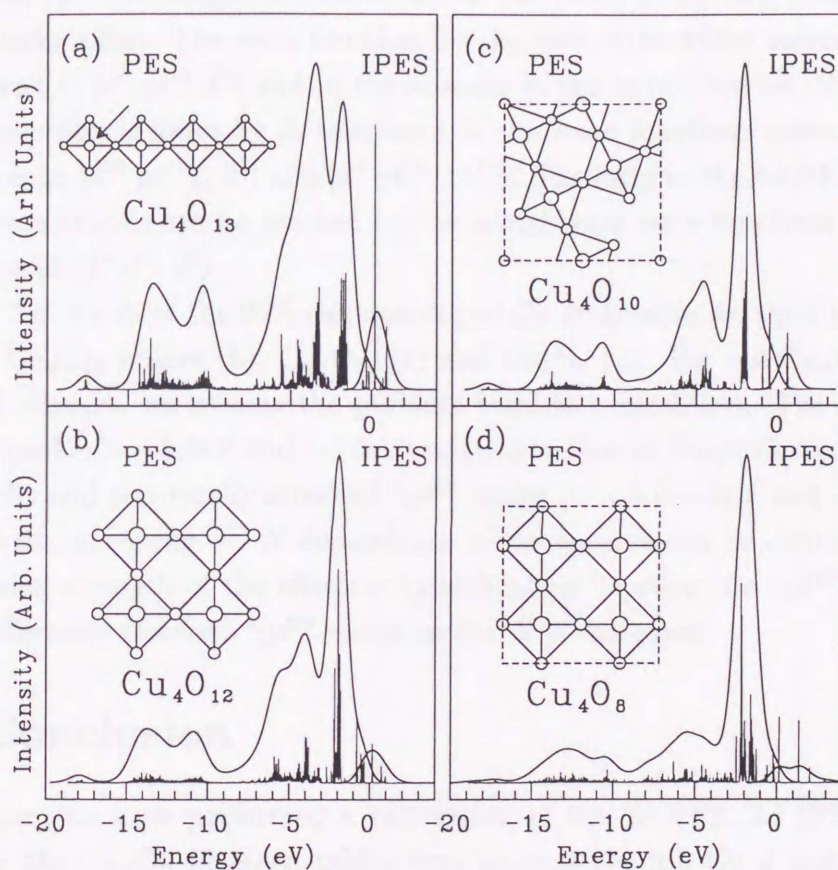


Figure 3.4: Calculated 3d PES and 3d IPES spectra for the electron-doped Cu_4O_{13} linear chain (a) and Cu_4O_{12} square (b) clusters and Cu_4O_{10} (c) and Cu_4O_8 (d) with the periodic boundary condition (25 % doping); μ is taken to be the origin of energy; the edge Cu site is excited site for the linear chain; the chemical potential is at the origin.

transfer to the state inside the insulating gap of the undoped spectra.

In Figs. 3.5(a), (b) and (c), we show the calculated Cu 2*p* XPS spectra for the 33% hole doped, undoped and 33% electron doped Cu₃O₁₀ linear chain clusters, respectively. In Fig. 3.5(c), we show Cu 2*p* XPS for the 33% electron doped Cu₃O₁₀ cluster. In addition to the structures observed in the undoped spectrum, a new peak D (D') corresponding to mainly $\underline{c}d^{10}$ character appears in the energy region $\sim 2\text{eV}$ lower from the main structure in 2*p*_{3/2} (2*p*_{1/2}) edge. Similarly to the electron-doped 3*d* PES, the spectral weight is transferred to the peak, indicating strong intersite charge transfer effect. The wave function for the final state which corresponding to the new peak is $|d^9 \underline{c}d^{10} d^9\rangle$ and in the absence of the hybridization, the energy of the wave function is lower by Δ compared to the wave functions corresponding to the main peak: $|d^{10} \underline{c}d^{10} \underline{L} d^9\rangle$ and $|d^9 \underline{c}d^{10} \underline{L} d^{10}\rangle$. Similarly to the 3*d* PES, the three of the wave functions can be reached by the initial state wave functions $|d^9 d^9 d^{10}\rangle$, $|d^{10} d^9 d^9\rangle$ and $|d^9 d^{10} d^9\rangle$.

In Fig. 3.6, we show the 25% electron doped Cu 2*p* spectra for the Cu₄O₁₃ linear chain (a), Cu₄O₁₂ square (b), Cu₄O₁₀ (c) and Cu₄O₈ (d). For the Cu₄O₁₀ (c) and Cu₄O₈ (d) clusters, we assume the periodic boundary condition. The intensity of the " $\underline{c}d^{10}$ " peaks ($\sim -9.5\text{eV}$ and $\sim 10\text{eV}$) relative to that of the peaks corresponding to the locally and non-locally screened " $\underline{c}d^9$ " states (~ -8.5 — -6eV and ~ 12 – 15eV) increases with increasing *N*. *N* dependence of the spectra can be explained by the the increasing strength of the effective hybridization between the " $\underline{c}d^{10}$ " state and the two differently screened " $\underline{c}d^9$ " states as the *N* is increased.

3.5 Conclusion

In conclusion, we have performed a calculation of the 3*d* PES, 3*d* IPES, and Cu 2*p* PES for the Cu_{*n*}O_{*m*} clusters, taking into account the full Cu *d* and O *p* orbits and the full intraatomic multipole interaction as a model of the CuO₂ plane. For the undoped 3*d* PES, analogous to the result of the van Veenendaal for that of the 2*p* XPS spectrum, the main peak structure consists of the " $d^9 \underline{L}$ " state, which has an excess hole introduced by the photoexcitation in the neighboring oxygen sites, and the " d^9 " state with the hole in the neighboring CuO₄ unit forming ZRS state. These two kinds of states are hybridized with each other through the charge transfer beyond a single CuO₄ unit. The main peak and its shoulder structure correspond to the bonding and antibonding states of the two, respectively. The interference of the initial and final state wave functions of the two leads to a spectral weight transfer to the bonding state. The degree of the spectral weight transfer is increased as the number of the nearest neighbor Cu sites of the excited Cu site is increased. For the

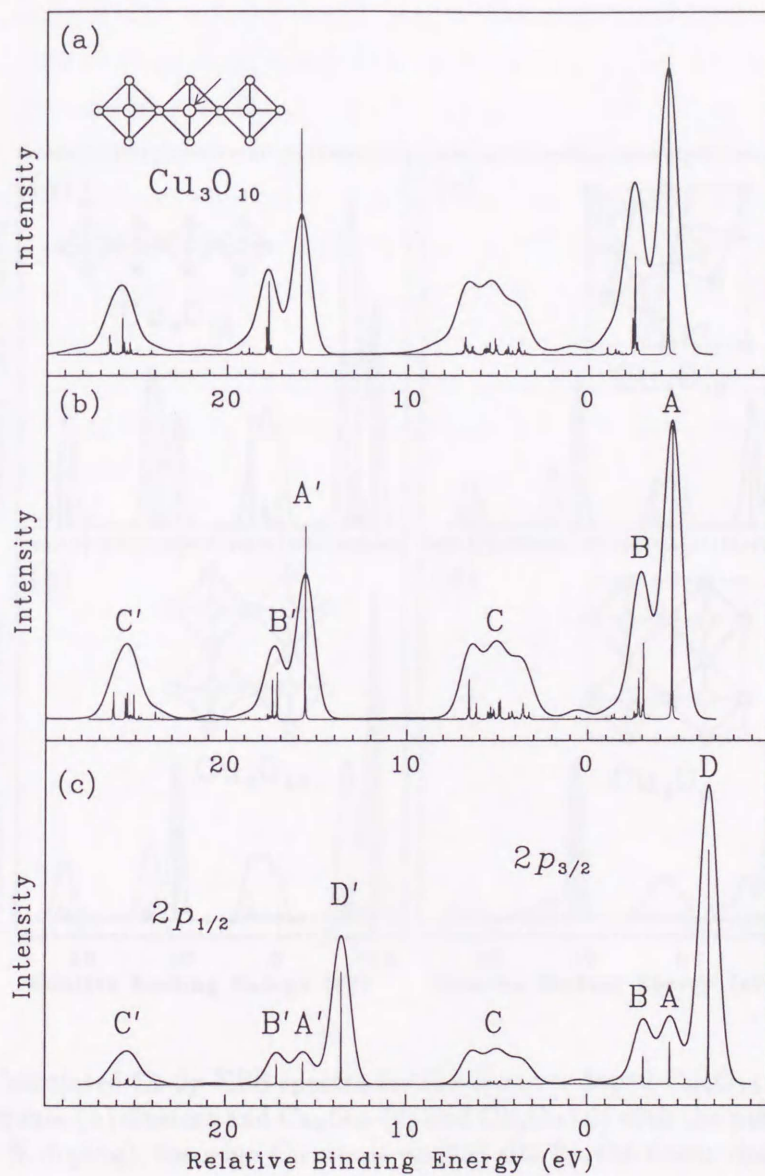


Figure 3.5: Calculated Cu 2p XPS spectra for the 33% hole doped (a), undoped (b) and 33% electron doped (c) Cu_3O_{10} linear chain clusters.

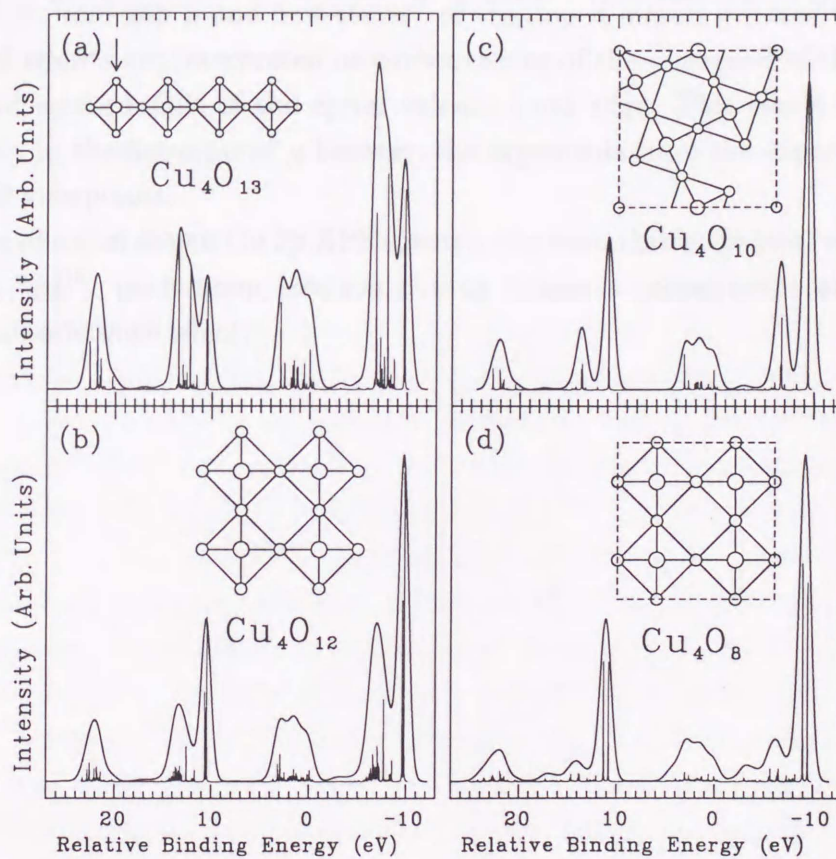


Figure 3.6: Calculated Cu 2p XPS spectra for the electron-doped Cu_4O_{13} linear chain (a) and Cu_4O_{12} square (b) clusters and Cu_4O_{10} (c) and Cu_4O_8 (d) with the periodic boundary condition (25 % doping); the edge Cu site is excited site for the linear chain.

undoped Cu 2*p* XPS spectrum, the situation is similar to the 3*d* PES spectrum.

For the doped 3*d* PES and 3*d* IPES, upon the electron doping, the chemical potential shifts to the lower edge of the conduction band and two new states appear inside the insulating gap. Upon hole doping, on the other hand, the chemical potential shifts to the upper edge of the valence band and new states appear in the vicinity of the upper edge of the valence band. Due to the strong non-local interference of the initial and final state wave functions, upon both electron and hole doping, the spectral weight is drastically transferred to the states inside the gap of the undoped system. The "mid-gap μ and new states" of the doped metals inferred from the experimental results are interpreted as consequences of the disregard of the character change and upward shift of the upper valence band edge. This result removes the discrepancy in the behavior of μ between the arguments from the experimental and theoretical viewpoints.

For the electron doped Cu 2*p* XPS spectra, the remarkable spectral weight transfer to the " $\underline{c}d^{10}$ " peak upon electron doping is also a consequence of the strong non-local interference effect.

Chapter 4

Systematic Basis Set Reduction

4.1 Introduction

In the previous chapter, we have shown that both the multiple-Cu-site effect and the $3d$ orbitals degeneracy are important to understand various high-energy spectroscopies for Cu-oxides. However, rapid increase of the number of the basis functions with the number of the site prevents us from calculating on the cluster models containing more than four Cu ions with the full degeneracy of $3d$ and oxygen $2p$ orbitals. Even a Cu_5O_{16} cluster with 5 holes has about 5×10^8 basis functions which is untractable with today's computers. To overcome this difficulty, systematic reduction of the basis set which does not affect the spectrum should be required to calculate spectra for the clusters containing several transition metal ions. In this chapter we will present a formalism for such a systematic reduction of the basis set of transition-metal-oxide clusters as a model of transition metal (TM) compounds and also some numerical results on the Cu_nO_m clusters containing up to five Cu atoms.

As a model for $3d$ TM compounds, we now think about TM-oxide clusters which consist of the TMO_6 octahedron or TMO_4 square units connected by sharing their oxygens. For simplicity, here, we consider the case of the $3d$ PES spectrum only. The discussion below can also be applied to other high-energy spectroscopies like the TM $2p$ XPS or the $3d$ IPES. The wave function of the ground state for the cluster would be approximately described by the linear combination of the direct products of the low-lying eigenstates of the TMO_n units ($n = 4$ or 6). Namely, considering that each of the two units sharing an oxygen site is overlapped only on the oxygen site, we try to remove double counting of bases including the orbitals on the shared oxygen site using an appropriate method. The wave function of the final states for the $3d$ PES spectrum reached by the photoexcitation in the absence of the interactions in the final states are, on the other hand, the direct products of the wave functions of the ground state and a hole created by the photoexcitation. This requires high-energy

eigenstates for the photoexcited TMO_n unit. By switching on the interactions in the final states, the additional hole causes further mixing among the states in the photoexcited TMO_n unit. Furthermore, the high-energy eigenstates on the photoexcited TMO_n unit are mixed with high-energy eigenstates on the neighboring TMO_n units. Because the high-energy eigenstates on the neighboring TMO_n units, however, do not participate the initial states, they do not concern the spectral weight transfer caused by the interference of the initial and final state wave functions. This means that they do not change center of gravity of the spectral weight, though they could broaden or deform some of the structures in the spectrum without them. Assuming such a final-state-effect caused by the high-energy eigenstates on the neighboring TMO_n units is small, we use the full set of the basis constructed from the TM $3d$ and O $2p$ orbits only on the photoexcited TMO_n unit. For the rest of the cluster, on the other hand, we use a reduced basis set extracted from the low-lying eigenstates of the TMO_n units using the density matrix method [76], which will be discussed below. This is a outline of our method.

Furthermore, in the Sect.4.3, we will propose a effective one-Cu-site model which can well reproduce the spectra for the undoped Cu_5O_{16} cluster with the reduced basis set.

4.2 Density matrix method

In this section, we present detailed description of the way to reduce the basis set of the cluster using the case of Cu_5O_{16} cluster as an example. Figure 4.1 shows how to reduce the basis set for the Cu_5O_{16} cluster schematically. The central Cu site is assumed to be the photoexcited site. First, to obtain the reduced basis set for four CuO_3 units surrounding the central CuO_4 unit, we calculate low-energy eigenfunctions of the CuO_4 unit with various total electron numbers N . Next, we remove the $2p$ orbits on the oxygen site which will be shared with the central CuO_4 unit. The density matrix approach used by White [76] in the context of real-space renormalization-group calculation is suitable to doing this. To do this end, we rewrite the obtained the g -th lowest energy eigenfunction with total electron numbers N $|\Psi_g^N\rangle$ to the direct product form of the two wave functions

$$|\Psi_g^N\rangle = \sum_{i,j} c_{ij} |\psi_i\rangle |\varphi_j\rangle ,$$

where $\{|\psi_i\rangle\}$ is the complete set of the state on the CuO_3 unit and $\{|\varphi_j\rangle\}$ is the complete set of the state on the removed oxygen site. After this, diagonalizing the

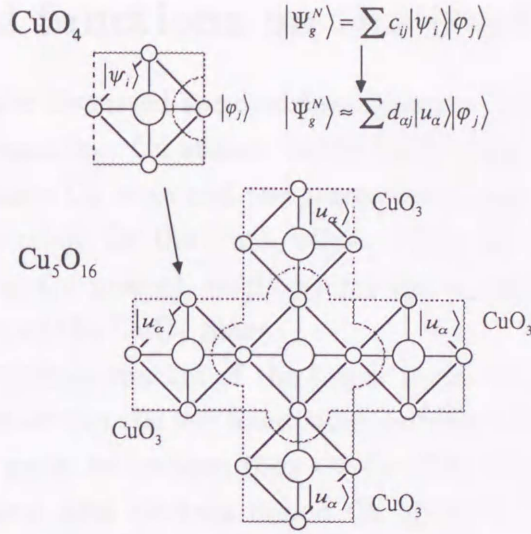


Figure 4.1: Schematic construction of the reduced basis set for the Cu_5O_{16} cluster. We first calculate the ground state wave functions of the CuO_4 clusters with various total electron numbers N . Using the density matrix method, we extract the reduced basis set for the CuO_3 units. Finally, we construct the basis set for the Cu_5O_{16} cluster from the reduced basis sets for the four CuO_3 units and the full basis set for the central CuO_4 unit.

density matrix of the reduced basis set

$$\rho_{i,i'} = \sum_j c_{ij}^* c_{i'j},$$

we obtain the eigenvalues $\{w_\alpha\}$ and eigenfunctions $\{|u_\alpha^N\rangle\}$ of the density matrix. It is easily shown that to use a set of the eigenfunctions $|u_\alpha^N\rangle$ ($\alpha = 1 \dots m$) with largest m eigenvalues as the basis of the CuO_3 unit is the optimal choice in the sense that the basis set minimize the error

$$\left| |\Psi_g^N\rangle - \sum_{\alpha,j} d_{\alpha j} |u_\alpha^N\rangle |\phi_j\rangle \right|,$$

with respect to both arbitrary basis set with fixed m on the CuO_3 unit $\{|u_\alpha^N\rangle\}$ ($\alpha = 1 \dots m$, $\langle u_\alpha^N | u_{\alpha'}^N \rangle = \delta_{\alpha\alpha'}$) and $d_{\alpha j}$. Finally, we assemble the Cu_5O_{16} cluster from all the units. The full set of the basis on Slater determinants constructed from the Cu $3d$ and O $2p$ orbitals are used on the central CuO_4 unit (photoexcited unit) and for four CuO_3 units surrounding this, we use the reduced basis set extracted from the low-lying eigenstates of the CuO_4 units with the various total electron number. We perform the calculation in the same way as in Chap. 3 on the reduced basis set. Note that, we do not introduce further approximation except using the reduced basis set.

4.3 Spectral functions on the Cu_5O_{16} cluster

In Chap. 2, we have discussed spectral functions on CuO_2 plane using Cu_nO_m cluster containing at most four Cu atoms. In the CuO_2 plane, however, each Cu site has four nearest neighbor Cu sites and the cluster with four Cu ions is not enough to obtain quantitative result for the CuO_2 plane. Thus, the spectra on the Cu_5O_{16} cluster which have four Cu nearest neighbors for the central Cu site is suitable to investigate the spectra of the CuO_2 plane.

Figure 4.2 shows various spectra of the linear chain Cu_3O_{10} cluster calculated with the reduced basis set (on the left hand side) and the full basis set (on the right hand side). From top panel to bottom, they are the 33% electron doped $3d$ spectra, undoped $3d$ spectra and 33% electron doped Cu $2p$ XPS. The basis functions of CuO_3 clusters are extracted from the ground state eigenfunctions of CuO_4 clusters with total hole number 0, 1 and 2. The number of the basis functions for the CuO_3 clusters with hole numbers 0, 1 and 2 are 1, 4 and 1, respectively. The number of the basis functions for the final state of the undoped $3d$ PES spectrum is $\sim 2.6 \times 10^6$ whereas the number is $\sim 10^5$ for the reduced basis set. Except for peaks with low intensity, which may arise from high-energy eigenstates on CuO_4 units other than the photoexcited site, the spectra using the reduced basis set well reproduce the full basis ones.

To investigate the nearest neighbor Cu sites dependence of the $3d$ PES and the Cu $2p$ XPS spectra more quantitatively, we have calculate the spectra for the Cu_4O_{13} and Cu_5O_{16} clusters. In Figs. 4.3(a), (b) and (c), we show $3d$ PES spectra of the CuO_4 , Cu_2O_7 and Cu_3O_{10} clusters calculated with the full basis set and in Fig. 3(d) and (e) we show that of of Cu_4O_{13} and Cu_5O_{16} clusters calculated with the reduced basis set. The geometry of the clusters are also shown in the figure. The nearest neighbor Cu sites N of the central CuO_4 unit are 0, 1, 2, 3 and 4 for the clusters in the Figs. 4.3(a), (b), (c), (d) and (e), respectively. The energy separation of the main and its shoulder peaks is increased and the relative intensity of the shoulder peak is decreased with the increasing N (indicated by arrows in Fig. 3.1). For the Cu_5O_{16} cluster, however, the effect is much smaller compared to the Cu_4O_8 cluster (see Fig. 3.1). In Chap. 3, for the Cu_4O_8 cluster, we use the periodic boundary condition and in reality the nearest neighbor Cu sites for the central Cu site is two. This could lead to an artificial result. Figure 4.4 shows Cu $2p$ XPS spectra for the same clusters in the Fig. 4.3.

To understand the N dependence of the $3d$ PES spectra more quantitatively, we discuss the wave function of the undoped Cu_5O_{16} cluster. In the ground state of the undoped Cu_5O_{16} cluster, the dominant configuration has a hole on central CuO_4 unit

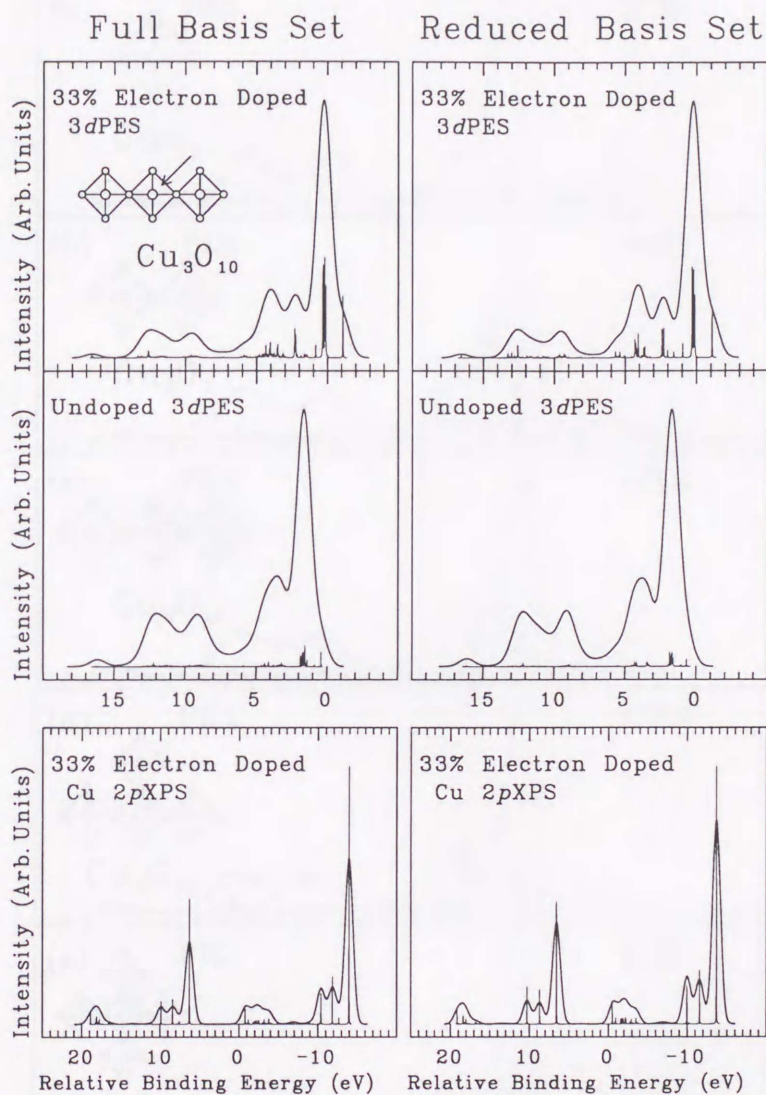


Figure 4.2: Comparison of the calculated spectra of the linear chain Cu_3O_{10} cluster using the reduced basis set (on the right hand side) with those using the full basis set (on the left hand side). From top to bottom: 3d PES spectra for the 33% electron doped cluster, 3d PES spectra for the undoped cluster and Cu 2p XPS spectra for the 33% electron doped cluster.

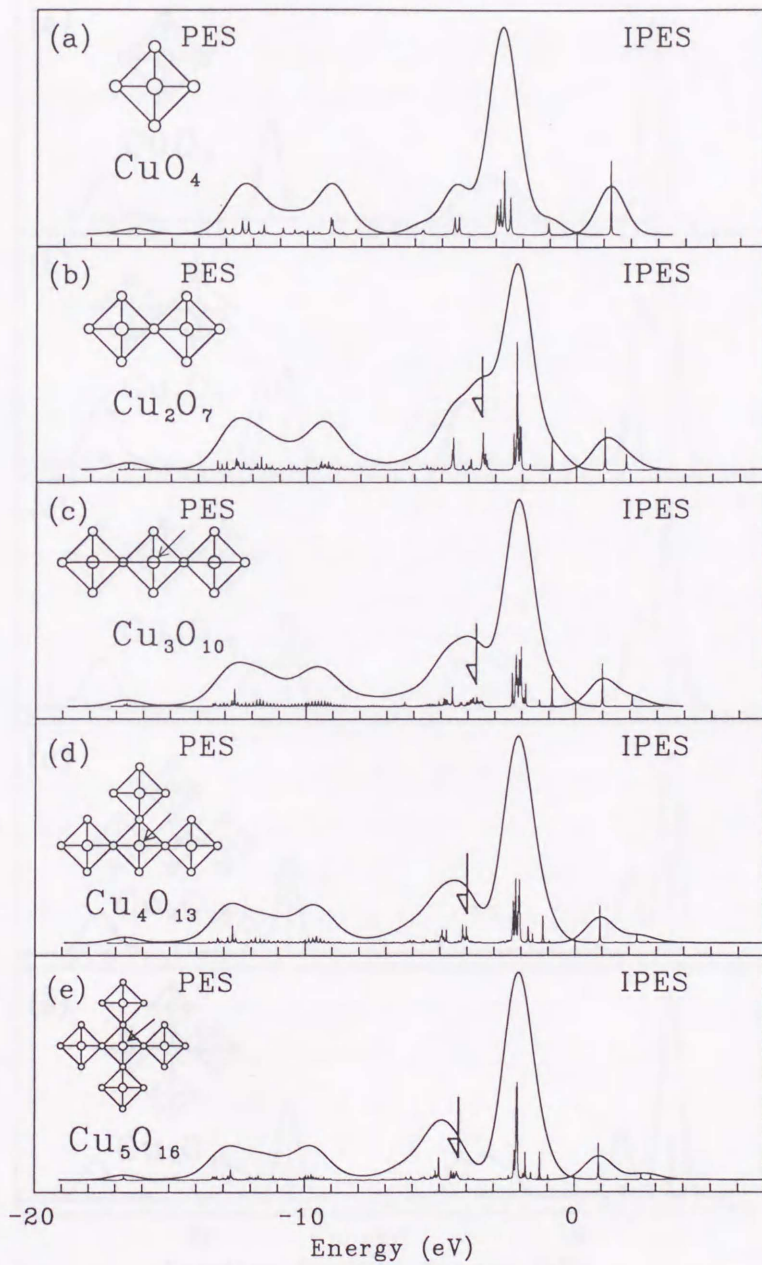


Figure 4.3: Calculated 3d PES and 3d IPES spectra for various undoped clusters with the full basis set for CuO_4 (a), Cu_2O_7 (b) and Cu_3O_{10} (c) and with the reduced basis set for Cu_4O_{13} (d) and Cu_5O_{16} ; the chemical potential is at the origin.

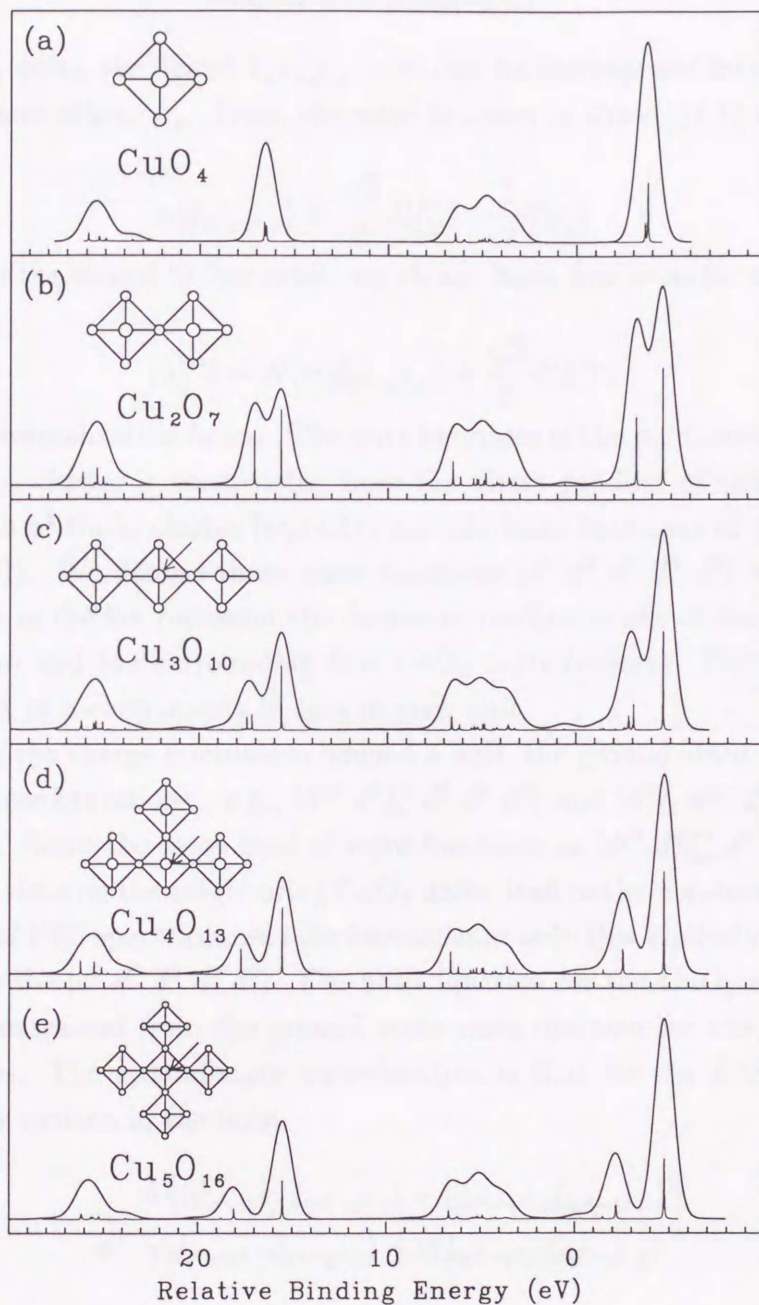


Figure 4.4: Calculated Cu 2p XPS spectra for various undoped clusters with the full basis set for CuO_4 (a), Cu_2O_7 (b) and Cu_3O_{10} (c) and with the reduced basis set for Cu_4O_{13} (d) and Cu_5O_{16} .

and also in each of surrounding four CuO₃ units. The ground-state wave-function of the CuO₄ cluster with a hole is written in the form

$$\alpha|\underline{d}_{x^2-y^2,\sigma}\rangle + \beta|\underline{L}_{x^2-y^2,\sigma}\rangle. \quad (4.1)$$

For the CuO₃ units, the ligand $L_{x^2-y^2,\sigma}$ orbit can be decomposed into the shared O $2p\sigma$ orbit p_σ and others L'_σ . Then, the wave function in the eq.(4.1) can be rewrite in the form

$$\alpha|\underline{d}_{x^2-y^2,\sigma}\rangle + \frac{\sqrt{3}}{2}\beta|\underline{L}'_\sigma\rangle + \frac{1}{2}\beta|p_\sigma\rangle. \quad (4.2)$$

Removing the the shared O $2p\sigma$ orbit, we obtain basis functions for the CuO₃ unit with a hole

$$|u_\sigma^{(1)}\rangle = \mathcal{N}(\alpha|\underline{d}_{x^2-y^2,\sigma}\rangle + \frac{\sqrt{3}}{2}\beta|\underline{L}'\rangle) \quad (4.3)$$

where \mathcal{N} is a normalization factor. The wave functions of the dominant configuration for the Cu₅O₁₆ cluster is constructed from the direct product of the ground state wave functions of CuO₄ cluster (eq.(4.1)) and the basis functions of the four CuO₃ units (eq.(4.3)). We denote these wave functions $|d^9 d^9 d^9 d^9 d^9\rangle$ where the five configurations in the ket represent the dominant configurations of the central CuO₄ unit (first one) and the surrounding four CuO₃ units (others). For simplicity, we omit the index of z -components of spin in each unit.

Because of the charge fluctuation beyond a unit, the ground-state wave-function also contains configurations, e.g., $|d^{10} d^9 \underline{L}' d^9 d^9 d^9\rangle$ and $|d^9 \underline{L} d^{10} d^9 d^9 d^9\rangle$, with small weights. Since the same kind of wave functions as $|d^{10} d^9 \underline{L}' d^9 d^9 d^9\rangle$, which have the ZRS state on the neighboring CuO₄ units, lead to the non-local interference effect on the $3d$ PES spectrum, we take into account only this kind of wave functions in addition to the $|d^9 d^9 d^9 d^9 d^9\rangle$. The basis function for the CuO₃ units with two holes can be extracted from the ground state wave function for the CuO₄ cluster with two holes. The ground-state wave-function is that for the ZRS state and is approximately written in the form

$$\begin{aligned} & \delta \left\{ |\underline{d}_{x^2-y^2,\uparrow} \underline{L}_{x^2-y^2,\downarrow}\rangle + |\underline{d}_{x^2-y^2,\downarrow} \underline{L}_{x^2-y^2,\uparrow}\rangle \right\} \\ & + \gamma |\underline{d}_{x^2-y^2,\uparrow} \underline{d}_{x^2-y^2,\downarrow}\rangle + \varepsilon |\underline{L}_{x^2-y^2,\uparrow} \underline{L}_{x^2-y^2,\downarrow}\rangle \end{aligned} \quad (4.4)$$

Rewriting the eq.(4.4) with use of the L' and p orbits instead of the L orbit and retaining states which have two holes on the CuO₃ unit, we obtain a approximate basis function for the CuO₃ unit with two holes

$$\begin{aligned} |u^{(2)}\rangle = \mathcal{N}' \left[\frac{\sqrt{3}}{2} \delta \left\{ |\underline{d}_{x^2-y^2,\uparrow} \underline{L}'_{x^2-y^2,\downarrow}\rangle + |\underline{d}_{x^2-y^2,\downarrow} \underline{L}'_{x^2-y^2,\uparrow}\rangle \right\} \right. \\ \left. + \gamma |\underline{d}_{x^2-y^2,\uparrow} \underline{d}_{x^2-y^2,\downarrow}\rangle + \frac{3}{4} \varepsilon |\underline{L}'_{x^2-y^2,\uparrow} \underline{L}'_{x^2-y^2,\downarrow}\rangle \right] \end{aligned} \quad (4.5)$$

where \mathcal{N}' is a normalization factor. Finally, we obtain an approximate ground-state wave-function in the form

$$A|d^9 d^9 d^9 d^9 d^9\rangle + \frac{1}{2}B\{s_1|d^{10} d^9 \underline{L}' d^9 d^9 d^9\rangle + s_2|d^{10} d^9 d^9 \underline{L}' d^9 d^9\rangle + s_3|d^{10} d^9 d^9 d^9 \underline{L}' d^9\rangle + s_4|d^{10} d^9 d^9 d^9 d^9 \underline{L}'\rangle\}. \quad (4.6)$$

s_i ($i = 1 \dots 4$) denote phase factors which satisfy $|s_i| = 1$. In addition to this, s_i should satisfy the relation:

$$\langle d^9 d^9 d^9 d^9 d^9 | \mathcal{H} | d^{10} d^9 \underline{L}' d^9 d^9 d^9 \rangle = s_1 \beta T, \quad (4.7)$$

$$\langle d^9 d^9 d^9 d^9 d^9 | \mathcal{H} | d^{10} d^9 d^9 \underline{L}' d^9 d^9 \rangle = s_2 \beta T, \quad (4.8)$$

$$\langle d^9 d^9 d^9 d^9 d^9 | \mathcal{H} | d^{10} d^9 d^9 d^9 \underline{L}' d^9 \rangle = s_3 \beta T, \quad (4.9)$$

$$\text{and } \langle d^9 d^9 d^9 d^9 d^9 | \mathcal{H} | d^{10} d^9 d^9 d^9 d^9 \underline{L}' \rangle = s_4 \beta T \quad (4.10)$$

where T has a positive value. Since the wave function $|d^9 d^9 d^9 d^9 d^9\rangle$ is hybridized with the rest of four wave functions through the hopping of a hole on $L_{x^2-y^2}$ orbit in the central CuO_4 unit to the one of the CuO_3 unit, the relative phases of the four wave function and that of the four $p\sigma$ orbits in $L_{x^2-y^2}$ should be the same.

To obtain an effective Cu site model, we further simplify the model. If we neglect the spin degree of the freedom on the CuO_3 units with a hole (so we can eliminate all the d^9 's for the CuO_3 units in the kets from eq.(4.6)) and substitute

$$|\mathcal{V}_{x^2-y^2}\rangle = \frac{1}{2}\{s_1|d^{10} d^9 \underline{L}' d^9 d^9 d^9\rangle + s_2|d^{10} d^9 d^9 \underline{L}' d^9 d^9\rangle + s_3|d^{10} d^9 d^9 d^9 \underline{L}' d^9\rangle + s_4|d^{10} d^9 d^9 d^9 d^9 \underline{L}'\rangle\} \quad (4.11)$$

and eq.(4.1) into eq.(4.6) then, the effective ground-state wave-function can be written in the form:

$$A\alpha|\underline{d}_{x^2-y^2,\sigma}\rangle + A\beta|\underline{L}_{x^2-y^2,\sigma}\rangle + B|\underline{\mathcal{V}}_{x^2-y^2,\sigma}\rangle. \quad (4.12)$$

In addition to the ligand L , we have a hole reservoir state $\mathcal{V}_{x^2-y^2}$ which is regarded as a effective ligand. The $|\underline{\mathcal{V}}_{x^2-y^2,\sigma}\rangle$ state corresponds to the state having a excess hole on the neighboring CuO_3 units. Using eq.(4.1), eq.(4.7)-(4.10) and eq.(4.11), we can obtain the effective hybridization strength between the ligands \mathcal{V} and L :

$$\langle \underline{L}_{x^2-y^2,\sigma} | \mathcal{H} | \underline{\mathcal{V}}_{x^2-y^2,\sigma} \rangle = 2T. \quad (4.13)$$

Similarly to this the effective hybridization strength for the Cu site with N neighbors is found to be $\sqrt{N}T$. For the Cu_4O_8 cluster, on the other hand, since the number of the nearest neighbor Cu sites is two and the effective hybridization strength in each is doubled, the value should be $\sqrt{8}T$. Thus, the effective hybridization strength for the Cu_4O_8 cluster is $\sqrt{2}$ times larger than that for the Cu_5O_{16} cluster.

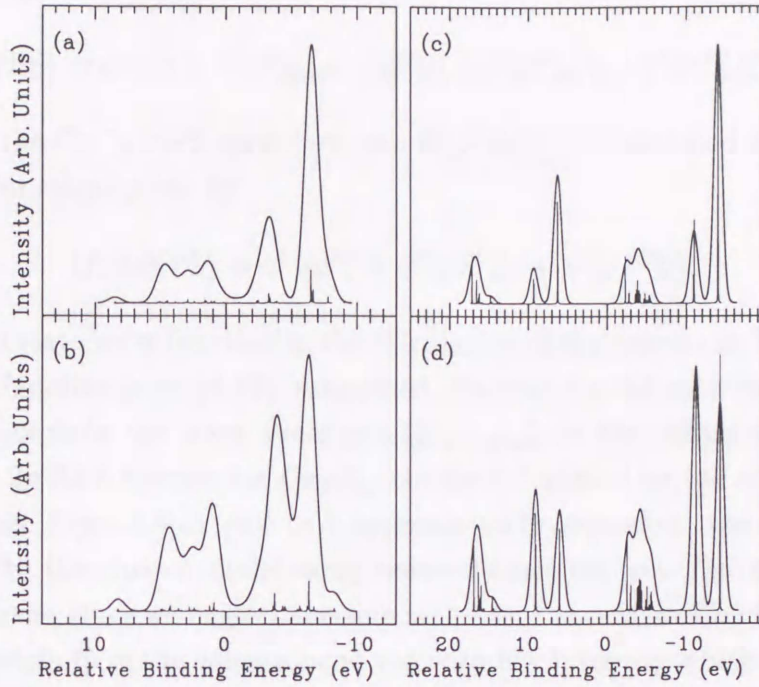


Figure 4.5: Calculated 3d XPS and Cu 2p XPS spectra for undoped Cu_5O_{16} cluster using the simplified model described in the text. 3d PES (a) and Cu 2p XPS spectra (c) with the $|\mathcal{V}\rangle$ states in the initial state and 3d PES (b) and Cu 2p XPS spectra (d) without the $|\mathcal{V}\rangle$ states in the initial state.

Using the density matrix method, we obtain $T=0.65\text{eV}$ and the energy difference of the two ligands $E(\mathcal{V}) - E(\underline{L}) = -2.13\text{eV}$. The weight of the three configurations $|\underline{d}_{x^2-y^2,\sigma}\rangle$, $|\underline{L}_{x^2-y^2,\sigma}\rangle$ and $|\mathcal{V}_{x^2-y^2,\sigma}\rangle$ in the ground state are 55%, 35% and 10%, respectively. For the final state of the 3d PES and the Cu 2p XPS, because the hole is also located on the $L_{3z^2-r^2,\sigma}$ orbitals, we should take into account another linear combination of above four wave functions hybridized with the $|\underline{L}_{3z^2-r^2,\sigma}\rangle$ states. We denote this linear combination of the wave functions by $|\mathcal{V}_{3z^2-r^2,\sigma}\rangle$. The effective hybridization strength between $|\mathcal{V}_{3z^2-r^2,\sigma}\rangle$ and $|\underline{L}_{3z^2-r^2,\sigma}\rangle$ can be obtained in a similar way as that for the orbitals with $x^2 - y^2$ symmetry

$$\langle \underline{L}_{3z^2-r^2,\sigma} | \mathcal{H} | \mathcal{V}_{3z^2-r^2,\sigma} \rangle = \frac{2}{\sqrt{3}} T. \quad (4.14)$$

Applying the method described in Chap. 2, we can calculate the spectra for this effective one Cu site model with the two ligands L and \mathcal{V} .

Figure 4.5 shows the 3d PES and Cu 2p XPS spectra for the undoped Cu_5O_{16} cluster using the effective one Cu site model. The final-state wave-functions which we assumed in the calculation of the 3d PES (see Fig.4.5(a)) are written in terms of

a superposition:

$$|f; 3d\text{PES}\rangle = \alpha'|d^8\rangle + \beta'|d^9\bar{L}\rangle + \gamma'|d^9\bar{\mathcal{V}}\rangle + \delta'|d^{10}\bar{L}^2\rangle + \varepsilon'|d^{10}\bar{L}\bar{\mathcal{V}}\rangle. \quad (4.15)$$

and that for the Cu 2*p* XPS spectrum (see Fig.4.5(c)), we assumed a superposition of the wave functions given by

$$|f; 2p\text{XPS}\rangle = \alpha''|\underline{c}d^9\rangle + \beta''|\underline{c}d^{10}\bar{L}\rangle + \gamma''|\underline{c}d^{10}\bar{\mathcal{V}}\rangle. \quad (4.16)$$

For the initial state wave function in the calculation of the spectra in Figs.4.5(a) and (c) the wave function in eq.(4.12) is assumed, whereas for the spectra in Figs.4.5(b) and (d), we exclude the wave functions $|\bar{\mathcal{V}}_{x^2-y^2,\sigma}\rangle$ in the initial state. The 3*d* PES and Cu 2*p* XPS spectra for Cu₅O₁₆ cluster calculated by the effective one Cu site model (see Figs. 4.5(a) and (c)) approximately reproduce the spectra which calculated with the cluster model using reduced basis set (see Fig. 4.3(e) and Fig. 4.4(e)). However, since we neglect the spin states on the neighboring CuO₃ unit, the states in the vicinity of the valence band top with low intensity which corresponding to the spin and quasi-particle excitations are incorrect for the 3*d* PES spectrum.

To show the importance of the non-local interference of the initial and final wave functions, we exclude the $|\bar{\mathcal{V}}_{x^2-y^2,\sigma}\rangle$ state, which corresponds to the state having the extra hole on the neighboring CuO₃ units, in the initial state (see Figs. 4.5(b) and (d)). Though the weight of the $|\bar{\mathcal{V}}_{x^2-y^2,\sigma}\rangle$ state is only about 10% in the initial state, the result is remarkable both in the 3*d* PES and Cu 2*p* XPS spectra. The relative intensity of the structures, which is suppressed by the non-local interference effect in the presence of the $|\bar{\mathcal{V}}_{x^2-y^2,\sigma}\rangle$ state, in the high energy side are now strongly enhanced. It is clear that the resemblance of the main peak structure between the spectra for the CuO₄ cluster and the much larger cluster is only accidental. For the Cu₅O₁₆ cluster, the states having the excess hole on the ligand *L* and that having the hole on neighboring CuO₄ units (the ligand $\bar{\mathcal{V}}$) are highly mixed in the final state and the resultant bonding and anti-bonding states are mixtures of the two states with almost the same weight. The non-local character of the states corresponding to main peak structure is also expected in other TM oxides appeared in Chap. 2. In Chap. 2, we assumed the ligand *L* is localized within the nearest neighbor oxygen sites. However, we have shown that the assumption at least not true for the CuO₂ plane. The excess hole introduced by the photoexcitation, in reality, should also be distributed over several TMO_{*n*} units in other TM oxides. The values of the charge transfer energy Δ and the effective 3*d*-3*d* interaction strength U_{dd} obtained with the TMO₆ cluster by analyzing the experimental valence band spectra in Chap. 2 should be then reinterpreted as those obtained with an effective ligand which accommodates the hole more extensive region including the neighboring TMO_{*n*} units.

4.4 Conclusion

We have presented a formalism of the systematic reduction of the basis set for the transition-metal-oxide clusters using density matrix method proposed by White. The spectra obtained by using the reduced basis set well reproduce those obtained by the full basis set. Using this method, we have calculated the $3d$ PES and Cu $2p$ XPS spectra for the Cu_5O_{16} cluster having four nearest neighbor Cu sites around the photoexcited Cu site.

We also propose an effective one Cu site model for the Cu_5O_{16} cluster. In addition to the ordinary ligand, which consists of the nearest-neighbor oxygen $2p$ orbits, the model has a hole reservoir level corresponding to the state having an extra hole on nearest neighbor CuO_4 units. Apart from the low intensity states located in the vicinity of the valence band top, the spectra calculated by using the model are consistent with those obtained by the cluster model with reduce basis set.

The non-local character of the states corresponding to main peak structure of the $3d$ PES and Cu $2p$ XPS spectra are also expected in other TM oxides. The values of the charge transfer energy Δ and the effective $3d$ - $3d$ interaction strength U_{dd} obtained with the TMO_n cluster by analyzing the experimental valence band spectra in Chap. 2 should be reinterpreted as those obtained with an effective ligand containing the states on the neighboring TMO_n units.

Acknowledgments

I would like to express my sincere thanks to Prof. Takeo Jo for his fruitful discussions and continuous encouragement. I would also like to thank Prof. Tamio Oguchi for his valuable discussions. I gratefully acknowledge stimulating discussions and also instructions on the computational algorithm with Prof. Junjiro Kanamori, Prof. Macoto Kikuchi, Dr. Manabu Takahashi, Dr. Tomotoshi Nishino, Dr. Shin Imada and Dr. Tomomi Ohtuka. It is my pleasure to thank Prof. Hisazumi Akai and Prof. Junichi Igarashi for providing me a useful program and discussions on the resonant photoemission. I would also like to thank Prof. Shik Shin and Prof. Makoto Okusawa for sending me unpublished data.

[1] A. Fujimori, T. Mizuno and T. Jo, *Phys. Rev. Lett.* **62**, 2724 (1989).

[2] A. Fujimori and T. Mizuno, *Phys. Rev. Lett.* **63**, 2700 (1989).

[3] J. Zaanen, G. A. Sawatzky and J. W. Allen, *Phys. Rev. Lett.* **55** (1985) 1695.

[4] T. Jo, K. Kobayashi, S. Nishino, J. Phys. Chem. **94**, 1000 (1990).

[5] T. Mizuno, *Ph.D. Thesis* (1989), The University of Tokyo.

[6] F. C. Zhang and T. H. Ren, *Phys. Rev. Lett.* **77**, 2370 (1996).

[7] J. van Elp, H. Kalkbrenner, P. Klotz and G. A. Sawatzky, *Phys. Rev. B* **45** (1992) 1012.

[8] T. van Elp, J. T. Michard, H. Kalkbrenner, P. Klotz, G. A. Sawatzky, R. W. F. de Groot and T. T. Tran, *Phys. Rev. B* **49** (1994) 1144.

[9] J. van Elp, *Ph.D. Thesis* (1991), The University of Groningen.

[10] H. A. van den Brink, *Ph.D. Thesis* (1990), The University of Groningen.

[11] G. D. Mahan and J. W. Anderson, *Phys. Rev.* **163**, 710 (1967).

References

- [1] J. H. de Boer and E. J. W. Verwey: Proc. Phys. Soc. London **49** (1937) 59.
- [2] N. F. Mott and R. Peierls: Proc. Phys. Soc. London **49** (1937) 72.
- [3] N. F. Mott, Proc. Phys. Soc. London **A 62** (1949) 416.
- [4] J. Hubbard: Proc. R. Soc. London **A276** (1963) 238.
- [5] J. Hubbard: Proc. R. Soc. London **A277** (1964) 237.
- [6] J. Hubbard: Proc. R. Soc. London **A281** (1964) 410.
- [7] A. Fujimori, F. Minami and S. Sugano: Phys. Rev. **B29** (1984) 5225.
- [8] A. Fujimori and F. Minami: Phys. Rev. **B30** (1984) 957.
- [9] J. Zaanen, G. A. Sawatzky and J. W. Allen: Phys. Rev. Lett. **55** (1985) 418.
- [10] T. Uozumi, K. Okada, A. Kotani: J. Electron Spectrosc. Relat. Phenom. **78** (1996) 103.
- [11] T. Uozumi: PhD Thesis 1994, The University of Tokyo.
- [12] F. C. Zhang and T. M. Rice: Phys. Rev. **37** (1988) 3759.
- [13] J. van Elp, H. Eskes, P. Kuiper and G. A. Sawatzky: Phys. Rev. **B 45** (1992) 1612.
- [14] J. van Elp, J. L. Wieland, H. Eskes, P. Kuiper, G. A. Sawatzky, F. M. F. de Groot, and T. S. Turner: Phys. Rev. **B 44** (1990) 6090.
- [15] J. van Elp: PhD Thesis 1991, The University of Groningen.
- [16] M. A. van Veenendaal: PhD Thesis 1994, The University of Groningen.
- [17] F. D. M. Haldane and P. W. Anderson: Phys. Rev. **6** (1976) 2553.

- [18] K. Terakura, T. Oguchi, A. R. Williams and J. Kübler: Phys. Rev. **B30** (1984) 4734.
- [19] C. T. Chen and F. Sette: Phys. Scripta. **T31** (1990) 119.
- [20] J. G. Bednorz and K. A. Müller: Z. Phys. **B 64** (1986) 189.
- [21] See for example the review by E. Dagotto: Rev. Mod. Phys. **66** (1994) 763 and references cited therein.
- [22] E. Dagotto and J. R. Shrieffer: Phys. Rev. **B 43** (1991) 8705.
- [23] G. Dopf, A. Muramatsu and W. Hanke: Phys. Rev. Lett. **B 41** (1990) 9264.
- [24] T. Tohyama and S. Maekawa: J. Phys. Soc. Jpn. **60** (1991) 53.
- [25] T. Tohyama and S. Maekawa: Physica C **191** (1992) 193.
- [26] M. Alexander *et al.* : Phys. Rev. **B 43** (1991) 333.
- [27] Z. Tan *et al.* : Phys. Rev. **B 42** (1990) 1037.
- [28] H. Romberg, M. Alexander, N. Nucker, P. Adelman, J. Fink: Phys. Rev. **B42** (1990) 8768.
- [29] C. T. Chen, F. Sette, Y. Ma, M. S. Hybertsen, E. B. Stechel, W. M. C. Foulkes, M. Schluter, S.-W. Cheong, A. S. Cooper, L. W. Jr. Rupp, B. Batlogg, Y. L. Soo, Z. H. Ming, A. Krol, Y. H. Kao: Phys. Rev. Lett. **66** (1991) 104.
- [30] H. Matsuyama, T. Takahashi, H. Katayama-Yoshida, T. Kashiwakura, Y. Okabe, S. Sato, N. Kosugi, A. Yagishita, K. Tanaka, H. Fujimoto, H. Inokuchi: Physica C **160** (1989) 567.
- [31] T. Takahashi, H. Matsuyama, H. Katayama-Yoshida, K. Seki, K. Kamiya, H. Inokuchi: Physica C **170** (1990) 416.
- [32] J. W. Allen, C. G. Olson, M. B. Maple, J.-S. Kang, L. Z. Liu, J.-H. Park, R. O. Anderson, W. P. Ellis, J. T. Markert, Y. Dalichaouch, R. Liu: Phys. Rev. Lett. **64** (1990) 595.
- [33] A. Fujimori: Jpn. J. Appl. Phys. Series 7 (1992) 125.
- [34] H. Namatame, A. Fujimori, Y. Tokura, M. Nakamura, K. Yamaguchi, A. Misu, H. Matsubara, S. Suga, H. Eisaki, T. Ito, H. Takagi, S. Uchida: Phys. Rev. **B41** (1990) 7205.

- [35] T. Suzuki, M. Nagoshi, Y. Fukuda, K. Oh-ishi, Y. Syono, M. Tachiki: Phys. Rev. **B42** (1990) 4263.
- [36] J. W. Allen, O. Gunnarsson, J. J. Joyce, A. J. Arko: Phys. Rev. Lett. **70** (1993) 3163.
- [37] A. Svane and O. Gunnarsson: Phys. Rev. Lett. **65** (1990) 1148.
- [38] M. Arai and T. Fujiwara: Phys. Rev. **B 51** (1995) 1477.
- [39] G. A. Sawatzky and J. W. Allen: Phys. Rev. Lett. **53** (1984) 2339.
- [40] A. Fujimori: in *Core Level Spectroscopy in Condensed Systems*, ed. J. Kanamori and A. Kotani (Springer-Verlag, Berlin, 1988).
- [41] G. A. Sawatzky: in *Core Level Spectroscopy in Condensed Systems* (ref.[28]).
- [42] S.-J. Oh: in *Core Level Spectroscopy in Condensed Systems* (ref.[28]).
- [43] A. Fujimori, A. E. Bocquet, T. Saitoh and Mizokawa: J. Electron Spectrosc. Relat. Phenom. **62** (1993) 141.
- [44] A. Fujimori, N. Kimizuka, T. Akahane, T. Chiba, S. Kimura, F. Minami, K. Siratori, M. Taniguchi, S. Ogawa and S. Suga: Phys. Rev. **B42** (1990) 7580.
- [45] J. van Elp, R. H. Potze, H. Eskes, R. Berger and G. A. Sawatzky: Phys. Rev. **B44** (1991) 1530.
- [46] A. Kotani and K. Okada: in *Recent Advances in Magnetism of Transition Metal Compounds*, ed. A. Kotani and N. Suzuki (World Scientific, Singapore, 1993).
- [47] K. Okada and A. Kotani: J. Electron Spectrosc. Relat. Phenom. **62** (1993) 131.
- [48] K. Okada and A. Kotani: J. Phys. Soc. Jpn. **61** (1992) 4619.
- [49] L. H. Tjeng, C. T. Chen, J. Ghijsen, P. Rudolph and F. Sette: Phys. Rev. Lett. **67** (1991) 501.
- [50] M. F. Lopetz, A. Hoehr, C. Laubschat, M. Domke and G. Kaindl: Europhys. Lett. **20** (1992) 357.
- [51] T. Miyahara, T. Hanyu, H. Ishii, T. Mitsuishi, S. Muto and S. Nakai: J. Phys. Soc. Jpn. **62** (1993) 4129.
- [52] S. Suga *et al.* : private communication.

- [53] M. Okusawa *et al.* : private communication.
- [54] A. Tanaka and T. Jo: J. Phys. Soc. Jpn. **61** (1992) 2669.
- [55] A. Tanaka and T. Jo: J. Phys. Soc. Jpn. **61** (1992) 3837.
- [56] A. Harasaki, A. Tanaka and T. Jo: J. Phys. Soc. Jpn. **62** (1993) 2220.
- [57] Y. Seino, H. Ogasawara, A. Kotani, B. T. Thole and G. van der Laan: J. Phys. Soc. Jpn. **61** (1992) 1859; G. van der Laan, B. T. Thole, H. Ogasawara, Y. Seino and A. Kotani: Phys. Rev. **B46** (1992) 7221; G. van der Laan, M. Surman, M. A. Hoyland, C. F. J. Flipse, B. T. Thole, Y. Seino, H. Ogasawara and A. Kotani: Phys. Rev. **B46** (1992) 9336.
- [58] See for example L. C. Davis: J. Appl. Phys. **59** (1986) R25.
- [59] J.-H. Park, L. H. Tjeng, J. W. Allen, R. Claessen, C. T. Chen, P. Metcalf and H. R. Harrison: preprint.
- [60] Y. Tezuka, S. Shin, A. Agui, M. Fujisawa and T. Ishii: J. Phys. Soc. Jpn. **65** (1996) 312.
- [61] A. Tanaka and T. Jo: J. Phys. Soc. Jpn. **62** (1993) 1118.
- [62] J. Ghijsen, L. H. Tjeng, H. Eskes, A. Sawatzky and R. L. Johnson: Phys. Rev. **B42** (1990) 2268.
- [63] E. U. Condon and G. H. Shortley: *Theory of Atomic Spectra* (Cambridge University, London, 1959).
- [64] T. Jo, A. Kotani, J. C. Parlebas and J. Kanamori: J. Phys. Soc. Jpn. **52** (1983) 2581.
- [65] K. Okada and A. Kotani: J. Electron Spectrosc. Relat. Phenom. **62** (1993) 131.
- [66] V. Heine: *Solid State Physics*, ed. H. Ehrenreich, F. Seitz and D. Turnbull (Academic Press, New York, 1980) Vol. 35, p.87.
- [67] J. Igarashi: Prog. Theor. Phys. Suppl. No. 101 (1990) 317.
- [68] O. Gunnarsson and K. Schonhammer: Phys. Rev. **B28** (1983) 4315.
- [69] T. Jo and A. Kotani: J. Phys. Soc. Jpn. **55** (1985) 2457.
- [70] H. Eskes, M. Meinders and G. A. Sawatzky: Phys. Rev. Lett. **67** (1991) 1035.

- [71] H. Eskes, G. A. Sawatzky and L. F. Feiner: *Physica C* **160** (1989) 424.
- [72] H. Eskes and G. A. Sawatzky: *Phys. Rev.* **B43** (1991) 119.
- [73] R. Haydock, V. Heine and M. J. Kelly: *J. Phys. C* **5** (1972) 2845.
- [74] M. A. van Veenendaal and G. A. Sawatzky: *Phys. Rev. Lett.* **70** (1993) 2459.
- [75] M. A. van Veenendaal, H. Eskes, and G. A. Sawatzky: *Phys. Rev. B* **70** (1993) 11462.
- [76] S. R. White: *Phys. Rev. Lett.* **69** (1992) 2863.
- [77] H. Sato, M. Tamura, N. Happo, T. Mihara, M. Taniguchi, T. Mizokawa, A. Fujimori and Y. Ueda: *Solid State Commun.* **92** (1994) 921.
- [78] A. Kakizaki, K. Sugeno, T. Ishii, H. Sugawara, I. Nagakura and S. Shin: *Phys. Rev. B* **28** (1983) 1026.

公表論文

- (1) Resonant $3d$, $3p$ and $3s$ Photoemission in Transition Metal Oxides Predicted at $2p$ Threshold
(遷移金属酸化物の $2p$ しきい値領域における共鳴 $3d$, $3p$ および $3s$ 光電子放出の予言)
共著者 田中新、城健男
(学会誌) Journal of the Physical Society of Japan Vol. 63, No. 7, pp. 2788-2807
平成 6 年 7 月 15 日出版 (日本物理学会)
- (2) Strong $3d$ -Ligand Hybridization in TiO_2 and Satellite Structures in Ti $3d$ and $3p$ Photoemission
(TiO_2 における $3d$ -配位子間の強い混成と Ti $3d$ および $3p$ 光電子分光放出のサテライト構造)
共著者 城健男、田中新
(学会誌) Journal of the Physical Society of Japan Vol. 64, No. 2, pp. 676-677
平成 7 年 2 月 15 日出版 (日本物理学会)
- (3) Effect of Electron Doping on Spectral Function of Cu-Oxide Cluster Model Including Full Multiplet: Shift of Valence Band Edge
(銅酸化物クラスターモデルにおけるスペクトル関数の電子ドーピング効果~価電子帯上端の移動~)
共著者 田中新、城健男
(学会誌) Journal of the Physical Society of Japan Vol. 65, No. 4, pp. 912-915
平成 8 年 4 月 15 日出版 (日本物理学会)
- (4) Spectral Function of Electron-Doped Cu-Oxide Cluster Model Including Full Multiplet
(多重極相互作用を取り入れ、電子をドーピングした銅酸化物クラスターモデルにおけるスペクトル関数)
共著者 田中新、城健男
(学会誌) Physica B に平成 9 年出版予定 (Elsevier Science)

参考論文

- (1) Temperature Dependence of $2p$ Core X-Ray Absorption Spectra in $3d$ Transition Metal Compounds
($3d$ 遷移金属化合物における $2p$ 内殻 X 線吸収スペクトルの温度依存性)
共著者 田中新、城健男
掲載誌 Journal of the Physical Society of Japan Vol. 61, No. 6, pp. 2040-2047 (平成 4 年出版)

- (2) Configuration Interaction in Ni Metal and Ni Alloys and High-Energy Spectroscopy
(金属 Ni と Ni 合金における配置間相互作用と高エネルギー分光)
共著者 田中新、城健男、G. A. Sawatzky
掲載誌 Journal of the Physical Society of Japan Vol. 61, No. 8, pp. 2636-2639 (平成 4 年出版)

- (3) Resonances and Magnetic Circular Dichroism in Valence Band Photoemission Predicted at Ni $2p$ Threshold for Ferromagnetic Nickel
(強磁性 Ni の Ni $2p$ しきい値領域における価電子帯光電子放出の共鳴と円偏光依存性に対する予言)
共著者 田中新、城健男
掲載誌 Journal of the Physical Society of Japan Vol. 61, No. 8, pp. 2669-2672 (平成 4 年出版)

- (4) Resonances in $3d$ Electron Photoemission Predicted at Ni $2p$ Threshold for NiCl₂ and NiO
(NiCl₂ と NiO の Ni $2p$ しきい値領域における $3d$ 光電子放出の共鳴)
共著者 田中新、城健男
掲載誌 Journal of the Physical Society of Japan Vol. 61, No. 11, pp. 3837-3840 (平成 4 年出版)

- (5) Spin Polarization of $3d$ Photoemission at $3p$ Threshold in Ferromagnetic Ni Expected from Configuration Interaction Model
(配置間相互作用を取り入れたモデルにより予言された $3p$ しきい値領域における $3d$ 光電子放出のスピン偏極)
共著者 田中新、城健男
掲載誌 Journal of the Physical Society of Japan Vol. 62, No. 4, pp. 1118-1122 (平成 5 年出版)

- (6) Capability of Resonant Photoemission with the Soft X-Ray in Rare Earth Systems
(希土類を含む系の軟 X 線領域での共鳴光電子放出の有用性)
共著者 原崎亜紀子、田中新、城健男
掲載誌 Journal of the Physical Society of Japan Vol. 62, No. 7, pp. 2220-2223 (平成 5 年出版)
- (7) Selection Rules in Resonant $4f$ Photoemission for Rare Earths
(希土類の共鳴 $4f$ 光電子分光の選択則)
共著者 甲斐優、田中新、城健男
掲載誌 Journal of the Physical Society of Japan Vol. 64, No. 7, pp. 2356-2359 (平成 7 年出版)
- (8) Spin Polarization of $3d$, $3p$ and $3s$ Photoemission in Ferromagnetic Nickel Predicted at Ni $2p$ Core Threshold
(強磁性ニッケルにおける Ni $2p$ しきい値領域での $3d$, $3p$ および $3p$ 光電子放出のスピン偏極に対する予言)
共著者 田中新、城健男
掲載誌 Journal of the Physical Society of Japan Vol. 64, No. 10, pp. 4013-4022 (平成 7 年出版)
- (9) Configuration Dependent Hybridization Strength Revealed by Analysis of Resonant Inverse Photoemission in $CeNi_2$
($CeNi_2$ の共鳴逆光電子放出の解析により明らかになった混成の強さの配置依存性)
共著者 田中新、城健男
掲載誌 Physica B Vol. 206 & 207, pp. 74-76 (平成 7 年出版)
- (10) Theory of Resonant Inverse Photoemission Spectroscopy in Ce Compounds: Selection Rule and Hybridization Strength
(Ce 化合物の共鳴逆光電子分光に対する理論~選択則と混成の強さ~)
共著者 田中新、城健男
掲載誌 Journal of the Physical Society of Japan Vol. 65, No. 2, pp. 615-621 (平成 8 年出版)

- (11) Effect of Coulomb Interaction on the X-Ray Magnetic Circular Dichroism Spin Sum Rule in 3d Transition Elements

(3d 遷移元素における X 線磁気円二色性の Spin 総和則に対するクーロン相互作用の効果)

共著者 寺村善樹、田中新、城健男

掲載誌 Journal of the Physical Society of Japan Vol. 65, No.4, pp. 1053-1055 (平成 8 年出版)

- (12) Theory of Resonant Inverse Photoemission in Ce Compounds

(Ce 化合物の共鳴逆光電子分光の理論)

共著者 田中新、城健男

掲載誌 Journal of Electron Spectroscopy and Related Phenomena Vol. 78, pp. 131-134 (平成 8 年出版)

- (13) Selection Rules in Resonant Photoemission in Rare Earths

(希土類の共鳴光電子放出における選択則)

共著者 甲斐優、田中新、城健男

掲載誌 Journal of Electron Spectroscopy and Related Phenomena Vol. 78, pp. 63-66 (平成 8 年出版)

- (14) Effect of Coulomb Interaction on the X-Ray Magnetic Circular Dichroism Spin Sum Rule in Rare Earth

(希土類における X 線磁気円二色性の Spin 総和則に対するクーロン相互作用の効果)

共著者 寺村善樹、田中新、B. T. Thole、城健男

掲載誌 Journal of the Physical Society of Japan Vol. 65, pp. 3056-3059 (平成 8 年出版)